NOTE TO USERS

Manufacturing of Braided Thermoplastic Composites with Commingled Fibers

Louis Laberge-Lebel

A Thesis

in

The Department

of

Mechanical and Industrial Engineering

Presented in Partial Fulfilment of the Requirements
for the Degree of Master of Applied Science (Mechanical Engineering) at
Concordia University
Montreal, Québec, Canada

April 2005

Your file Votre référence
ISBN: 0-494-10265-9
Our file Notre référence
ISBN: 0-494-10265-9

ABSTRACT

Manufacturing of Braided Thermoplastic Composite with Commingled Fibers

Louis Laberge-Lebel

Through this work, an investigation on thermoplastic composites manufactured with braided commingled fibers is performed. Thermoplastic composites have the potential for complex shape part manufacturing with a cost-effective perspective. However they present a manufacturing challenge because of the high melt viscosity of their matrices. Among the many solutions to this problem commingled yarns present a promising avenue. The commingled yarn studied here is a carbon/nylon yarn from Schappes Techniques France. Braiding is used to manufacture preforms from this yarn. Bi-axial braiding is described with the mathematical relations regulating the process. The machine available in the lab has been calibrated and seven fabrics have been produced with seven different braiding conditions to explore the preforming method. The fabrics have been consolidated using compression molding. A model to predict the final thickness of the consolidated braid is proposed. The evaluation of the quality of the consolidation was performed using a constituent content method and a qualitative observation by microscopy. Both methods were developed in the scope of this work. Flexural and tensile mechanical properties of the consolidated laminates are tested. The tensile modulus data are compared to a mathematical model using the classical lamination theory.

ACKNOWLEGEMENTS

I would first like to thank my family and friends for their support and encouragements during my stay at Concordia University. Also, I would like to thank my university colleagues for the great exchanges realised with them and all the different views they made me discover. I would like to thank Dr. Asami Nakai, Dr. Philippe Merle, John Elliot, Janet Boyles, Brian Cooper, and the guys from the machine shop for their precious advices. They are all persons that have been of great help but I also discovered their nice personalities. Finally, I am very thankful to Dr. Suong V. Hoa, for the way he guided me through this thesis process, by giving me all the freedom and opportunities to explore the fascinating worlds of composite and research.

TABLE OF CONTENTS

LISTE OF FIGURES

LISTE OF TABLES

NOMENCLATURE

a	Diamond shaped yarn cross over height
abd_{11}	Laminate compliance matrix term 1,1
abd_{22}	Laminate compliance matrix term 2,2
A_C	Braid unit cell covered area by fibers
A_D	Area of the diamond shaped yarn crossover in the braid unit cell
A_T	Braid unit cell area
A_Y	Yarn consolidated cross-section area
b	Diamond shaped yarn cross over widthTg Glass transition temperature
B_S	Braider head set speed
C	Braid circumference
C_S	Capstan set speed
C_f	Cover factor
d	Distance between parallel yarns in the braid
D	Braiding mandrel diameter
e	Braid unit cell length.
E_{AXIAL}	Consolidated braid axial tensile modulus
E_{HOOP}	Consolidated braid hoop tensile modulus
η	Viscosity of polymer melt
L	Impregnation distance
M_a	Weigh of a composite sample in air

m_B Slope of the braider head set-vs-real speed curve

m_C Slope of the capstan head set-vs-real speed curve

$m_{C/B}$ Slope of the dependency of the capstan set-vs-real slope upon braider set speed

M_d Weigh of a dry filter in a weighing pan containing clean fibers

M_f Weigh of a dry filter in a weighing pan

M_w Weigh of a composite sample immersed in water

N Total rotational numbers of carriers involved in the braiding operation. Total number of bias yarns in the braid.

n_D Number of yarn crossovers in braided fabric.

N_F Number of reinforcement filaments in a yarn

N_L Number of braided layers in a preform

ω Angular velocity of the carriers around the braider.

p Pitch distance, axial distance on braiding mandrel for one fiber to completely turn around mandrel

P Pressure

ϱ_L Tow linear weight.

ϱ_a Actual density of the consolidated composite

ϱ_t Theoretical density of the consolidated composite

ϱ_f Reinforcement density

ϱ_m Matrix density

R_C Compression Ratio

R_F Reinforcement filament radius

S Braid unit cell width.

S_F	Permeability of a fiber bed
t_C	Consolidated thickness
θ	Braid Angle
θ_F	Braid angle for full cover condition
Tm	Melting point
t_P	Preform thickness
v	Linear speed of the braiding mandrel
V	Impregnation flow front speed
V_f	Fiber volume fraction
V_m	Matrix volume fraction
w	Yarn width.
W_b	Braided fabric aerial weight
W_f	Fiber weight fraction
W_m	Matrix weight fraction
X_V	Void content of a consolidated composite
Y	Diagonal length of a typical braid rectangle.

Chapter 1

INTRODUCTION

The field of composites has been going through many evolutions since its beginnings. The discovery of new materials, the mathematical modelling of the mechanical properties, and the establishment of new manufacturing techniques are just an overview of the many constantly renewing aspects of this field. One of the important challenges is the knowledge of manufacturing principles, which during the last 15 years, has changed from "descriptive art" to practice based on scientific and engineering principles [1]. Manufacturing science takes more importance today in the highly competitive market place, where efficiency and production speed are the keys to success. For example, the aerospace industry is actually finding new and inexpensive manufacturing techniques while keeping the high mechanical standards needed by the products. The path is going through composites for primary aircraft structures [2-5], trading the traditional aluminium riveted structures by high-strength and lightweight composites structures.

Thermoplastic composites offer a promising route for the aerospace industry. Their mechanical performances are greater in terms of damage resistance. Their chemical stability gives them a strong resistance to aircraft hydraulic fluids, aircraft fuel and other chemical substances involved in the aircraft industry. Their post-forming, re-shaping, and recycling ability demonstrate the potential for cost reduction.

The main drawback of thermoplastic composites is the high viscosity of their matrices, being 100 to 1000 times more viscous than thermoset matrices. This obstacle means difficulty

in impregnation of fiber beds, porosity in products and un-expected poor mechanical performance. That is where the manufacturing issues take all their importance. The elaboration of new strategies is of key importance to overcome this problem.

Among many solutions to this difficulty, commingled fibers, developed in the early 1990's, are gaining in popularity and use. Research has been made on different commingled yarns combining different materials. But more experimental data have to be collected on this manufacturing process to fully understand the form of material. Also, it is in combining the success in obtaining good consolidation to efficient preforming techniques such as braiding and weaving that the multiple potentials of this hybrid yarn will be confirmed.

1.1. Objective

The main objective of this thesis is to understand braided composites from thermoplastic commingled fiber form of materials. To do so, the investigation will go from a simple commingled yarn to the mechanical properties of a consolidated plate manufactured using braiding.

1.2. Outline

Chapter 2 presents an overview on thermoplastic composites; qualifying the different matrix and reinforcements available and introducing the main challenge when dealing with thermoplastic composites and the principal avenues to overcome this difficulty. Chapter 3 investigates the hybrid yarn used in this study: Schappe Technique's Carbon/Nylon commingled yarn. Chapter 4 is an analysis of the 2D biaxial braiding process and a characterization of the fabrics manufactured by this process using the commingled yarn of this

study. The braids have been consolidated in plates; the consolidation process and the results associated with these plates are presented in chapter 5. In chapter 6, a complete consolidation quality analysis is developed and performed on the plates manufactured in this study. The constituent content of the composite is quantified and the cross sections of the consolidated samples are observed using microscopy. Finally, chapter 7 shows the mechanical properties of the manufactured plates associated with prediction of properties. Tensile and flexural properties of the plates are measured. Using the classical lamination theory, the tensile modulus experimental data is compared to calculated values.

Chapter 2

THERMOPLASTIC COMPOSITES

Thermoplastic composites offer many advantages over thermoset composites such as higher fracture toughness and elongation, no chemical reaction time, unlimited shelf life, good solvent resistance, potential for fast, clean and automated manufacturing and greater recyclability [6]. However, the 100 to more than 1000 times higher viscosity of molten thermoplastic matrices compared to thermosets [7] requires different and novel manufacturing processes involving precursors such as pre-impregnated tapes and hybrid yarns.

This review will survey the different matrices and reinforcements available and the different strategies for combining themselves.

2.1. Matrices

In a composite, the matrix system serves several important functions. In addition to holding the reinforcing fibers together at the right orientation and in the product shape, the matrix protects the fiber from wear and abrasive damage and provides load transfer among the fibers.

In their nature, thermoplastics are long, threadlike molecules either lying closely packed together or intermingled with one another. When heated, the various forces linking the molecules together are weakened and the material softens until it reaches a viscous elastic liquid stage. Cooling results in an increase in viscosity followed by solidification.

Thermoplastics can be either semi-crystalline or amorphous. An amorphous polymer consists of long intermingled polymer chains arranged randomly. The glass transition temperature (Tg) is the temperature under which the long-range segmental motion ceases, as if all the long molecules movements were frozen. In semicrystalline polymers, a part of the polymer chains are arranged in crystals, distributed in an amorphous polymer phase. Semicrystalline polymers have a melting temperature (Tm) where all the crystals are melted and the polymer exists as a disordered melt.

All the different thermoplastics used in everyday life can be used as matrices for composites manufacturing, for example the low cost polyethylene, polypropylene or nylon. There are also high performance matrices such as polyphenylenesulfide (PPS), polyetherimide (PEI), polyetheretherketone (PEEK) or polyetherketoneketone (PEKK). The choice of the right matrix system is imposed by the application of the manufactured product and the manufacturing costs. Table 2.1, presents different matrices and their properties.

Matrix Polymer	Morphology	Tg	Tm	Processing Temperature	Tensile Strength	Tensile Modulus
		°C	°C	°C	MPa	GPa
Polyethelene (PE)	Semicrystalline	-120	140	175-275	55	2.5
Polypropylene (PP)	Semicrystalline	-18	170	200-260	45	1.4
Nylon (PA66)	Semicrystalline	50	265	270-325	50	2
Polyphenylenesulfide (PPS)	Semicrystalline	90	273	315-330	90	3.8
Polyetherimide (PEI)	Amorphous	217	-	335-426	105	3
Polyetheretherketone (PEEK)	Semicrystalline	143	343	350-380	100	3.5
Pelyetherketoneketone (PEKK)	Semicrystalline	156	306	330-380	90	3.4

Table 2.1: Properties of Selected Thermoplastics [8,9]

2.2. Reinforcements

The composite final mechanical properties are dependent to a large extent on the reinforcing fiber. High specific strength and modulus of reinforcement are of primary importance to obtain good mechanical properties. Also, the interface with the resin, in the fiber texture and functionality, has to promote adherence to the matrix to perform a good load transfer. Properties of selected reinforcements are presented in Table 2.2.

Reinforcement	Density	Tensile Strength	Tensile Modulus
	g/cm^3	MPa	GPa
S-Glass	2.50	4585	85
Kevlar 49	1.44	3034	138
Carbon AS-4	1.80	4000	248

Table 2.2: Properties of Selected Reinforcements [1,9]

2.3. Impregnation Strategies

Different parameters affect the flow speed of matrix in a fiber bed. Equation 2.1 presents the Darcy's law that governs flow in a porous media. The flow velocity V depends on the permeability of the fiber bed (S_F), the resin viscosity (η), the pressure gradient (ΔP), and the impregnation distance (ΔL).

$$V = -\frac{S_F}{\eta}\frac{\Delta P}{\Delta L} \tag{2.1}$$

From this relation it is clearly seen that a high matrix viscosity will reduce the flow speed and thus increase the impregnation time. So far, three main avenues are employed to reduce manufacturing costs in having low impregnation time at reasonable pressures. The first solution is the direct melt impregnation, leading to tapes and prepregs that are used to produce

parts in further manufacturing operations. The second solution is the intimate mixing prior to melting, also called post-impregnation technique. This solution includes the various hybrid yarns like powder impregnated yarns, commingled yarns and micro-braided yarns. The last solution, less developed, is to use precursors of low viscosity. For example, dissolving the polymer in a solvent before impregnation will give a low viscosity fluid that will easily impregnate the fiber bed.

2.3.1. Prepregs

Combining the matrix to the reinforcement prior to part manufacturing is called prepregging. With thermoplastic matrices, this operation usually gives a thin tape of unidirectional continuous fibers impregnated with the polymer to a desired fiber volume fraction. The result is a stiff, boardy and nontacky material (Figure 2.1). This tape is then used to manufacture parts to the desired shape using compression molding, autoclave processing, or tape placement techniques [10].

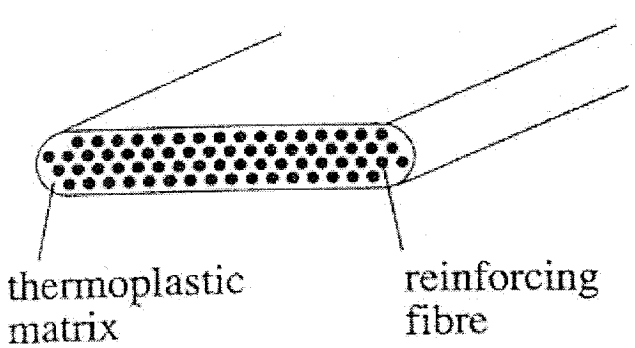

Figure 2.1: Thermoplastic Composite Tape Prepreg.

This combining method gives a good control on fiber orientation, a precise fiber content, and a uniform fiber distribution. The resulting product has a complete consolidation

state. All theses characteristics lead to high quality composites having consistency in mechanical properties.

However, the stiff, boardy and nontacky nature of the thermoplastic composite tape leads to difficult and costly manufacturing techniques rendering this form of material for high performance applications only.

2.3.2. Film Stacking

This method simply uses a reinforcement fabric placed in a sandwich between matrix thermoplastic films (Figure 2.2). Application of pressure and temperature then consolidates the new-formed stack.

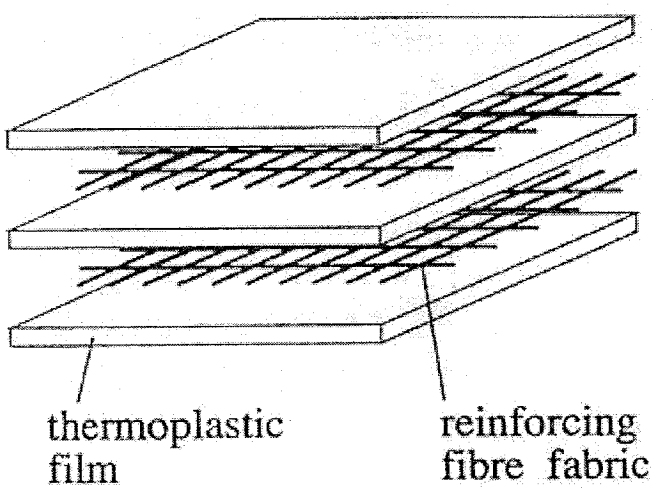

Figure 2.2: Thermoplastic Film Stacking.

This method is attractive for its simplicity and the availability of matrices in films. But it is also labour intensive and the preforms have low drapeability. Also, the impregnation distance, in the order of millimetres, is quite large for thermoplastic matrices, leading to difficult impregnation.

2.3.3. Hybrid yarns

Powder Impregnated Yarns

Powder impregnated (Figure 2.3) yarns are fibers impregnated with fine thermoplastic particles (5-15 μm). The processes to mix the matrix to the reinforcement employ fluidized bed or fluid slurry methods. Preforms are manufactured using weaving, knitting or braiding.

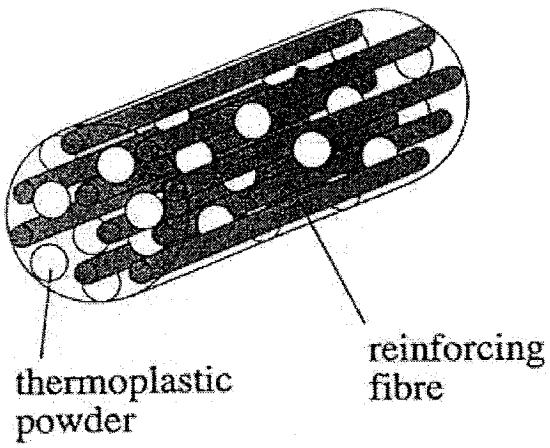

Figure 2.3: Powder Impregnated Yarns.

The advantage of the powder form in this kind of hybrid yarn gives the versatility in choice of matrix because of the availability of thermoplastic powders. But the combining step is difficult in order to obtain a good powder distribution. The resulting yarn has a high flexural rigidity and high friction. The yarn handleability is a problem since the polymer particles can be easily dislodged from the reinforcing filaments [9]. Finally, the high volumetric bulk factor of powder-impregnated yarns makes them difficult to mold.

Commingled Yarns

Commingled yarns are an intimate mix of reinforcement filaments and matrix filaments to form a yarn with desired fiber volume content. In post-impregnation techniques, Bernet et al. [11] showed that commingled yarns are suitable for rapid processing of complex

shapes involving modern manufacturing processes. Consolidation models are available from different sources and characterize the consolidation quality of the final composite by the amount of residual porosity in the part as function of the consolidation parameters i.e. time, pressure and temperature. Also, all models emphasize on the yarn architecture to predict the total laminate consolidation behaviour [12-14]. Ramasamy et al. [15-17] demonstrated the superiority of commingled yarns over powder-impregnated tows in the low-cost preforming method of braiding. Also, commingled yarns have made major breakthroughs in industry, for example in sports equipment like tennis rackets, demonstrating the viability of commingled yarn thermoplastic composites [18].

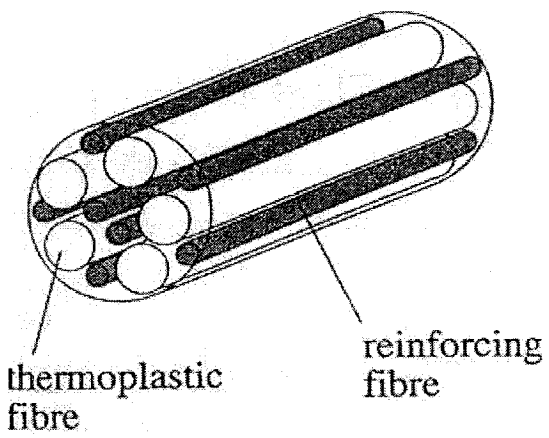

Figure 2.4: Commingled Yarn.

This form of hybrid yarn has a high degree of fiber matrix mixing, giving a short impregnation distance, in the order of micrometers. The resulting yarn is also flexible, and is of low friction. However, availability issues make commingled yarns and fabrics a difficult choice when dealing with thermoplastic composites because of the scarcity of matrix/reinforcement on the market and the high cost of the commingled form of material.

Micro-Braided Yarns

A different mixing strategy is under development since the 1990's in Japan, which is called micro-braiding. The micro-braiding is a post impregnation technique using braiding as a way of intimate mixing of the thermoplastic matrix and the reinforcement at the tow level (Figure 2.5). Previous studies at Kyoto Institute of Technology [19-21], have shown the great potential of this post-impregnation technique in low cost: micro-braiding offers great versatility in terms of the infinite material combinations available, and also the variability of matrix/reinforcement ratios that can be obtained without having to rely on material suppliers.

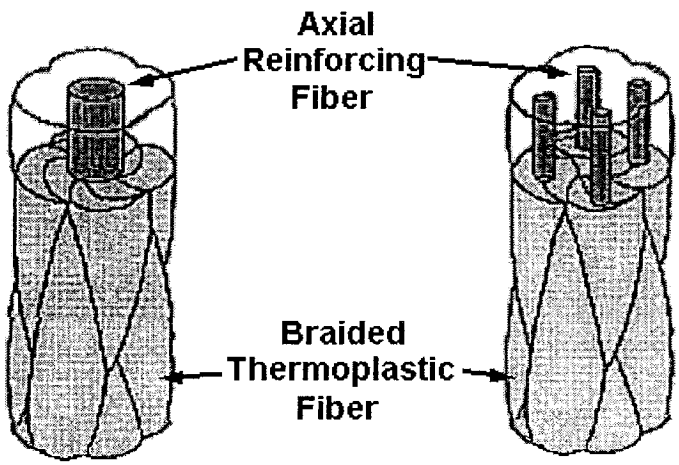

Figure 2.5: Micro-Braided Yarns.

The resulting yarn is flexible; offer a great protection of the reinforcement has a low coefficient of friction; and has low yarn manufacturing costs. On the other hand, the impregnation time is higher than the other form of hybrid yarns because the impregnation distance from the braided sheath to the centre of the reinforcing tow is fairly large (0.2 to 0.4 mm)

Chapter 3

COMMINGLED YARN

3.1. Background

Among the different hybrid-yarns, commingled yarns are a blend of thermoplastic matrix filaments and reinforcement filaments at the tow level. They have been developed in the 1990's to overcome the major manufacturing issue when dealing with thermoplastic composites, the high melt viscosity. The very good fiber/matrix distribution in non-molten state before manufacturing reduces the impregnation distance, i.e. the flow length that the matrix has to do to cover the reinforcing fibers, to the order of hundreds of microns, enhancing the manufacturing time.

This form of material also gives the opportunity to take full advantage of the cost reduction given by textile technologies, such as weaving and braiding. There is good freedom in choice of matrix-reinforcement combination.

Various techniques are used to manufacture commingled yarns. The objective is to produce a uniform reinforcement/matrix distribution when reducing the damage inflicted to the reinforcing filament. The blend can be realized by passing superposed reinforcement and matrix bundles in a high-pressure air or water jet through a nozzle. The uniformity of the blend is dependent of the similarity of the two mingled fibers in their configuration; they should be as similar as possible.

Another technique is to use stretch-broken filaments of matrix and reinforcement in a predetermined length and twisted together in a yarn. The fiber length is considerably higher than the critical fiber length. The longitudinal properties of the composite may be affected by the imperfectly aligned fibers coming from the stretch-broken twisted yarn. However, the interlaminar properties may be enhanced [6].

The material used in this study has been developed at École Polytechnique of Lauzanne [22]. Carbon and nylon have been selected for matrix and reinforcement on the basis of drapeability, processing cycle time and material cost. Then an optimization of the fibre/matrix interface is realized. A mathematical model is developed to predict consolidation time to obtain void-free composites. Further discussed in chapter 5, this model takes into account the yarn characteristics such as the heterogeneity of the commingling in the yarn, properties of materials, permeability of the fiber network and the resin viscosity.

3.1.1. Carbon/Nylon Commingled Yarn

The materials used in this study are commingled yarns manufactured by Schappes Techniques (France). The yarn is composed of nylon matrix and carbon reinforcement.

Matrix

The matrix is from the nylon family. It is a polyamide 12 coming from EMS CHEMIE AG (Switzerland) and named Grilamid 12. Selection of this particular matrix formulation has been based on various criteria such as viscosity, wetting, adhesion, durability and costs [22]. Properties of the matrix are presented in Table 3.1. PA12 is a semi-crystalline thermoplastic polymer having a crystallinity of about 41% for solidification rates between 1 and 100°C/min

[22]. For the commingling step, the nylon filament comes in a staple fiber form having an average diameter of 20 μm.

Matrix Polymer	Density	Melt Viscosity at low shear rates (>1 sec^{-1})	Glass Transition Temp. - Tg	Melting Point - Tm	Bending Modulus	Tensile Modulus
-	g/cm^3	Pa.s	DSC,°C	DSC,°C	MPa	MPa
PA12	1.01	250	42	178	1200	1400

Table 3.1: Matrix Properties [22]

Reinforcement

The reinforcement of the composite material involved in this study is carbon fiber from Tenax Fibers GmbH (Germany). Schappes Techniques transforms the 5-7 μm diameter continuous carbon filaments into stretch-broken filaments having an average length of 80 mm. The typical tension breaking apparatus (Figure 3.1) comprises many sets of drafting rolls, the peripheral speed of the delivery rolls being considerably greater than that of the feed rolls, causing the drafted filaments to be stressed beyond the breaking point, the length of the stapled fibers produced being determined (at least in part) by the spacing of the roll pairs [23]. Prior to this operation, the fibers are coated with a sizing agent that keep the tow integrity during stretch breaking. Also, the sizing improves wettability and interfacial strength. The density of the carbon filaments is 1.78 g/cm^3.

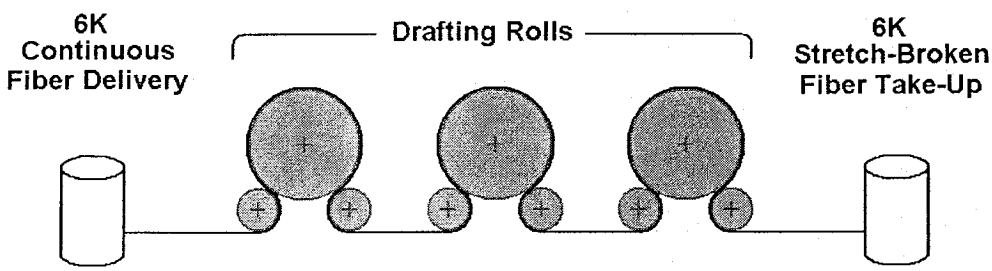

Figure 3.1: Stretch-Breaking Apparatus.

Commingling

The commingling is realised by Schappes Techniques in France. The process uses the stretch-broken carbon filaments and staple nylon fibers and blends them in commingled yarns having 6000 carbon filaments. The blend is realized so that the stretch-broken carbon fibers and the staple nylon fibers stay parallel to the yarn direction.

Material Architecture

The yarns used for braiding are an assembly of two 6K commingled tows wrapped together by a continuous nylon bundle to keep the yarn integrity. Prior to this assembly, nylon wrapping is also done on each of the two 6K tows to prevent the un-commingling during preforming operations like braiding. It also reduces the friction of the yarn on other yarns and machine elements in preforming and manufacturing operations. The architecture of the yarn is presented in figure 3.2. The fiber volume fraction including the wrapping is 53% and the metric count is .84 Mc (Km per Kg) (as mentioned by the manufacturer)

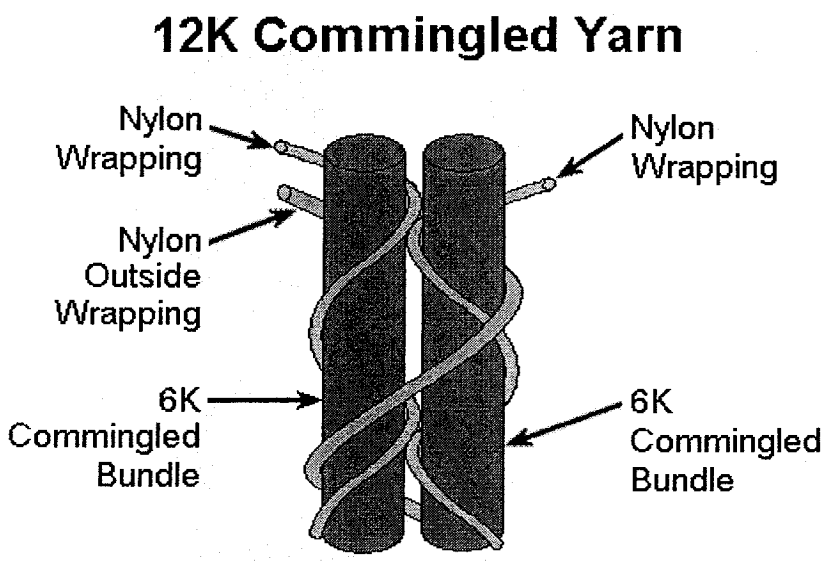

Figure 3.2, Commingled Fiber Architecture

3.2. Experimental

Further analysis is made in this study on the yarn architecture. First a fiber content analysis is made to confirm the fiber/matrix ratio in the yarn form. Procedure for this analysis is presented in section 6.4. Then, six yarns are embedded in clear room-temperature-curing epoxy mounts and polished using an automatic surface preparation machine. During curing of the mounts, a load of approximately 5 grams is applied on the yarns to tension them as installed on the braiding machine. The surface preparation method is used as described further in section 6.3.1. Using a microscope and an image analysis system, width and thickness measurements are taken on the polished cross section of the yarn. Finally, linear weight of the raw yarns is measured.

3.3. Results and Discussion

The yarn cross-section examination under the microscope gives interesting insights on the yarn architecture. A picture is presented at Figure 3.3

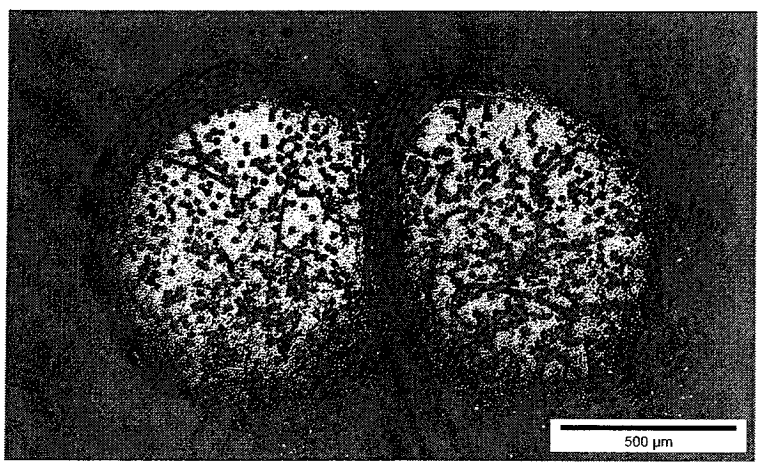

Figure 3.3, Cross-Section of a Commingled Yarn

In this figure, the two big circular areas contain a multitude of grey and white dots in the 6K commingled tows. The white small dots are the carbon fibers. Their highly crystalline structure reflects the light projected by the microscope. The grey dots are the nylon fibers. In each of the 6K commingled tows, the distribution of the grey dots is not even, confirming the heterogeneity of the commingling. Also, by the circularity of the dots, the different orientations of the fibers may be estimated. As presented in Figure 3.4, where a map of the different regions of the commingled yarn is shown, three distinctive nylon bundles are observed in the yarn cross-section. They act as wrappings: two on each 6K commingled tow, preventing the un-commingling, and one that wraps everything, keeping the 12K yarn integrity.

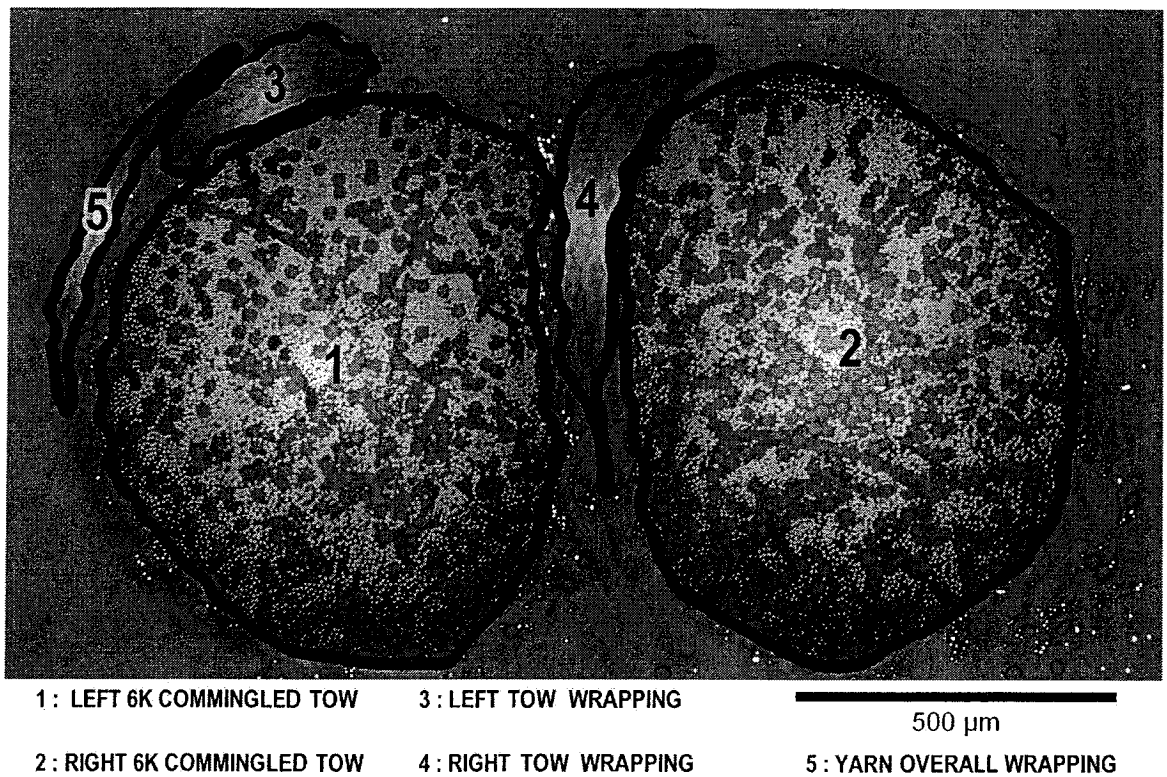

Figure 3.4: Commingled Yarn Parts

3.3.1. Thickness and Width

Measurements on the 6 cross-sections observed using the microscope gave the outside dimensions of the yarn. As the yarn has a quasi-rectangular shape, 6 thicknesses and 6 widths have been measured on each micrograph. Results are given in Table 3.2.

Measurement	No of Measures	Dimension	95% Conf. Int.
-	-	µm	µm
Width	36	1768	± 33
Thickness	36	971	± 21

Table 3.2: Measured Dimensions on the Yarn Cross-Section

3.3.2. Fiber Mass Content

The dissolution experiment (Section 6.4) gave an average fiber mass content of W_f = 65.3%. Using the density values of the nylon and the carbon, the corresponding fiber volume content of the fiber is V_f = 51.6%. This number is slightly less than what is reported by the manufacturer (53%).

3.3.3. Linear Weight

Linear weight of the yarn, determined by 5 measurements, is presented in Table 3.3 first as a linear density in g/m but also in the different units for yarn weight used in industry. The metric count is the length of the yarn in kilometers that weigh 1 Kg. Denier is the weight in grams of 9000 m of yarn. Finally, Tex is the weight in grams of 1000 meters of yarn.

Measurment	Metric Count	Denier	Tex
g/m	-	-	-
1.103 ± 0.025	0.91 wt	9929 - denier	Tex 1103

Table 3.3: Commingled yarn Linear Weight

The linear weight of the yarn found in this study is 8.7% more than what is mentioned by the manufacturer.

3.4. Conclusion

The Carbon/Nylon commingled yarn used in this study is compliant to the manufacturer specifications and other studies. The values obtained in this chapter will help to predict the braid properties, and the final properties of the braided laminate.

Chapter 4

BRAIDING

4.1. Introduction

Braiding is a preforming process that manufactures braided fabrics in flat or tubular form by intertwining three or more yarn systems together [1]. The properties of braids, such as high conformability, shear-resistant, and tolerance to impact damage are given by their bias interlacing structure. Braids can be produced as 2D structures in flat or tubular forms but they can also be produced in 3D structures having various shapes and yarn orientations.

2D braidings are produced with braiding machines similar to Figure 4.1. The machine has a track and horn gear system guiding the intertwining carriers, and a take-up mechanism to collect the formed braid. Triaxial braids are formed by adding a 0° yarn in between the bias yarns to enhance the reinforcement in the axial direction.

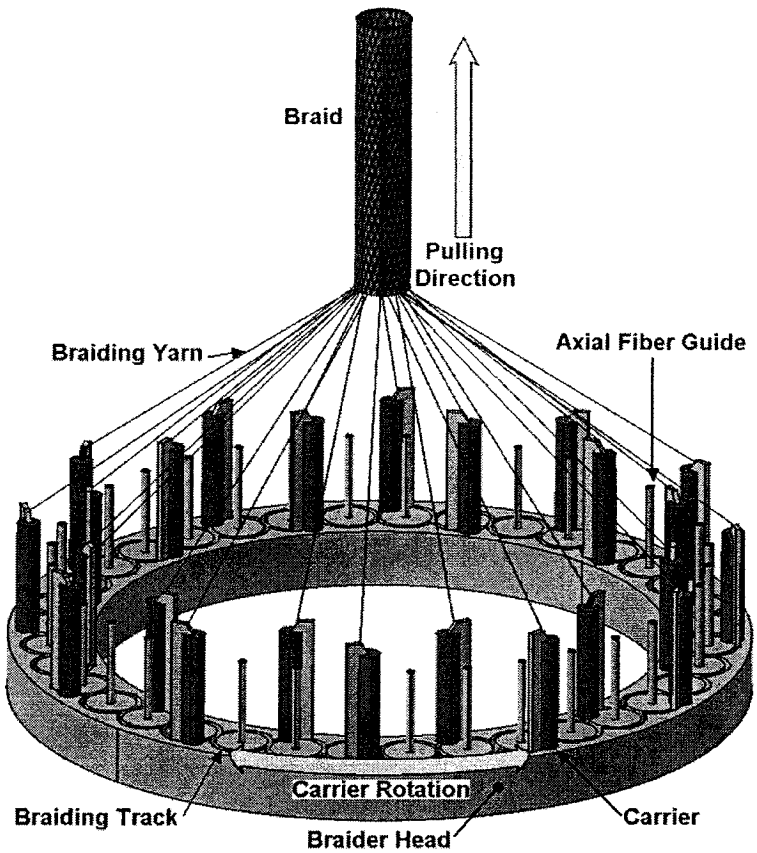

Figure 4.1: Braiding Machine Configuration.

The architecture of the braid is influenced by the configuration of the tow, the rotation speed of yarn carriers around the braiding track, the number of yarns carriers used in the braiding process, the pulling speed of the braid, and the shape and diameter of the braiding mandrel, i.e. the object onto which the braid is formed.

4.2. Theoretical Background

Through time, modelling of the structural geometry of the braid has been realized using various models. Ko and Pastore [24], introduced the mathematical relations between the braid properties such as the angle and the cover factor to the braiding conditions: the braider rotational speed, the mandrel axial speed, the mandrel diameter and the number of yarns in the

braid. Since then, research on braiding [25-27], refinements of the model introduced by Ko and Pastore, and automation of the process [25] have been done. Yan [28] modelled the braid structure by incorporating the intertwining path of the yarns, and used the yarn filament packing fraction along with the filament dimensions to predict the dimensions of the yarn, thus the configuration of the braid. Works have also been done to predict braid configuration when using braiding mandrels of various shapes [29-31].

Here will be introduced, using the various models, the mathematical relations linking the different braid properties together and also the braiding conditions to the final braid properties.

4.2.1. Braid Angle

Braid angle is function of the braider rotational speed and the capstan advancement speed. As shown in Figure 4.2, this angle can be determined as the inverse tangent of the circumference on the pitch distance ratio (Equation 4.1, D is the diameter of the mandrel, and p is the pitch distance).

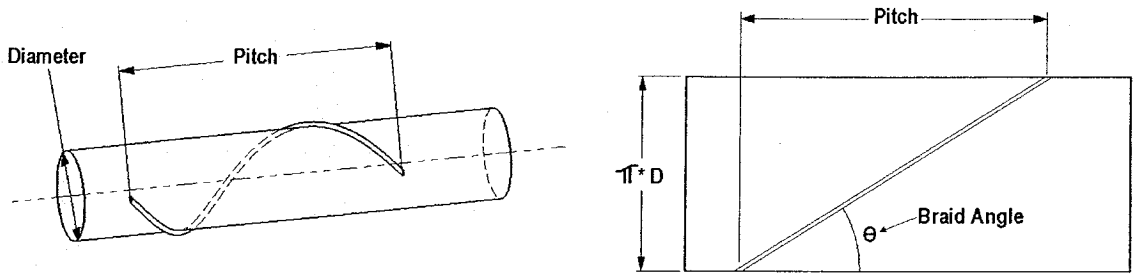

Figure 4.2: Pitch Distance and Braid Angle.

$$\tan\theta = \frac{\pi D}{p} \tag{4.1}$$

The pitch is the axial distance from a point on the mandrel where a braided fiber is passing until the same fiber passes, after one rotation around the mandrel, on the axial line of the first point on the mandrel (Figure 4.2). In steady state, the pitch distance is found using the mandrel linear speed v [m/sec] and number of revolutions per seconds ω [sec^{-1}] accomplished by a carrier on the braider head (Equation 4.2).

$$p = \frac{v}{\omega} \tag{4.2}$$

Using the pitch distance and the circumference of the braid, a typical braid rectangle [32] can be constructed. This rectangle is defined by cutting the tubular braid along the axial direction and then making two perpendicular cuts at the intersection of one bias yarn at each edge (Figure 4.3).

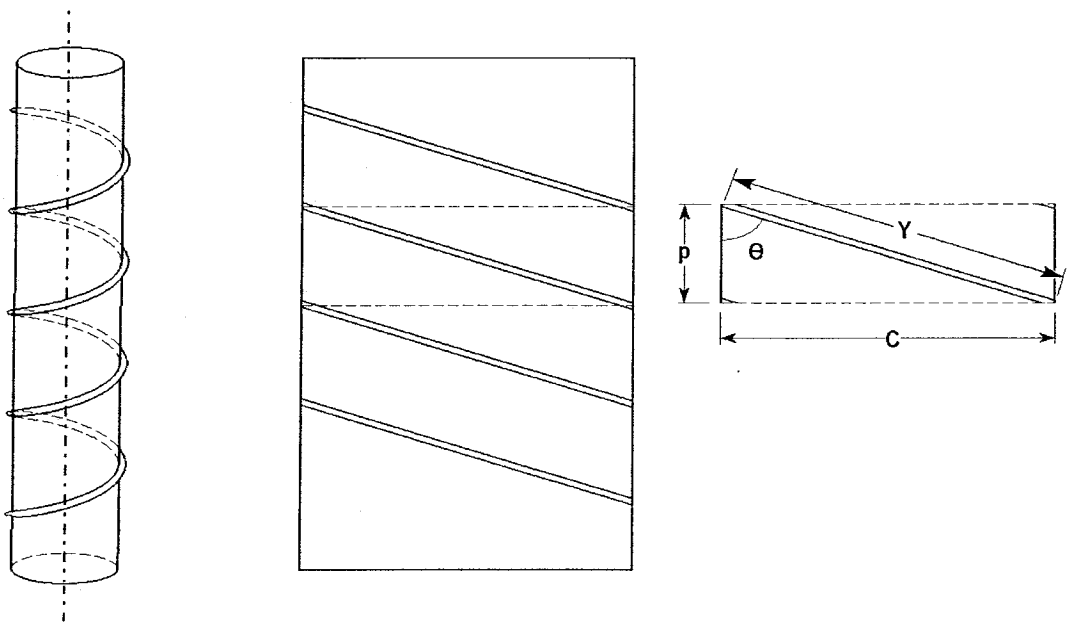

Figure 4.3: Typical Braid Rectangle

This rectangle leads to important deductions on a certain manufactured braid properties concerning the braid angle. First, the yarn length Y, consisting of the diagonal of the rectangle, is constant assuming that the braided material is not elastic. It can be determined using the braid circumference C and the braid angle (Equation 4.3).

$$Y = \frac{C}{\sin\theta} \tag{4.3}$$

Then, even if the braid is tensioned or compressed along the axial direction, the yarn length Y does not change. This leads to a relation between the braid angle and the circumference C, which can be determined for two stretching conditions of the same braid. (Equation 4.4)

$$\frac{C_1}{\sin\theta_1} = \frac{C_2}{\sin\theta_2} \tag{4.4}$$

4.2.2. Aerial Weight

In the rectangle pC of figure 4.3, it can be considered that each contained-in yarn is of length Y by grouping the yarn ends that are cut by the edges of the rectangle. This approach is explained in figure 4.4 for a small portion of the rectangle.

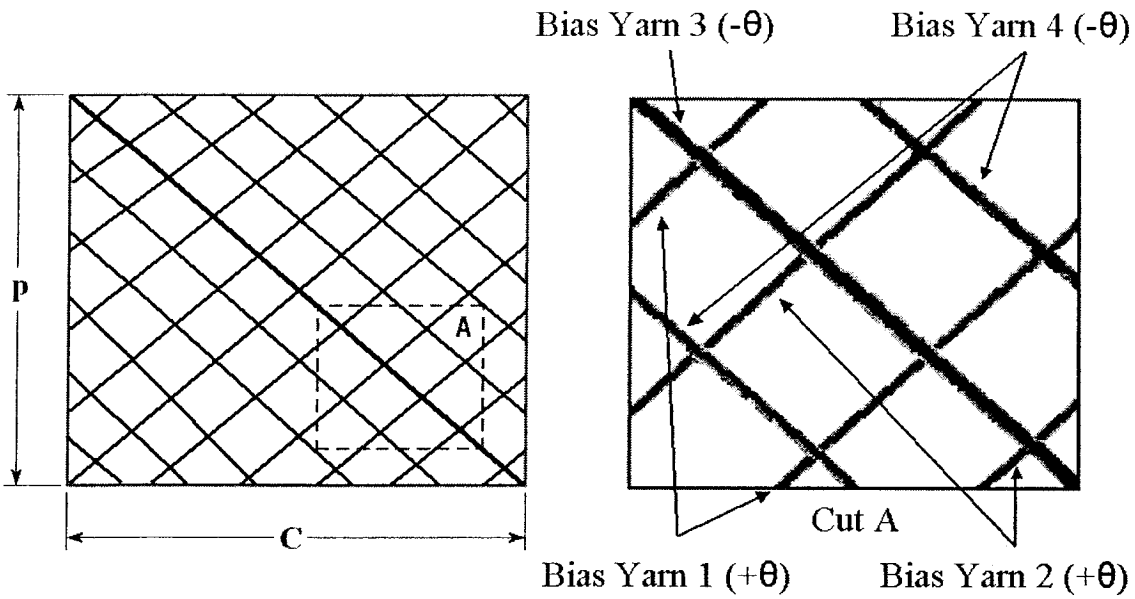

Figure 4.4: Yarn Length in Typical Braid Rectangle

Also, if the braid is realised with N carriers, N yarns will cross the rectangle pC of Figure 4.3. Furthermore, half of the N yarns (N/2) are oriented in one direction (+θ) and the other half (N/2) is in the other direction (-θ). Then, as seen in the enlarged view (Cut A) of Figure 4.4, because each bias yarn oriented in one direction crosses twice each of the yarns in the other direction, the number of yarns crossovers n_D contained in the rectangle pC will be calculated by (Equation 4.5):

$$n_D = 2 \cdot \frac{N}{2} \cdot \frac{N}{2} = \frac{N^2}{2} \tag{4.5}$$

This relation is used later in this text. Moreover, because N yarns crosses the rectangle pC, the sum of all lengths of the yarns contained in a typical braid rectangle is the length Y multiplied by N carriers. Using this length, the linear weight of a fiber ϱ_L and the area of the rectangle pC leads to the expression of the aerial weight of a braid (Equation 4.6).

$$W_B = \frac{\rho_L \cdot N \cdot Y}{p \cdot C} \tag{4.6}$$

Therefore, it is possible to express equation 4.6 in terms of the braid angle, the number of carriers, the braid diameter and the fiber linear weight, using equation 4.1 and 4.3:

$$W_B = \frac{\rho_L \cdot N}{\pi D \cos\theta} \tag{4.7}$$

Finally, for design purposes, using equation 4.1, 4.1 and 4.3, the aerial weight may be expressed in terms of the number of carriers, the machine speed ratio ω/v, the mandrel diameter, and the linear weight of the yarn ϱ_L. Note that the machine speed ratio is the inverse of the pitch distance presented in Equation 4.2

$$W_B = \rho_L N \sqrt{\frac{1}{(\pi D)^2} + \left(\frac{\omega}{v}\right)^2} \tag{4.8}$$

4.2.3. Unit Cell

In the literature, different unit cells are identified. They are determined by extracting a small repeating unit in the braid. They all lead to the same mathematical relations. Here will be employed the rhombus shaped unit cell, presented in figure 4.5

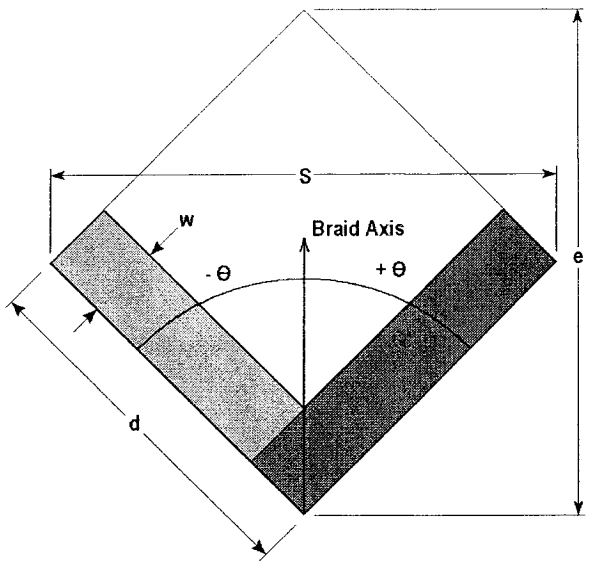

Figure 4.5: Unit Cell Geometry

Equation 4.9 calculates its width S. It is obtained by dividing the circumference of the braid by the number of carriers rotating on the same side, i.e. the total number of carriers divided by two.

$$S = \frac{2\pi D}{N} \tag{4.9}$$

The length e of the unit cell may be expressed as a function of the braid angle and the yarn spacing as in Equation 4.10:

$$e = \frac{S}{\tan\theta} = \frac{2\pi D}{N\tan\theta} \tag{4.10}$$

From Equation 4.1, the unit cell length e can be expressed by:

$$e = 2\frac{p}{N} \tag{4.11}$$

The distance d is the distance between parallel yarns in the braid, which is calculated by Equation 4.12.

$$d = \frac{e}{2\cos\theta} = \frac{\pi D}{N\sin\theta} \tag{4.12}$$

4.2.4. Cover Factor

Unit Cell Approach

The cover factor is the ratio of the area covered by the fibers on the total mandrel area. It is developed using the unit cell of previous section. First, the area of the unit cell A_T, is given by Equation 4.13.

$$A_T = \frac{S \cdot e}{2} = \frac{2 \cdot (\pi D)^2}{N^2 \tan\theta} \tag{4.13}$$

The fibers are covering the unit cell on twice the side length d of the cell, but there is an overlapping diamond at the bottom of the cell that needs to be subtracted. Thus, the area covered by fibers is:

$$A_C = 2dw - A_D \tag{4.14}$$

Where w is the width of the fiber. The configuration of the diamond is shown in figure 4.6

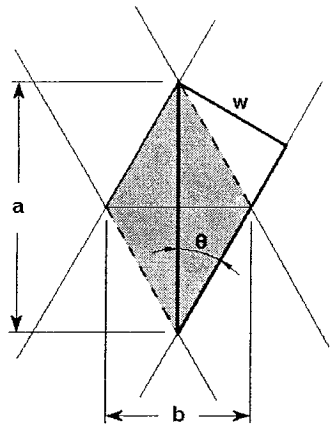

Figure 4.6: Overlapping Diamond Configuration

The dimensions a and b of this diamond may be expressed by:

$$a = \frac{w}{\sin\theta} \tag{4.15}$$

$$b = a\tan\theta = \frac{w}{\cos\theta} \tag{4.16}$$

The area A_D of the diamond is:

$$A_D = \frac{1}{2}ab = \frac{w^2}{2\sin\theta\cos\theta} \tag{4.17}$$

From equations 4.12, 4.14, and 4.17, the covered area becomes:

$$A_C = \frac{2\pi Dw}{N\sin\theta} - \frac{w^2}{2\sin\theta\cos\theta} \tag{4.18}$$

The cover factor can be calculated by equation 4.19, in terms of the mandrel diameter D, the total number of carriers N, the braid angle theta and the fiber width[30].

$$C_f = \frac{A_C}{A_T} = \frac{4N\pi Dw\cos\theta - N^2w^2}{4\pi^2 D^2\cos^2\theta} \tag{4.19}$$

Typical Rectangle Approach

The cover factor may also be obtained by using the typical rectangle pC of Figure 4.3. First, the covered area is expressed by the total length of fibers minus the area occupied by all the yarn crossovers, i.e. the diamonds.

$$A_C = NYw - n_D A_D \tag{4.20}$$

The cover factor will be expressed by:

$$C_f = \frac{A_c}{p\cdot\pi D} \tag{4.21}$$

Substituting equations 4.1, 4.3, 4.5, and 4.17 in equation 4.21 will lead to the same cover factor expression as in equation 4.19. This confirms that the two approaches lead to the same results.

4.2.5. Lock Angle

The lock angle is the angle for full cover. It can be found setting C_f=1 in equation 4.19. Equation 4.22 expresses lock angle as a projection of the width of half of the yarns in the braid (Nw/2) on the mandrel circumference.

$$\cos\theta_F = \frac{Nw}{2\pi D} \tag{4.22}$$

4.3. Braiding Machine

The braiding equipment at Concordia University has been bought and installed in 1998. A homemade capstan apparatus has been manufactured and installed to support a moving mandrel at the centre of the braiding ring. A photograph of the braider is shown in figure 4.7

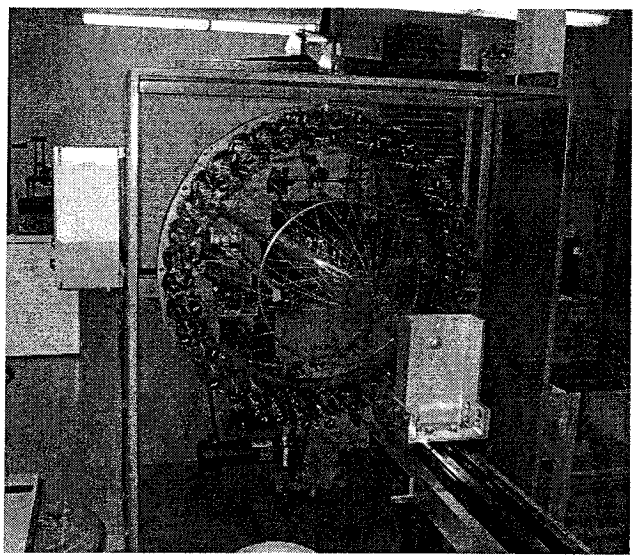

Figure 4.7: Braiding Machine at Concordia Centre for Composites

4.3.1. Machine-Braiding head

The braiding head has 108 carriers, 72 rotating in the circular braiding track ring and 36 installed behind the braiding ring, providing axial (0°) fiber placement interlocked by the bias yarns. Half (36) of the rotating carriers are rotating clockwise, and the other half is rotating the counter-clockwise in an intertwining motion. Rotation is controlled by an electronic speed

controller regulating both the rotation speed and the capstan linear speed in a closed circuit. The machine is fixed, vertical, and has a circular ring shape.

4.3.2. Machine-Capstan

The capstan, having 1 degree of freedom, insures the horizontal displacement of the mandrel through the braider head. Its heavy-duty construction allows the use of heavy braiding mandrels. The maximum displacement length is 12 feet (3.66 m). The displacement is driven by a 1/15 HP electric motor linked to a gearbox having a 133/1 ratio, regulated by the speed controller.

4.3.3. Braiding Mandrels

Two mandrels are used in this study. The first is a 2-3/8 inches (60 mm) diameter mandrel, having a 14-feet (4.28 m) length, already manufactured and available in the braiding lab. The other is designed to produce a braid preform having a circumference of 12.56 inches (319 mm). This circumference is the perimeter of a squared section molding mandrel of 3-3/16 inches (81 mm) sides having rounded corners of 3/16 inches (5 mm) radius. This molding mandrel was used for the manufacturing of a wingbox structure using thermoplastic commingled yarn. The braiding mandrel outside diameter is 4 inches (102 mm) to obtain the desired circumference of 12.56 inches (319 mm). The length is 10-feet (3.04 m). Two end-caps are fitted to an aluminium tube of 4 inches (102 mm) outside diameter to form the mandrel. The end-caps have centred and threaded holes to attach the mandrel to the capstan. Drawings of the mandrel are included in Appendix A.

4.3.4. Control

The braiding machine is driven by an electronic drive that regulates the speed as a function of two numbers entered into the controller. The first number is for the braider rotation speed, called braider set speed, and the second is for the capstan speed, called capstan set speed.

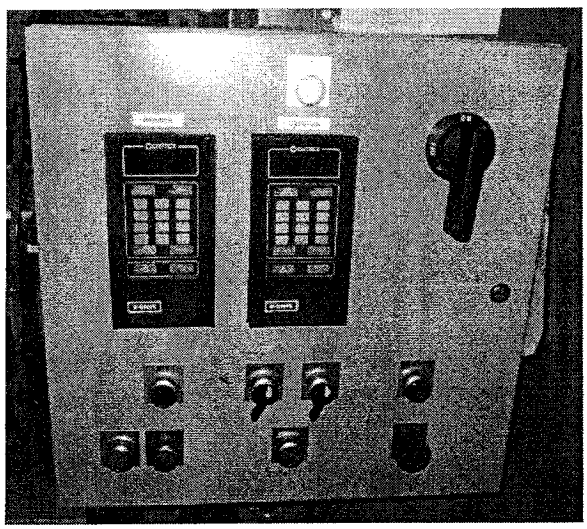

Figure 4.8: Braiding Machine Controller

4.3.5. Security

Braider operation has some security and safety issues. First, in case of jam or injury, the machine can be turned off using the two kill-switches situated on both sides of the braider outside box. Also, the preforming operation induces a lot of yarn-to-yarn friction. This friction emits a lot of carbon microscopic dust from the carbon fiber yarns that can be harmful to skin, eyes and respiratory system. To protect the operator, a proper coverall suit, a dust mask with proper filters, goggles and gloves need to be worn.

4.4. Braiding Machine Calibration

The rotation speed and the mandrel linear speed determine the angle of the manufactured braid. The real speeds of both the capstan and braider are functions of the numbers entered in the controller. For calibration purposes, an experiment is done to find the relation between the entered numbers and the real speeds of the equipment. Speeds are measured with a chronometer to find the time for one rotation for braider speed and the time for a certain length for the capstan speed. Table 4.1 shows the measurements realized for the 9 possible combinations between three different braider set speeds (25, 30, 35) and three different capstan set speeds (0.75, 1.5, 2.25). Results for the set speed pair 2.25 and 25 are not available because the experiment could not be performed.

Braider Head and Capstan Measured Speeds for different Set Speeds				
Set Speeds / Braider Head		25	30	35
Capstan		Measured Speeds		
0.75	Braider [RPM]	1.41	1.7	1.97
	Capstan [m/s]	0.0025	0.0029	0.0034
1.5	Braider [RPM]	1.41	1.69	1.97
	Capstan [m/s]	0.0049	0.0059	0.0068
2.25	Braider [RPM]	n/a	1.7	1.97
	Capstan [m/s]	n/a	0.0087	0.0103

Table 4.1: Speed Measurement Results

Results of those speed measurements at different settings showed the linear dependency of the speeds upon the set speed numbers entered in the controller (Figures 4.9 and 4.10).

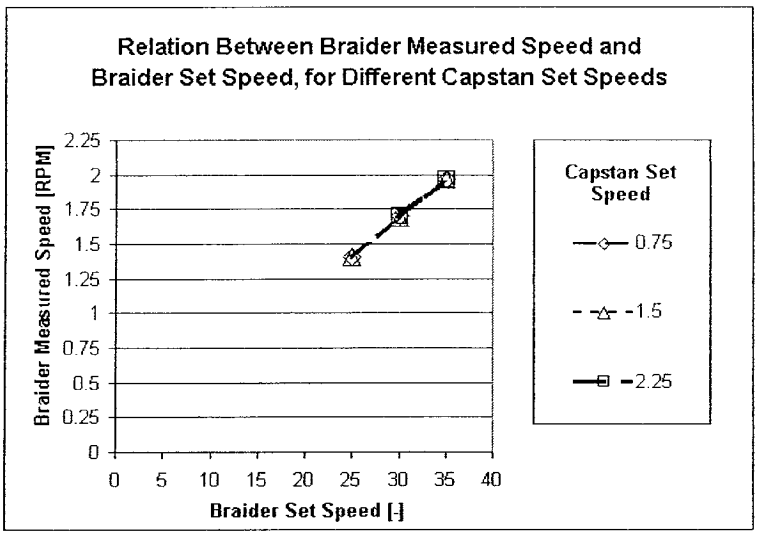

Figure 4.9: Braider Head Set Speed Versus Measured Speed Relations

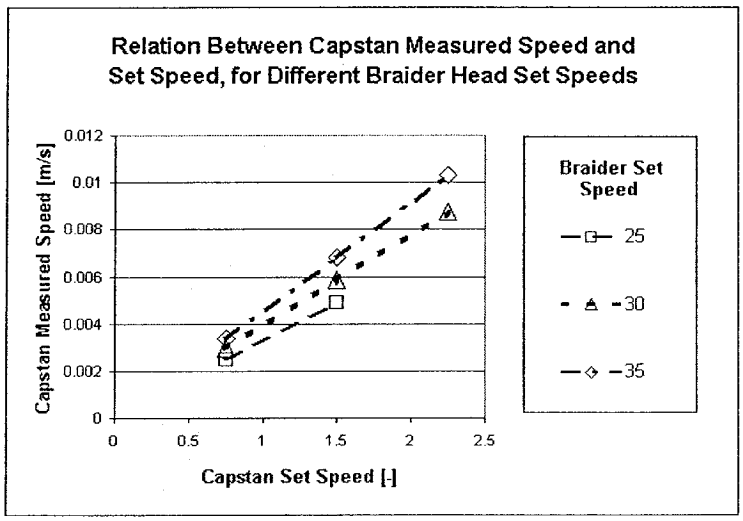

Figure 4.10: Capstan Set Speed Versus Measured Speed Relations

Moreover, it is seen from Figure 4.9 that the braider head rotation speed is completely independent of the capstan set speed. But there is a dependency of the capstan measured-vs-set speed slope upon the entered braider head set speed, as shown in Figure 4.10. As every curve is linear on the examination area, slopes are extracted from the data giving one number for the braider head speed dependency upon the braider head set speed in the controller, and 3

numbers for the capstan linear speed dependency upon capstan set speed. The slopes are presented in Table 4.2

Machine	Conditions	Symbol	Slope	Unit
Braider	All Conditions	m_B	0.0564	RPM
Capstan	Braider @ 25	m_{C25}	0.0033	m/s
	Braider @ 30	m_{C30}	0.0039	m/s
	Braider @ 35	m_{C35}	0.0046	m/s

Table 4.2: Braider Head and Capstan Speed Relations

Using a graph showing the relation between the slopes of the capstan set speed versus the measured speed (m_{C25}, m_{C30}, m_{C35}) and the braider set speed, the following conclusion is extracted: the influence of the braider set speed upon the capstan measured-vs-set speed slope is linear. Figure 4.11 show this linear relation and the slope is extracted.

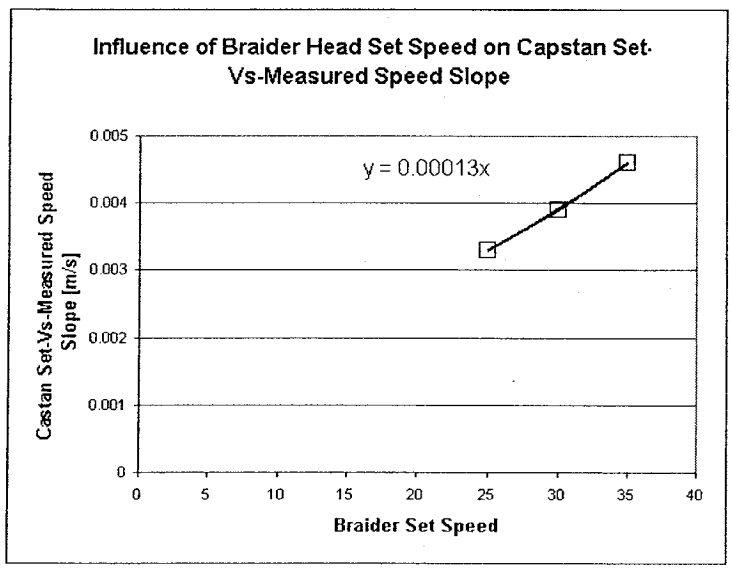

Figure 4.11: Capstan Set-Vs-Measured Slope Dependency upon Braider Set Speed.

Predicting the braider head true rotation speed ω, in RPM, is done using equation 4.23, the braider head set speed B_S, and the braider head true-vs-set speed slope m_B = 0.0564 RPM.

The same principle is applied in equation 4.24 for the capstan true-vs-set speed, where v stands for the capstan true speed [m/s], C_S for capstan set speed, and m_C for the capstan true-vs-set speed slope.

$$\varpi = m_B \cdot B_S \tag{4.23}$$

$$v = m_C \cdot C_S \tag{4.24}$$

Predicting the capstan true-vs-set speed slope can be done using equation 4.25, where $m_{C/B}$ is the slope of Figure 4.11. Then, the capstan true speed v can be expressed, as seen in equation 4.26, in function of the braider head set speed B_S and the capstan set speed C_S.

$$m_C = m_{C/B} \cdot B_S \tag{4.25}$$

$$v = \lfloor m_{C/B} \cdot B_S \rfloor \cdot C_S \tag{4.26}$$

Using equation 4.23 and 4.26, and the values of Table 4.3, the true speeds of the braider head and capstan can be determined.

Type	Symbol	Value	Unit
Braider	m_B	0.0564	RPM
Capstan/Braider	$m_{C/B}$	0.00013	m/s

Table 4.3: Final Slope Values For True Speed Calculations

Finally, it can be useful to express the machine setting in terms of a ratio of the braider rotational speed and the capstan linear speed as established in equation 4.27.

$$\varpi/_{v} = \left[\frac{m_B}{m_{C/B}}\right] \cdot C_S \tag{4.27}$$

Note that because m_B is expressed in RPM, the speed ratio ω/v is expressed here in RPM/m/s. In conclusion, it is seen from this equation that the braider head set speed does not have an effect on the speed ratio. Thus, only the capstan set speed will affect the braiding angle; the braider head set speed will change the rapidity of the process.

4.5. Braiding – Experimental

The aim of this experimental braiding investigation is to produce braids using different braiding conditions: braid diameter, speed settings, number of carriers mounted on the braider. The properties of the braids are measured to compare with mathematical relations presented in section 4.1. From the braids are extracted preforms for the continuation of the study, the consolidation and mechanical properties investigations are discussed in subsequent chapters.

4.5.1. Braid Diameters

The diameter of the braids will be considered to be the same as the mandrels diameters. Therefore, one set of braids will have a diameter of 4 inches (102 mm), and the other set will have a 2-3/8 inches (60 mm) diameter.

4.5.2. Speed Settings

To cover a range of angles, braider and capstan speeds have been selected quasi-randomly. Three different speed settings are found by observation and measurements on each mandrel to produce braid angles in the range of 30°, 45°, and 60°. The braider head and capstan set speeds were noted when the measured braid angle was in the ± 5° range of the

goal angle. Also, one experiment was conducted to approach the full cover angle and its settings on the 4 inch (102 mm) O.D. mandrel with 72 carriers. Calculated with formula 4.22, and using the yarn width found in table 3.2, this angle is 78.5°. All the speed settings are presented in Table 4.4.

No	Desired Angle	Number of Carriers	Mandrel Diameter	Mandrel Set Speed	Braider Head Set Speed	Braid Name
-	Deg	-	inch (mm)	-	-	-
1	± 30 ± 5	72	4 (102)	3.39	30	30B72
2	± 45 ± 5	72	4 (102)	1.95	30	45B72
3	± 60 ± 5	72	4 (102)	1.13	30	60B72
4	± 78.5 ± 5	72	4 (102)	0.7	35	78B72
5	± 30 ± 5	72	2-3/8 (60)	2	30	30S72
6	± 45 ± 5	68	2-3/8 (60)	1.16	30	45S68
7	± 60 ± 5	60	2-3/8 (60)	0.75	30	60S60

Table 4.4: Braiding Experimental Settings

The last entry in Table 4.4 is the name of the braid constructed from the braid parameters. First number identifies the target angle, and then a letter specifies the mandrel type, B for the 4-inch (102mm) O.D. mandrel and S for the 2-3/8 inch (60mm) mandrel. The final number is for the total amount of carriers mounted on the machine for the braiding operation.

4.5.3. Number of Carriers

The number of yarns in each braid was selected so no overlapping occurs between yarns in the final braided preform. When braiding at 45° (45S68) and 60° (60S60) on the small mandrel, it was necessary to reduce the numbers of mounted carriers to 68 and 60 respectively because of the high yarn content in the braid, giving yarn-overlapping situations. But all the other braids were done using the full capacity of the machine, 72 rotational yarn carriers.

4.5.4. Pitch Measurements

To determine the braiding angle, the pitch is measured directly on the mandrel after the braid is realised at each 5 inches (127 mm) in length. This distance helps to calculate the braid angle using equation 4.1. The resulting calculated value is the mean braid angle at the middle point of the measured pitch distance on the mandrel.

4.5.5. Mandrel Removing

Prior to removing the braid from the mandrel, a long 5 cm wide band of the braided fabric was fused along its length using an electrical soldering gun. Two other bands were done all around the mandrel at the beginning and at the end of the braid. This operation locally melted the nylon matrix and fixed the fibers with respect with other fibers when cooling down. It insured that the braid angle would not change during the subsequent preforming operations. At the end, the fused braid band was cut all around the mandrel at its beginning and its end. It was finally cut along its length at the middle of the fused band. At this point, the braid could be removed by unrolling it from the mandrel and placed on a flat table as a flat braided fabric.

4.5.6. Local Angle Measurement

Along the length of the preform, three local angles of the braid were measured on the lateral axis of the flat preform at 5 inches (127mm) intervals. The angle measurement tool is an angle finder in a transparent semi-disc form (Figure 4.12). The angle was taken between 2 yarns at an intersection in the braid. The local angle is then calculated as a mean of three measurements. It is then divided by two to get the angle with respect to the axis of the braid.

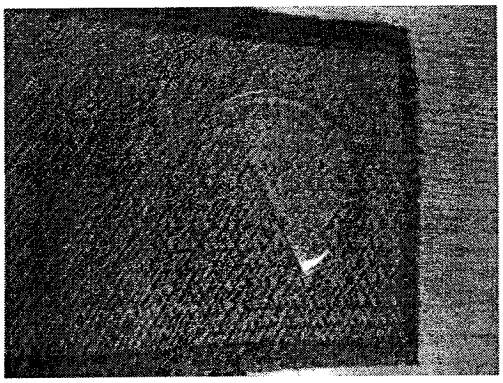

Figure 4.12: Angle Measurement on Braided Fabric

4.5.7. Preforming

Knowing the evolution of the angle along the length of the flat braid, square pieces were fused and cutout of the braid at specific positions where the angle is constant. The sides of those square pieces are parallel and perpendicular to the braid axis and their dimensions are selected to fit the molds (see Section 5.2.2). Three layers of same angle were stacked together to mold one plate.

4.5.8. Braided Fabric Measurements

Different pieces of information were extracted from the preform. First the longitudinal and lateral dimensions, the weight, and the local angle were measured and averaged out from each layer. These data lead to the calculation of the aerial weight and the local angle.

Thickness was taken for each individual layer, the thickness of a two-layer combination and a thickness of the three-layer preform stacking, giving 7 measurements in total. The measurement was performed using a vertical calliper (±0.01 mm) on a flat granite table. The braid was placed on the table with a 1 square inch parallel block on top at the measurement place. The measurement was taken when the tip of the calliper touches the parallel block. The thickness was calculated as the average of 8 local measurements on a layer or a stack of layers.

4.6. Results and Discussion

4.6.1. Braid Angle

Here will be presented the angle measurements when the braid angle attained its steady state, depending on the machine settings. Those are the angles from the braid where the preforms are cut out. Table 4.5 presents the results coming from the three different measurement methods, which are taken at different steps on the preforming process.

No	Braid Name	Mandrel Set Speed	Braider Set Speed	Pitch angle	Local Angle	Laminate angle
-	-	-	-	Deg	Deg	Deg
1	30B72	3.39	30	n/a	± 35.0 ± 0.5	n/a
2	45B72	1.95	30	± 49.3 ± 0.3	± 49.4 ± 0.2	n/a
3	60B72	1.13	30	± 63.6 ± 0.2	± 64.0 ± 0.3	n/a
4	78B72	0.7	35	± 72.7 ± 0.1	± 72.3 ± 0.3	± 72.8 ± 0.7
5	30S72	2	30	± 34.8 ± 0.4	± 35.4 ± 0.5	± 36.5 ± 0.5
6	45S68	1.16	30	± 49.9 ± 0.2	± 50.0 ± 0.5	± 49.6 ± 0.7
7	60S60	0.75	30	± 61.4 ± 0.4	± 60.3 ± 0.5	± 60.6 ± 0.3

Table 4.5: Braid Angle Measurements

Relation Between Measurements

As seen in Table 4.5, where all the angle measurements are presented, there is no significant variation of the angle between the measurement methods. This indicates first that all the measurements methods gave about the same results. Also, preforming operations such as removing the braid from the mandrel and cutting the open braid into laminates do not disturb the angle. For the rest of the study, the measured local angle will be considered as the braid angle.

Angle Prediction

Using equations 4.1 and 4.2, the braid angle can be calculated in terms of the braiding parameters: machine speed ratio ω/v [m^{-1}], and the mandrel diameter (equation 4.28). Results are presented in Table 4.6.

$$\theta = \tan^{-1}\left(\frac{\pi D\omega}{v}\right) \tag{4.28}$$

No	Braid Name	Mandrel Set Speed	Braider Set Speed	Mandrel Diameter	Speed Ratio	Predicted Angle	Local Angle
-	-	-	-	mm	1/m	Deg	Deg
1	30B72	3.39	30	102	2.1	± 34.4	± 35.0 ± 0.5
2	45B72	1.95	30	102	3.7	± 49.9	± 49.4 ± 0.2
3	60B72	1.13	30	102	6.4	± 64.0	± 64.0 ± 0.3
4	78B72	0.7	35	102	10.3	± 73.2	± 72.3 ± 0.3
5	30S72	2	30	60	3.6	± 34.3	± 35.4 ± 0.5
6	45S68	1.16	30	60	6.2	± 49.6	± 50.0 ± 0.5
7	60S60	0.75	30	60	9.6	± 61.2	± 60.3 ± 0.5

Table 4.6: Prediction of the Braiding Angle

A graph is presented in Figure 4.13, showing the measured values of the braid angle along with the calculated values.

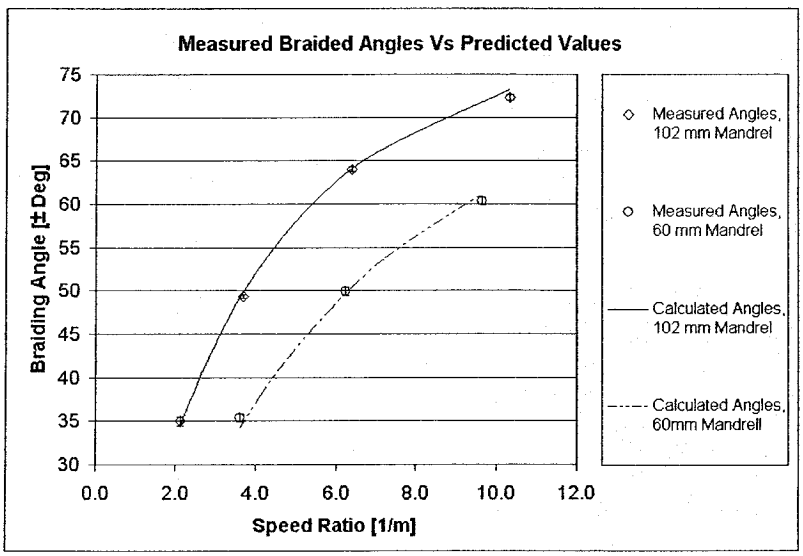

Figure 4.13: Comparison of Measured and Calculated Values of Braid Angle

It is seen that the measured and the calculated values are approximately the same. Not only this confirms the theoretical predictions but it also assesses the quality of the calibration curves extracted in section 4.3.

Lock Angle

From the 78B72, 45S68, and the 60S60 braids, it was impossible to decrease the mandrel speed to increase the braid angle or to add more carriers on the machine without having yarn-overlapping situations. As if the braid obtained were in lock angle situation, i.e. the angle at which the cover factor is 1. Those braids are presented in Table 4.7 along with their predicted lock angle calculated using equation 4.22 and the values in the Table. The width of the yarn used to calculate the lock angle is in Table 3.2

No	Braid Name	Number of Carriers	Mandrel Diameter	Predicted Lock Angle	Final Measured Lock Angle
-	-	-	inch (mm)	Deg	Deg
4	78B72	72	4 (102)	78.5	± 72.3 ± 0.3
6	45S68	68	2-3/8 (60)	71.4	± 50.0 ± 0.5
7	60S60	60	2-3/8 (60)	73.7	± 60.3 ± 0.5

Table 4.7: Braiding Lock Angle Situation

From the table, it is seen that the braid angles obtained at the limit of the yarn-overlapping situations are lower than the calculated lock angles. It is first due to low tension applied on the yarns by the carriers. The springs mounted on each carrier did not pull their yarns enough so they could take their place in the braid.

Moreover, the yarn width measurement performed in this study (section 3.3.1) may be inaccurate information to calculate the lock angle and the cover factor. The measurement was realized on individual tensioned yarn cross-sections. But the yarn cross section in the braid is deformed by the contact with the other interlocking fibers. Different studies incorporate yarn deformation models in the prediction of the lock angle [28,32], but no studies were found that are applicable to commingled fibers such as the one used here.

4.6.2. Aerial Weight Determination

The aerial weight of the braid was measured for all prepared preforms. Table 4.8 presents the measurements along with the number of carriers mounted on the braider, the diameter of the mandrel and the measured local angle.

No	Braid Name	Number of Carriers	Mandrel Diameter	Local Angle	Aerial Weight
-	-	-	inch (mm)		kg/m2
1	30B72	72	4 (102)	± 35.0 ± 0.5	0.299 ± 0.003
2	45B72	72	4 (102)	± 49.4 ± 0.2	0.393 ± 0.004
3	60B72	72	4 (102)	± 64.0 ± 0.3	0.581 ± 0.006
4	78B72	72	4 (102)	± 72.3 ± 0.3	0.901 ± 0.010
5	30S72	72	2-3/8 (60)	± 35.4 ± 0.5	0.521 ± 0.003
6	45S68	68	2-3/8 (60)	± 50.0 ± 0.5	0.634 ± 0.004
7	60S60	60	2-3/8 (60)	± 60.3 ± 0.5	0.748 ± 0.016

Table 4.8: Braid Aerial Weight

Using equation 4.8, the yarn linear weight calculated in section 3.3.3, and the braiding setting values, i.e. the speed ratio, the mandrel diameter and the number of carriers, the predicted areal weight can be calculated. Results are presented in Figure 4.14, where they are compared with the measured values.

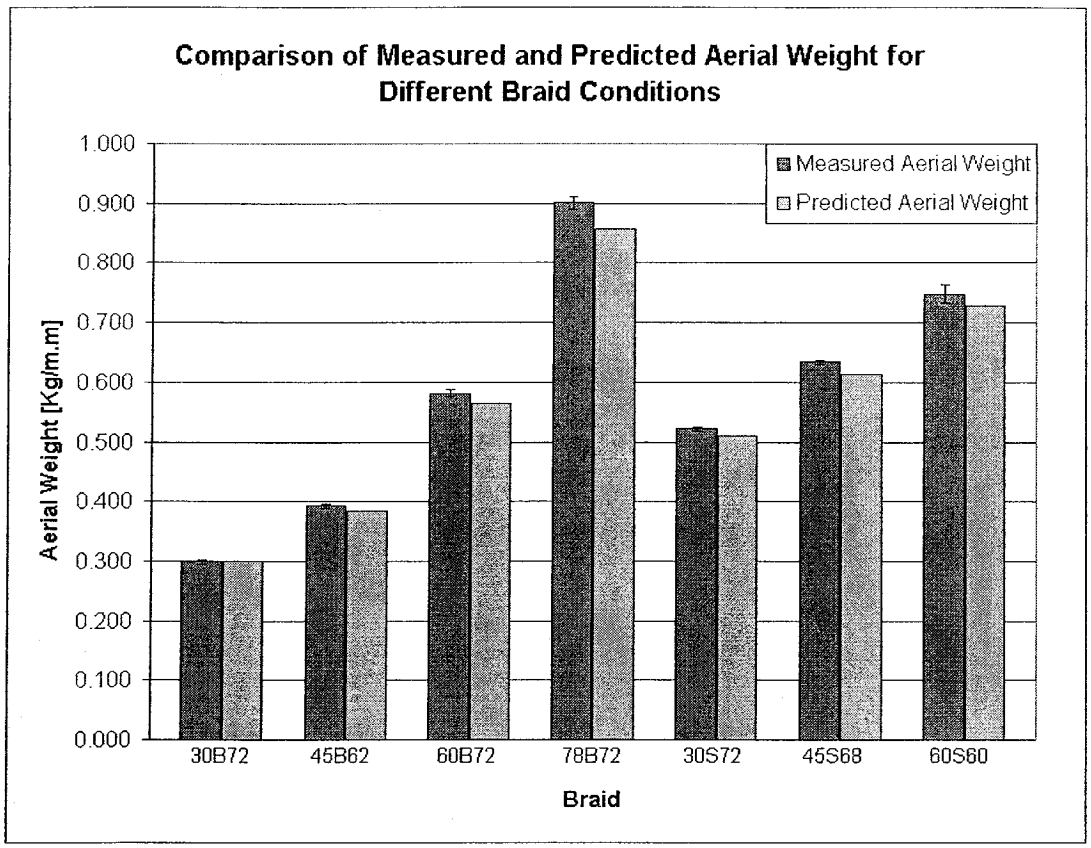

Figure 4.14: Comparison of Predicted and Measured Aerial Weight

The previous figure shows good accordance between measured values and theory. Table 4.9 present the calculated values in relation with the braid conditions and compared with the measured values.

No	Braid Name	Number of Carriers	Mandrel Diameter	Speed Ratio	Predicted Angle	Predicted Aerial Weight	Local Angle	Aerial Weight
-	-	-	mm	1/m	Deg	kg/m2	Deg	kg/m2
1	30B72	72	102	2.1	± 34.4	0.300	± 35.0 ± 0.5	0.299 ± 0.003
2	45B72	72	102	3.7	± 49.9	0.385	± 49.4 ± 0.2	0.393 ± 0.004
3	60B72	72	102	6.4	± 64.0	0.566	± 64.0 ± 0.3	0.581 ± 0.006
4	78B72	72	102	10.3	± 73.2	0.857	± 72.3 ± 0.3	0.901 ± 0.010
5	30S72	72	60	3.6	± 34.3	0.510	± 35.4 ± 0.5	0.521 ± 0.003
6	45S68	68	60	6.2	± 49.6	0.614	± 50.0 ± 0.5	0.634 ± 0.004
7	60S60	60	60	9.6	± 61.2	0.728	± 60.3 ± 0.5	0.748 ± 0.016

Table 4.9: Calculated And Measured Values for Different Braiding Conditions

4.6.3. Unconsolidated Thickness

All the thicknesses measured were averaged out in three numbers, the single layer thickness, the thickness of two layers stacked together, and the thickness of the 3-layers preform. Results are presented in Table 4.10, along with their corresponding braid information.

No	Braid Name	Measured Local Angle	Layer Thickness	2 Layers Preform Thickness	Global Preform (3 Layers)
-	-	Deg	mm	mm	mm
1	30B72	±35.0	1.83 ± 0.02	3.30 ± 0.06	4.88 ± 0.11
2	45B72	±49.4	1.88 ± 0.03	3.52 ± 0.05	5.06 ± 0.12
3	60B72	±64.0	2.09 ± 0.02	4.04 ± 0.03	6.01 ± 0.06
4	78B72	±72.3	2.23 ± 0.02	4.38 ± 0.03	6.58 ± 0.07
5	30S72	±35.4	2.15 ± 0.03	4.12 ± 0.05	6.17 ± 0.12
6	45S68	±50.0	2.25 ± 0.03	4.32 ± 0.04	6.37 ± 0.08
7	60S60	±60.3	2.58 ± 0.04	4.84 ± 0.07	7.21 ± 0.09

Table 4.10: Thickness Measurements on Un-Consolidated Braid

Confidence intervals of the single layer and 2-layer thicknesses are based on 24 measurements. For the global 3-layers preform thicknesses, it is based on 8 measurements, explaining the greater uncertainty on the preform thickness measurement.

One can be interested to see the effect of stacking on the thickness of a layer. Figure 4.15 shows the evolution of the thickness of layers taken individually, alone or in a stack of 2 or 3, for all the braids manufactured. The 2 latter data are obtained by dividing by 2, then 3 the two last columns of Table 4.10.

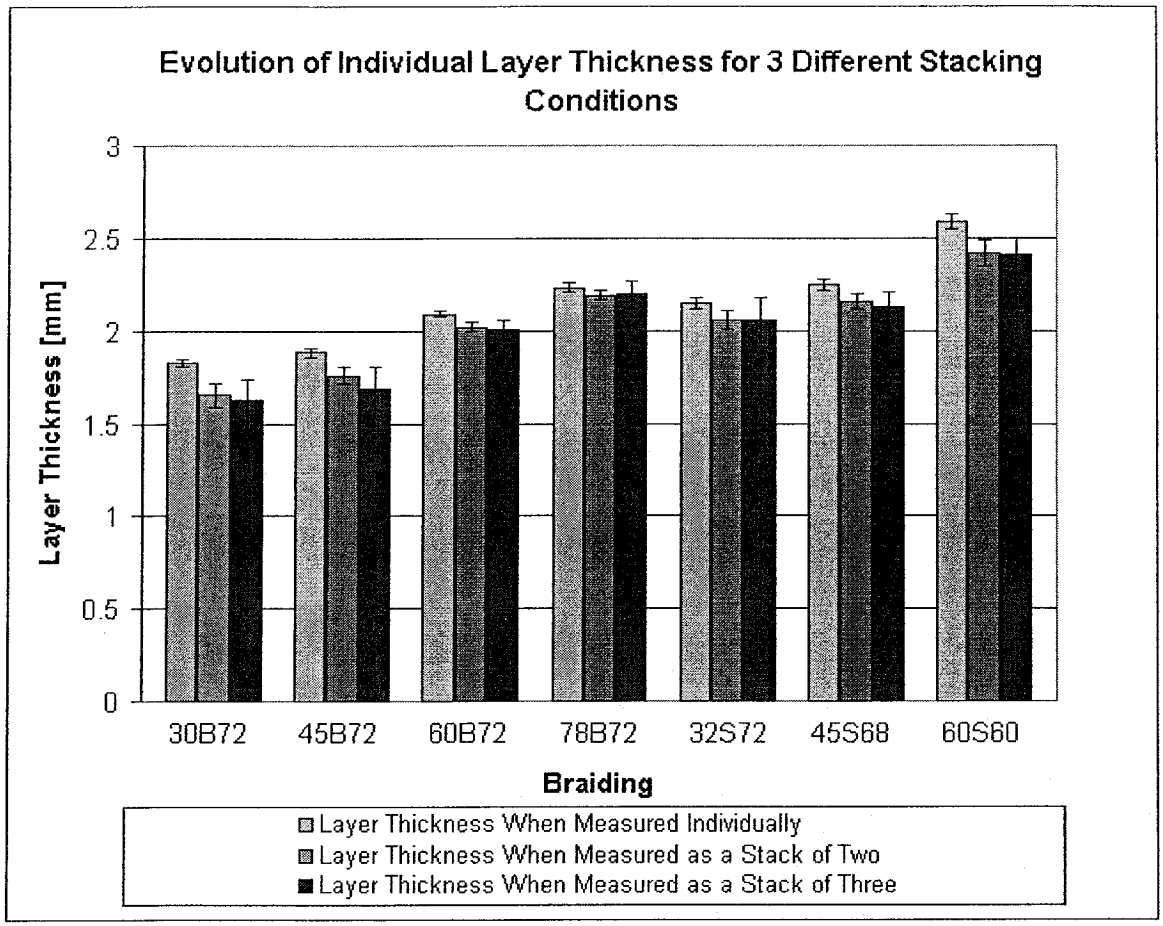

Figure 4.15: Layer Thickness Taken Individually or in Stack of 2 or 3 Layers.

It is seen from this graph that the thickness of each layer is reduced when taken in a stack compared to when they are measured individually. It is explained by the little intermingling between layers. The difference between when it is measured in a stack of 2 and 3 layers is generally little compared to the confidence interval of the measurement. Thus, the layer thickness in a stack will be considered as the global thickness of the 3-layers preform divided by three.

From a manufacturing point of view, especially with thermoplastic commingled yarns, the braid thickness will be of primary importance when designing complex molds. But, the

thickness of the braid cannot be found using the measured thickness of a yarn multiplied by two. Doing so, all the braids would have a thickness of 1.94 mm. The architecture of the yarn, the number of yarns mounted on the machine, the tension on each yarns during the braiding operation, the braid angle, and the mandrel diameter, are all factors that will influence the braid thickness. So, it is difficult to generalize braid thickness to any material and any machine.

4.7. Conclusion

This investigation used commingled yarns to manufacture 7 different braids. Angle, weight, and thickness measurements were taken to relate braid properties to theoretical predictions. The angle and the aerial weight prediction are reliable. Lock angle and Cover factor predictions are not accurate because they rely on fixed yarn architecture. But in reality, the commingled yarn cross-section configuration changes as it is incorporated into a braided preform.

Further studies could be realized to adapt available theories basing the braid property prediction on yarn architecture to the particular case of this carbon/nylon commingled yarn.

Chapter 5

MANUFACTURING

5.1. Background

The manufacturing process of thermoplastic composites can be divided into three major phases, melting, consolidation and cooling. First, the melting phase, depending on the tooling geometry and the power source, will bring the temperature of the molded material to the consolidation temperature above its melting point. Then, at the consolidation phase, pressure is applied for a certain time, called consolidation time, allowing the matrix to fully impregnate the fiber network. The final phase, solidification, depends on the tooling geometry and properties, affect final shape of the product, its internal stresses and the crystallinity of the matrix. De-molding is performed when the appropriate temperature, usually the glass transition temperature, is reached.

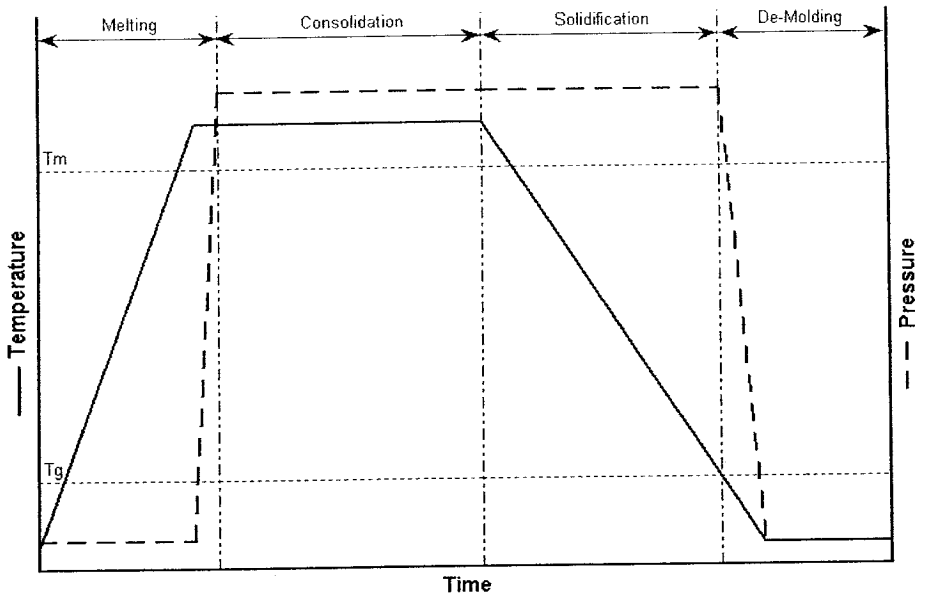

Figure 5.1: Typical Processing Cycle for Thermoplastic Composites

As stated in other studies [6, 12, 14, 21, 22, 33, 34], the consolidation process with thermoplastic composites coming from hybrid yarns precursors, such as powder-coated, commingled, and micro-braided yarn, generally starts with the coalescence of the melted resin in matrix pools between and around dry fiber bundles. This sub-stage of the consolidation is also called autohesion and generally takes a negligible time compared to the total consolidation time. The applied pressure is shared between the fiber network and the resin. The resin soon becomes a continuum where its pressure is acting on the dry fiber bundles. Then the impregnation process starts as a transverse flow towards the centre of each dry fiber bundles until closure of the voids. Simultaneously, a flow in the matrix rich regions, i.e. in between dry fiber bundles, can occur depending on the preform architecture. Those two flows are often referred to as micro- and macro-flows [35]. For the commingled yarn studied here, no macro-flow occurs along the tow length because the material distribution along the length of a fiber is

the same. Then the impregnation for the whole laminate can be represented by one single commingled yarn (see figure 5.2).

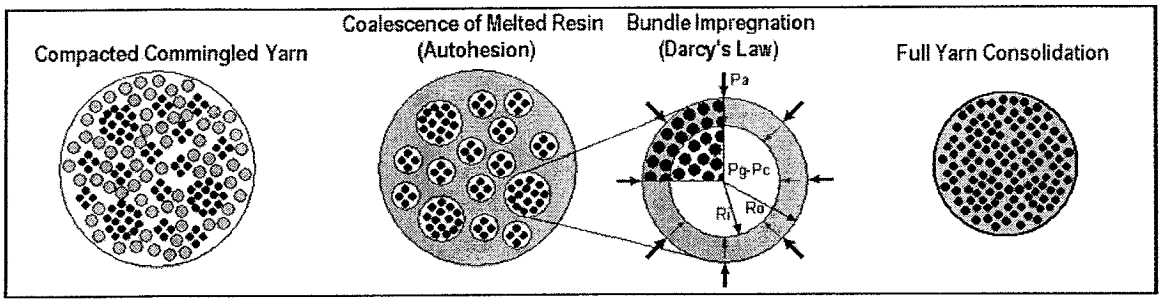

Figure 5.2: Impregnation Mechanism of Commingled Yarn [12]

With commingled yarns, because the commingling is heterogeneous, during consolidation, inside each commingled tow, the melted resin surrounds a population of cylindrical dry fiber bundles having different diameters. Bernet et al., for the development of an impregnation model for the same commingled material studied here, assumed that this population is constituted of 2 large bundles of 225 carbon fibers and 111 small bundles of 50-carbon fibers [22]. The impregnation of the whole laminate is then limited by the impregnation of the 2 large fiber bundles.

To obtain fully consolidated composites, 3 major parameters can be controlled: temperature, pressure and time. Schappes Techniques suggests a manufacturing window where temperature varies from 200°C to 250°C, pressure ranges from 7 to 50 bars (0.7 MPa to 5 MPa) and impregnation time goes up to 25 minutes. This window, presented in figure 5.3, relates the different parameters to obtain maximum properties and void free composites.

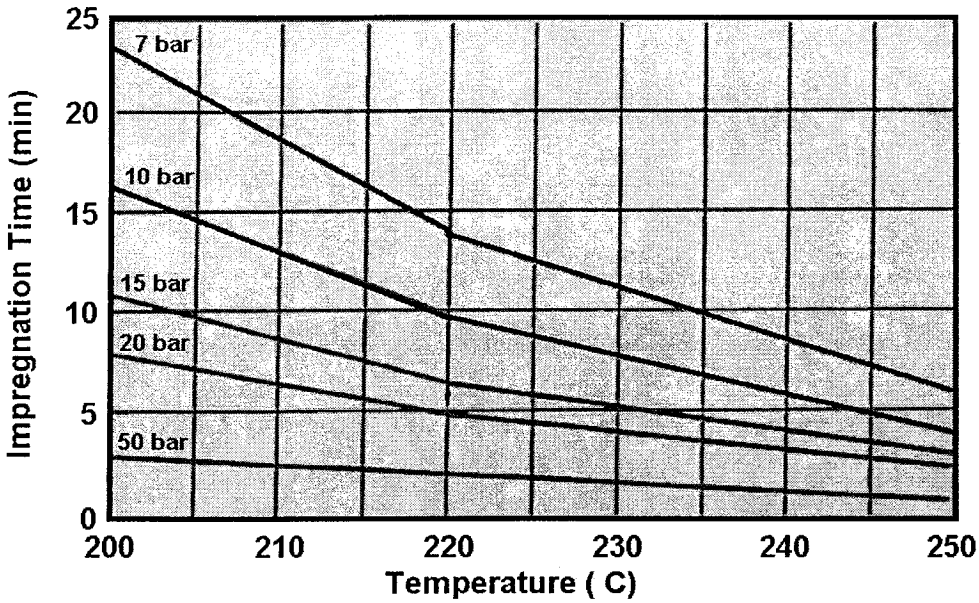

Figure 5.3: Process Windows for Schappes Techniques Carbon/PA12 Commingled Yarn

An internal report in Concordia University [36] showed that variation of ± 10% in pressure, impregnation time, and temperature produces no significant difference in tensile and flexural mechanical properties.

5.2. Plate Manufacturing

Manufacturing of plates from the braids is done in multiple operations where a couple of useful measures can be taken. This section describes the process of manufacturing of a plate from commingled fibers braids.

5.2.1. Preform Characteristics

The preforms are assembled using three layers of braided commingled fibers. The three layers come from the same braiding conditions. The braiding and preforming process was described in chapter 4. The preforms characteristics are summarized in Table 5.1.

No	Braid Name	Local Angle	Layer Thickness	Global Preform (3 Layers)	Aerial Weight
-	-		mm	mm	kg/m2
1	30B72	± 35.0 ± 0.5	1.63 ± 0.11	4.88 ± 0.11	0.299 ± 0.003
2	45B72	± 49.4 ± 0.2	1.69 ± 0.12	5.06 ± 0.12	0.393 ± 0.004
3	60B72	± 64.0 ± 0.3	2.00 ± 0.06	6.01 ± 0.06	0.581 ± 0.006
4	78B72	± 72.3 ± 0.3	2.19 ± 0.07	6.58 ± 0.07	0.901 ± 0.010
5	30S72	± 35.4 ± 0.5	2.06 ± 0.12	6.17 ± 0.12	0.521 ± 0.003
6	45S68	± 50.0 ± 0.5	2.12 ± 0.08	6.37 ± 0.08	0.634 ± 0.004
7	60S60	± 60.3 ± 0.5	2.40 ± 0.09	7.21 ± 0.09	0.748 ± 0.016

Table 5.1: Preform Characteristics.

5.2.2. Molds

Two molds are used in this study depending on the available circumference of the manufactured braids. The first one is a square picture frame mold having 10 inches (254 mm) side length. The other is a rectangular mold of 8 by 10 inches (203 x 254 mm). The molds are manufactured in aluminium. Figures 5.4 and 5.5 present isometric views of the molds. Both molds are designed for a vertical pressure on the braid without constraining the sides of the plate, allowing the resin to flow-out if necessary. The thickness of the top and bottom plates is 7/8-inch (22mm).

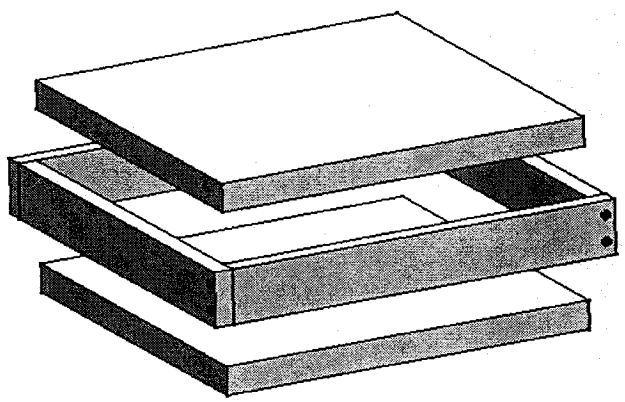

Figure 5.4: Isometric View of the 10-inch (254mm) Square Mold

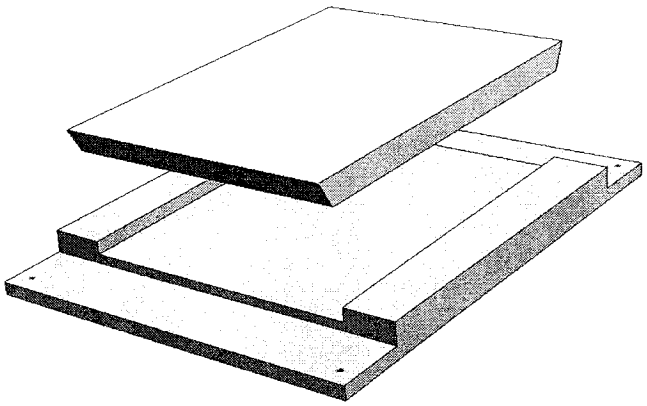

Figure 5.5: Isometric View of the 10 by 8-inches (254x203mm) Rectangular Mold

The molds are different in their configuration but are alike in the way they apply the pressure. The mold having an 8-inch (203 mm) wide cavity (Figure 5.5) was used to mold the preforms braided on the small mandrel (2-3/8 inches, 60 mm). Those preforms have a width of 7.5 inches.

5.2.3. Molding Cycle

For this study, a temperature of 220°C ± 5 °C, a pressure of 10 bars (1 MPa) for an impregnation time of 10 minutes was selected as manufacturing conditions in accordance with the processing window shown in Figure 5.3.

Molding is realized using a flat press with integrally heated and cooled platens. The manufacturer of the press is Wabash and the capacity is 30 tons. The press is first preheated at molding temperature. The preform is installed in the mold preconditioned with release agent. A thermocouple is placed in the middle layer to track temperature during molding with a data acquisition system. A kapton film is placed on each side of the preform for surface finish purpose. The mold is placed in the press and the pressure is applied when consolidation

temperature is reached at the middle layer. After consolidation time (10 min.) cooling is applied until de-molding temperature (30-40 °C).

5.2.4. Plate Measurements

Five local angle measurements are taken on each side of the plate using the method described in section 3.3.2. The final thickness is determined using the section measurements of the coupons used for mechanical testing (Chapter 7).

5.3. Consolidation Results

5.3.1. Consolidated Braid Angle

Table 5.2 presents the angle measured on the consolidated 3-layer braid preform (plate angle). It is seen that there is no significant angle change during consolidation. This result confirms that the angle does not change in all the manufacturing process from the braided mandrel until the final consolidated plate.

No	Braid Name	Measured Local Angle	Plate Angle After Consolidation
-	-	Deg	Deg
1	30B72	± 35.0 ± 0.5	± 35.0 ± 0.3
2	45B72	± 49.4 ± 0.2	± 49.3 ± 0.4
3	60B72	± 64.0 ± 0.3	± 63.7 ± 0.3
4	78B72	± 72.3 ± 0.3	± 72.0 ± 0.5
5	30S72	± 35.4 ± 0.5	± 36.6 ± 0.7
6	45S68	± 50.0 ± 0.5	± 50.9 ± 0.8
7	60S60	± 60.3 ± 0.5	± 61.0 ± 0.6

Table 5.2: Measured Angle and Thickness After Consolidation

5.3.2. Thickness, Cover Factor, and Compression Ratio

Consolidated 3-layer braided preform thicknesses (Plate Thickness) are presented in Table 5.3 along with corresponding predicted cover factor. The compression ratio (R_C) is

determined using the global preform thickness (t_P) over the consolidated plate thickness (t_C) (equation 5.1)

$$R_C = \frac{t_P}{t_C} \tag{5.1}$$

No	Braid Name	Local Angle	Cover Factor	Global Preform Thickness	Plate Thickness	Compression Ratio
-	-	Deg	-	mm	mm	mm
1	30B72	± 35.0 ± 0.5	0.423	4.88 ± 0.11	0.63 ± 0.004	771%
2	45B72	± 49.4 ± 0.2	0.522	5.06 ± 0.12	0.81 ± 0.005	622%
3	60B72	± 64.0 ± 0.3	0.701	6.01 ± 0.06	1.20 ± 0.005	503%
4	78B72	± 72.3 ± 0.3	0.902	6.58 ± 0.07	1.80 ± 0.015	366%
5	30S72	± 35.4 ± 0.5	0.650	6.17 ± 0.12	1.11 ± 0.011	558%
6	45S68	± 50.0 ± 0.5	0.742	6.37 ± 0.08	1.32 ± 0.008	482%
7	60S60	± 60.3 ± 0.5	0.827	7.21 ± 0.09	1.54 ± 0.010	469%

Table 5.3: Plate Thickness and Compression Ratio

Figure 5.6 shows a good correlation between cover factor and plate thickness. It is expected since the volume of fibers increases as the cover factor increases when the area on which the cover factor is calculated stays constant.

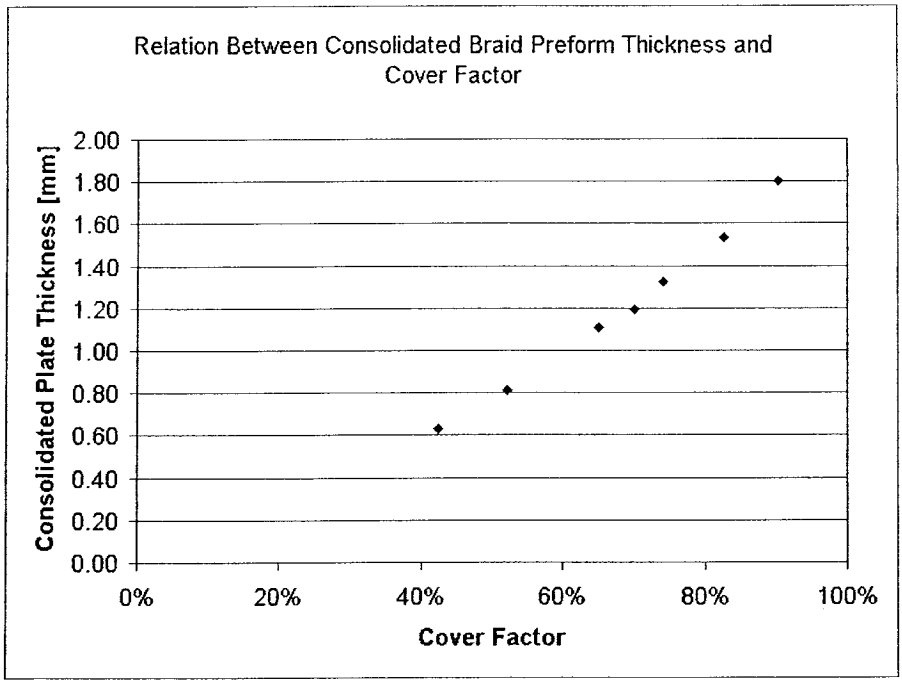

Figure 5.6: Plate Thickness as a Function of Cover Factor

To relate the two data together, it is first assumed that the unit cell area is (equation 4.13):

$$A_T = \frac{2\pi^2 D^2}{N^2 Tan\theta} \tag{5.2}$$

The volume of fibers in one cell is twice the inter fiber length d (equation 4.12), multiplied by the cross-section area of one consolidated yarn A_y.

$$V = 2dA_Y \tag{5.3}$$

The cross-section area of a consolidated yarn is function of the number of reinforcing filaments N_F in a yarn, the radius of one reinforcing filament and the fiber volume fraction:

$$A_Y = \frac{N_F \cdot \pi \cdot R_F^2}{V_f} \tag{5.4}$$

This leads to the equation of the consolidated laminate thickness, where N_L is the number of braided layers in the laminate:

$$t_C = \frac{N_L \cdot V}{A_T} = \frac{N_L \cdot N \cdot N_F \cdot R_F^2}{V_F D \cos\theta} \tag{5.5}$$

The prediction is shown in Figure 5.7 along with the cover factor predicted values. Each circle points are calculated using the parameters of the preforms in equation 5.5. The volume fraction V_F is set to 52%, the number of reinforcing filaments N_F is 12000, and the radius of a reinforcing filament R_F is 3.5 μm. The number of carriers N, the braid angle θ, and the mandrel diameter D are specific to each braid and are taken from Table 4.8.

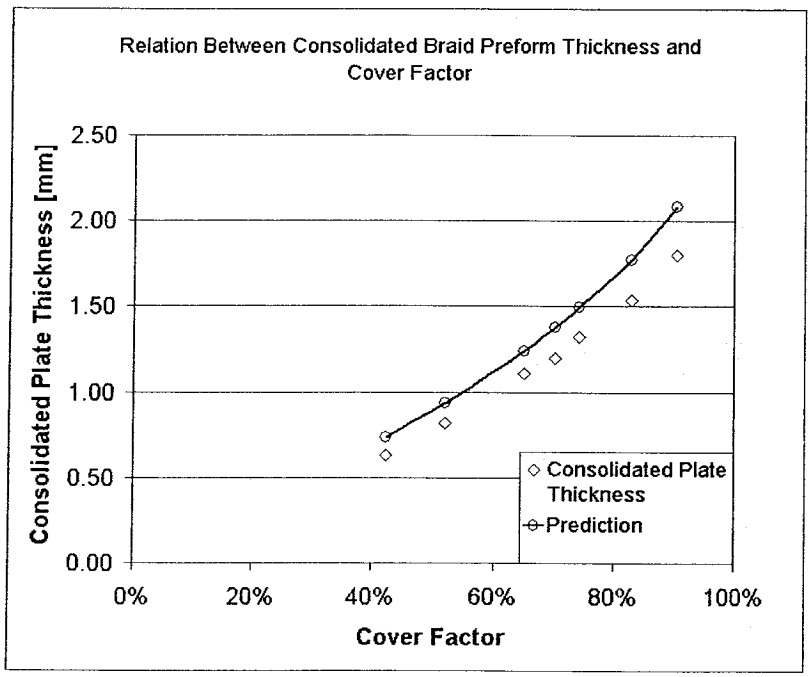

Figure 5.7: Prediction of Final Consolidated Laminate Thickness

An average difference of 15% is observed between the thickness measurements and the predicted values. This can be explained by the multiple sources of errors that can interfere with the predicted value, especially in the number of reinforcing fibers (N_F) and the fiber radius (R_F). This latter value is of greater importance because the error, even if is really small, is squared in equation 5.4. Furthermore, because of structure of the braid, the yarn area may not be parallel to the thickness direction of the consolidated plate. Equation 5.5 does not take in account the projected area of a consolidated yarn cross section by the angle induced by the intertwining of the yarns in the braid.

5.4. Conclusion

Manufacturing of plates from braided tubes does not disturb the braid angle. The final plate thickness can be related to the cover factor.

Chapter 6

CONSOLIDATION QUALITY

Evaluation of the consolidation quality gives a clear idea of the efficiency of the wetting stage of manufacturing, thus, it is also directly related to mechanical performance of the composite. There are different methods to state on the consolidation quality. Good examples of qualitative methods are visual aspect inspection, sound inspection when the product is tapped with a tap device, and microscopy. They inform on the presence or absence of defects, their distribution, their configuration, and their importance. Quantitative methods allow the evaluator, in quantifying the amount of constituents such as fibers, resin, voids and impurities, to compare mechanical result with theory and other works.

In this study, laminates are inspected using microscopy. Constituent content is determined using a chemical dissolution technique. This chapter will summarize the different methods for the evaluation of constituent and void content as reported in the literature. Methods to evaluate constituent content of consolidated laminates and to realize microscopy are described. Procedure will lead to the establishment of a protocol.

6.1. Background

The void content can be utilized to relate the mechanical performance and the process optimization. Ramasamy et al. [15] used an image analysis system linked to a microscope to measure the void content by means of thresholding. The magnification is 200 times and the void content determination takes 100 analyses per specimen. This method has one advantage;

it allows the evaluator to characterize the nature of the voids, i.e. their size, their location and maybe their cause

Also, void content determination is used to mathematically model the consolidation mechanisms. Bernet et al. [11, 12] in their investigation of consolidation of carbon/nylon commingled fabrics and Lin Ye et al.[13] in their investigation of the consolidation of carbon/PEEK commingled fibers, have both used the void content analysis to compare the results to mathematical properties predictions. Their void content is found using the following formula:

$$X_v = \frac{\rho_t - \rho_a}{\rho_t} \tag{6.1}$$

where ϱ_t is the theoretical density of the laminate and ϱ_a is the actual density of the manufactured laminate. This density is determined using ASTM-D792. The theoretical density can be calculated knowing the resin and fiber content of the laminate and using a rule of mixture. This rule can be expressed with the volume fraction (Eq. 6.2) or the weight fraction (Eq. 6.3).

$$\rho_t = V_f \rho_f + V_m \rho_m \tag{6.2}$$

$$\rho_t = \frac{\rho_f \rho_m}{W_f \rho_m + W_m \rho_f} \tag{6.3}$$

If there is no resin flow out of the mold during the consolidation, the resin and fiber content of the laminate should correspond to the resin and fiber content of the pre-impregnated fiber.

Weight or volume fraction can be obtained from the manufacturer of the material, but for accurate results, they can also be determined by experimentation. Ramasamy et al. have used a chemical dissolution procedure to determine the weight fraction of fibers and resin in the laminate. The process involves dissolution of a small sample of laminate of carbon fibers and Nylon 6 in a formic acid conical flask for two hours with a magnetic stirrer. Then, the fibers are filtered out, rinsed with formic acid, dried out at 100°C for 1 hour, and, finally, weighed. Moreover, the fibers were examined under SEM to see if there are traces of nylon on fibers. The resin residue can be precipitated by adding water to the solution of formic acid and nylon by filtering with a 15 μm filter funnel and dried at 100°C for 1 hour. This allows to back calculate by mass balance the fiber weight content in the laminate.

The densities of the materials involved have all been obtained by the manufacturer, but in the case of PEEK material, which is a semi-crystalline polymer, Ye Lin et al. have used the density of PEEK at the same crystallinity.

American Society for Testing Materials (ASTM) has developed a standardized test method for constituent content of composite materials (ASTM D3171-99). One approach of this method physically removes the matrix by digestion or ignition by seven different procedures. The first 6 procedures uses 6 different digestion media and the last procedure concerns ignition of the resin. But no particular medium is suggested for Nylon12. The standard also looks through all the possible causes of interferences such as errors in measurements of density of constituents, size of the coupon, mass change during digestion, and matrix retention.

Bayldon et al. [37] generally criticize destructive methods such as matrix digestion or ignition because they suffer from substantial inaccuracies. They address the difficulty of getting a pure void free resin sample for density determination. Furthermore, they point out that a great deal of care is required to separate the fibers from the matrix. Finally they mention that any volatile materials released and residual traces of matrix on the fibers can falsify the results.

On the other hand, Bayton et al. suggest an optical analysis method consisting in 4 major steps: sample preparation, image capture (and pre-processing), feature identification and separation, and finally feature measurement. They also emphasise on the fact that optical analysis not only gives a reading of the void content but can also give a lot of information on the void distribution and orientation.

6.2. Method Selection

Optical analysis can be considered as a good technique for constituent content determination, but some drawbacks have to be overcome. First the sample preparation step is crucial because the analysed surface has to be prepared with great precaution to avoid alteration. Then, the analysis images selection, so as the feature identification/separation step, is realized by the operator and can therefore falsify the results. Finally, to obtain precision, image analysis has to be done on a huge amount (~100 analyses per plate) of micrographs. The solution is to mechanically drive the experiment and to program analysis algorithms to reduce the operation time. But the development of such a set-up is expensive and needs a great deal of expertise.

Knowing this, in this work, micrographs are realized for qualitative needs only. The constituent content is determined using density measurements, chemical dissolution and proper calculation. This approach seems more adequate because of the availability of this technique in the lab, the accessibility of the expertise and because this method is widely used in the scientific community.

6.3. Micrography

6.3.1. Preparation Method

For visual inspection under microscope, two samples per manufactured plate are examined. One is cut along the plate axial direction to obtain a hoop view of the cross-section and the other is cut along the diameter direction of the plate to obtain an axial view of the braid cross-section. Thus, 14 samples are prepared for micrography.

The ¾ inch (19 mm) large coupons are molded in clear room-temperature-curing epoxy mounts of 1.25 inch (32 mm) in diameter and polished using an automatic surface preparation machine. The machine allows the preparation of 6 mounts at the same time placed in a sample holder. This holder is placed over a rotating disk where different grinding/polishing surfaces can be placed. A motorized head applies pressure onto the holder and action it in a rotating and oscillating movement, producing a sweeping movement of the grinded mounts onto the rotating disc. The method, developed for this particular material system in this study, is presented in Table 6.1.

Step	Repeat	Type	Disc Surface	Grit or Particule Size	Lubrification	Pressure for 6 Samples PSI (Pa)	Load/ specimen lbf (N)	Rotation Speed RPM	Time -
1	Until Flatness	Rough Grinding	SiC disc	320	Water	15 (103)	3 (13)	250	30 sec
2	X 2	Grinding	SiC disc	600	Water	10 (69)	3 (13)	250	30 sec
3	X 2	Fine Grinding	SiC disc	800	Water	15 (103)	3 (13)	250	45 sec
4	X 1	Rough Polishing	Victor	9 micron diamond suspension *	Water based diamond extendrer**	20 (138)	4 (18)	150	4 min
5	X 1	Polishing	Nylon Artic	3 micron diamond suspension *	Water based diamond extendrer**	25 (172)	5 (22)	150	4 min
6	X 1	Polishing	Nylon Artic	1 micron diamond suspension *	Water based diamond extendrer**	25 (172)	6 (27)	150	4 min
7	X 1	Fine Polishing	Imperial	0.05 micron SiC suspension ***	none	30 (207)	6 (27)	150	5 min

* : Add 5 drops of diamond suspention every 0:15 sec and 0:45 sec of the minute
** : Add 5 drops of lubricant every 0:00 sec and 0:30 sec of the minute
*** : Add SiC suspension every 20 sec.

Table 6.1, Microscopic Observation Surface Preparation Procedure

In the previous table, step one has to be repeated until all the samples installed on the machine rotating-disk are flat. It is observed when all the resin mounts containing the samples have the same grinded appearance. The commercial names of the polishing surfaces come from Anamet; the company information is available in Appendix B

The samples are observed using an optical microscope (Olympus, BX51M) and linked to a digital camera (Olympus, Qcolor5). A global picture of the sample is taken at 50X magnification and a representative section is taken at 200X magnification.

6.3.2. Observation Results

Microscopic observation showed the microstructure of the composite. All the micrographs are shown in Appendix C. Virtually no voids are observed in all the micrographs. Figure 6.1 shows a 50 times magnification picture taken from a plate made with the braid 45B72 ($\pm$ 49°).

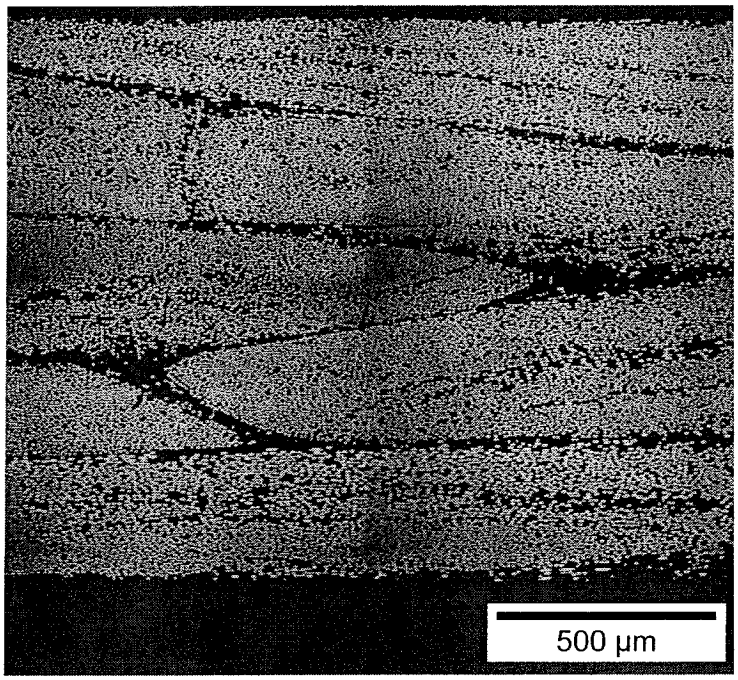

Figure 6.1: 200X Micrograph of a Consolidated ± 49° Braid (45B72), Seen in Axial View.

Boundaries between tows are observable as resin-rich regions. The tow regions are flattened compared to the round commingled tow shaped observed in Figure 3.3. Figures 6.2 and 6.3 show the axial views of the plates manufactured with the 30B72 and the 78B72 braids.

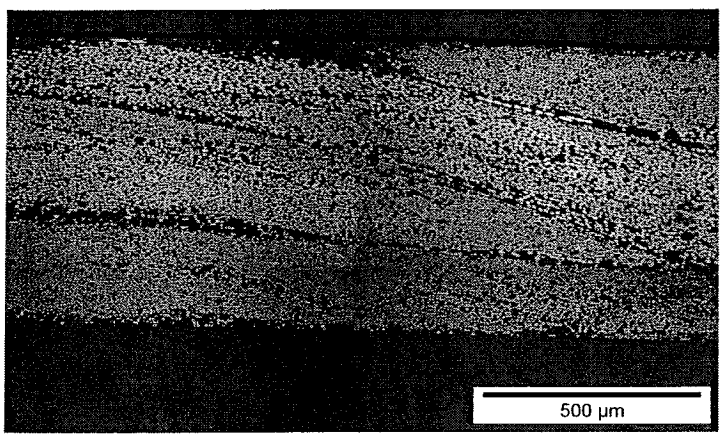

Figure 6.2: 200X Micrograph of a Consolidated ± 35° Braid (30B72), Seen in Axial View.

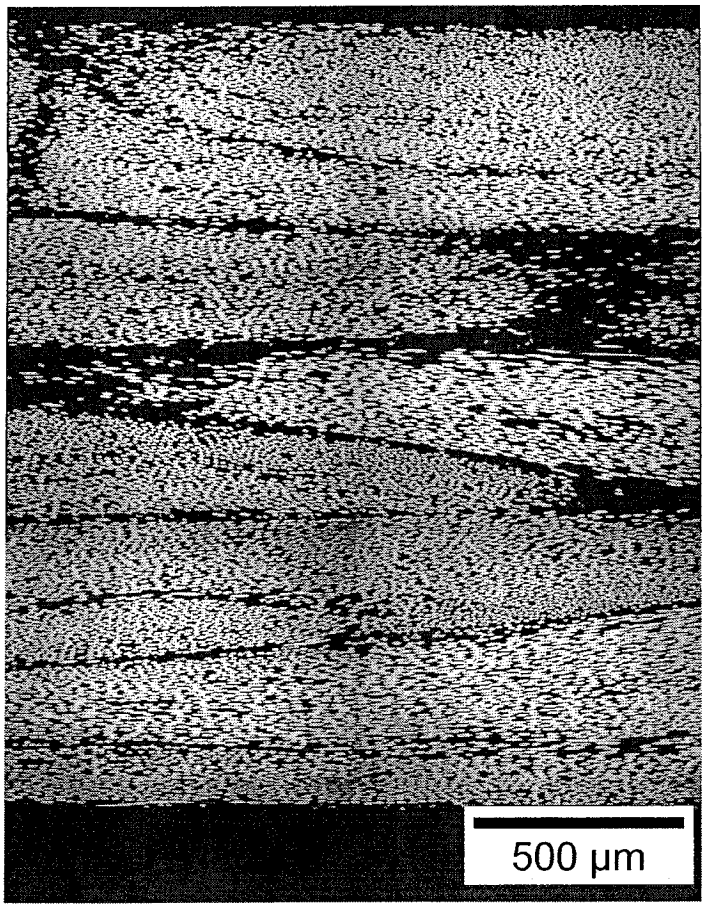

Figure 6.3: 200X Micrograph of a Consolidated ± 72° Braid (78B72), Seen in Axial View.

Only 4 different yarn regions are observed in Figure 6.2 from top to bottom of the picture. Figure 6.3 shows the presence of much more tow regions in the thickness. Each preform had 6 tows in its thickness, as each of the three layers is a braid that contains 2 yarns in its thickness. This indicates the presence of a flow of greater complexity than just an intra-bundle resin flow.

The plates seen in the last two pictures are coming from braids made with the same amount of yarn carriers and on the same mandrel, but with a different braid angle, thus a different cover factor. Figure 6.2 shows the plate manufactured with the lowest cover factor,

the 30B72 braid has a cover factor of 0.423. It is seen that the thickness is much lower and that only a few tow regions (4) are present in the observed area. The plate observed in Figure 6.3 is coming from the braid 78B72 having the highest cover factor of all the manufactured braids which is 0.902. Much more yarns are observed in the greater thickness. In both pictures, none has greater resin rich regions or better fiber distribution. This indicates that the matrix and the reinforcement are able to flow well to occupy all the open spaces in the braid even if its cover factor is very low. This leads to a good consolidation for a relatively short consolidation time (10 min.)

6.4. Constituent Content

Measuring the quantity of fibers, matrix and voids in the laminate is inspired from the standard test method ASTM D3171-99. The void content is determined by equation 6.1 using actual and theoretical density. The actual density can be obtained using ASTM-D792. The theoretical density (equation 6.3) can be obtained using the density of matrix and fibers from the manufacturer and the fiber weight content. This last data is calculated comparing the mass of fibers extracted by matrix digestion of a laminate sample, to the mass of the laminate sample.

This section will present in detail the elaboration and the justification of each step of the constituent content determination method and the calculations developed to process the data obtained in the lab. Finally, it will show and discuss the consolidation quality of the plates manufactured in this study.

6.4.1. Experimental

Drying

In order to get precise weight measurements, a drying procedure is developed to eliminate water presence prior to any weight measurements. In our case, there is humidity inside the laminate, the empty filters and the final product of the filtration step that needs to be removed before weighing. Drying is achieved using a vacuum oven for 2 hours. Then, a vacuum desiccator is used to cool down the specimen to be weighted after 45 minutes. Finally, dry air is used to re-equilibrate the pressure in the desiccator with the room atmospheric pressure in order to open it. The same procedure is employed before each weighing.

Density of Coupons

The desired density is the actual density (ϱ_a, see equation 6.1) of the laminate. The laminate bulk density consists of the mass of the coupon divided by the bulk volume of the coupon. The bulk volume is the total volume of the matrix plus the embedded fibers plus the inside closed pores and the open pores touching the surface of the solid. (See figure 6.4)

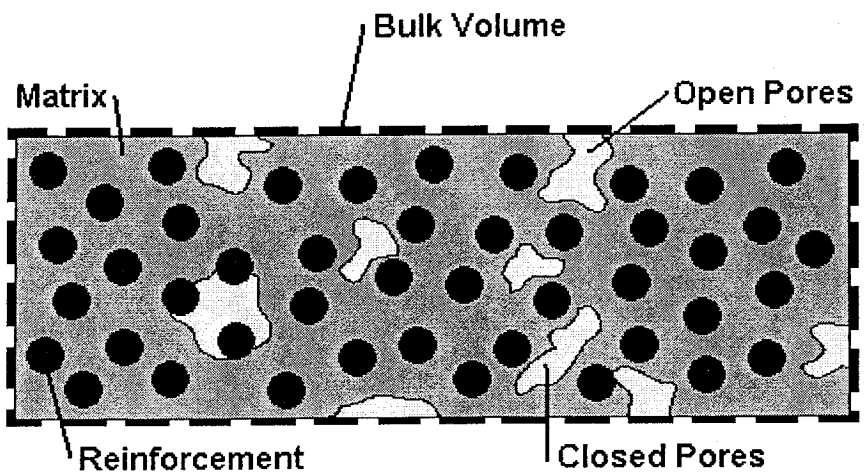

Figure 6.4: Bulk Volume of Coupon

There are many ways to get an accurate value of the bulk volume. Pycnometery is a common means using a wetting substance of known density and a pycnometer, i.e. a vessel of known volume. A difference of mass between the filled bottle and the filled bottle containing the sample leads to the density. Depending on the wetting nature of the liquid and the size of the open pores reaching the surface of the solid, the volume measured will include (bulk volume) or reject (skeletal volume) the cracks, defects and open pores. Mercury for example, bridges over the open cracks and pores resulting in a bulk volume determination. Another method is to use a high precision devices consisting of a piston compacting small sphere-shaped particles in a cylinder. The particle size is selected to conform to the shape of the measured coupon without entering the pores. Piston displacement comparison with and without the coupon leads to the bulk volume of the coupon.

Due to high cost of mercury-pycnometery or piston and particles devices, density measurements were done in accordance with standard ASTM D792-98, which is an accurate and widely used technique. The density value is obtained by dividing the weight of the sample in air by the buoyancy of the sample (weight of the sample in air minus the weight of the sample immersed in water). An ASTM D792-98 compliant density-measuring device can adapt an analytical scale to perform the experiments with the desired precision. The adherence of air bubbles on the laminates when weighing the sample in water and also water adherence on the forceps used to put the coupon on the water-immersed platen can change the readings. A good practice is to immerse the forceps in another water bath before grabbing and slowly place the coupon so no net change of water is done in the weighting bath.

Density of Materials

The density of the primary materials (matrix and fibers) have to be known precisely because theirs values are involved in the final void content result. Here, data from the manufacturer is employed. The Pa12 density is 1.01 g/m^3 and the carbon fiber density is 1.78 g/m^3

Weighting

A consistent weighting method has to be employed to insure good and repeatable results. One of the problems encountered with dry samples weighed in air is the water absorption by the sample during weighing. As no inert atmosphere scale is available, which would eliminate the presence of humidity during the weighing operation, the weighing procedure is to put the sample on the scale platen, and note the lowest weight indicated by the scale when the stabilisation sign appear. Forceps are used to prevent falsifying the results by addition of particles onto the weighing sample.

Digestion Medium

For the nylon 12 matrix used in this study, Schappes Techniques company, the manufacturer of the carbon/PA12 commingle fiber, recommends a digestion using formic acid at boiling temperature, around 107°C. For assurance of full digestion, 1 gram of laminate is dissolved in 200 ml of boiling ACS 88% concentrated solution formic acid in water for two hours. The operation is realised on a standard electrical hot plate equipped with a magnetic stirrer set at high mixing rate. The experimental set-up is shown in Figure 6.4. Formic acid is a highly corrosive and proper safety precautions should be taken. Furthermore, a condenser column is used when boiling formic acid to prevent evaporation of digestion medium.

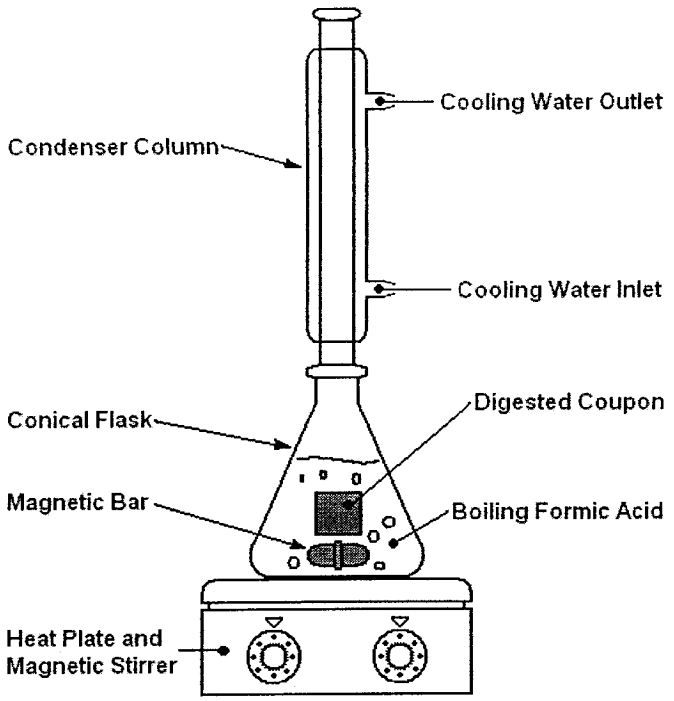

Figure 6.5: Dissolution Experimental Setup

To see if the digestion is efficient, manual inspection of the filtered and dried fibers is important. A complete digestion will leave the fibers easily detachable. On the contrary, an incomplete digestion will leave knots and rigid bundles in the recovered fiber sample. For certainty, Scanning Electron Microscopy (SEM) is used to examine the digested fibers and confirm that no traces of nylon are present.

Filtration

There are different filtration procedures available, by gravity in a conical filter, by vacuum filtration in Gooch type funnel or in porous Gooch type crucible. The latter solution has been tried but the glass crucibles (fig. 6.6) porosity is too high. An alternate way would be to use a ceramic fritted Gooch type crucible (fig 6.7) where small porosities are available.

These solutions still have drawbacks such as the slow filtration speed, the high costs and the high tarring weight that influences the precision.

Figure 6.6: Glass Frit Gooch Crucible

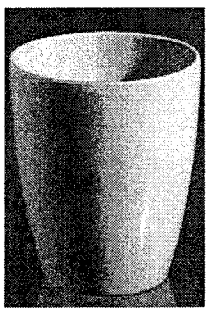

Figure 6.7: Ceramic Frit Gooch Crucible

The selected method is vacuum filtration developed for critical gravimetrical analysis. The method employs a round flat filter membrane squeezed between a coarse fritted glass surface and a glass funnel by means of a clamp (see figure 6.8). That method has the advantage that only the lightweight filter membrane is taken for weighing the product of filtration.

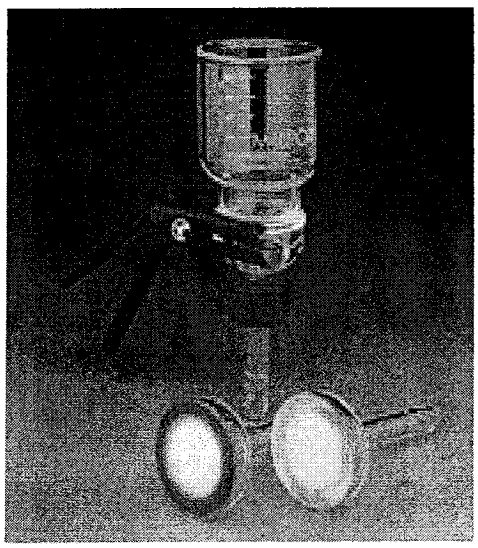

Figure 6.8: Analytical Filtering Apparatus.

Because the digestion is performed in formic acid at 107°C, the filtration has to be done at digestion temperature to prevent the matrix in solution to precipitate before it goes

through the filter. Depending on the filtration speed, different methods can be employed to keep the filtration apparatus at desired temperature. Preheating in an oven and using a hot air flow directed onto the funnel is a good solution in case of fast filtration. For slower filtering speeds, one may use a circulating hot fluid blanket or an electrical heating mantle. In our case, because of the fast filtration speed (less than 10 seconds), the first solution is employed. Also, a lot of hot rinsing digestion medium is employed to wash the matrix that can precipitate on the filter.

Finally, all the manipulations of the filter have to be done with extreme care, especially when the filter is wet, to prevent weight gain or loss. Handling has to be done using powder free gloves and forceps.

Filters

The filter was selected to meet specific requirements. First, it has to be dryable to constant weight under the selected drying conditions. Then, it has to be unaffected by the digestion medium. The solution of matrix and digestion medium has to flow through the filter under the filtration conditions without adherence of any kind. The pore size has to be under the smallest fiber particle that can be assumed to be a sphere of a diameter equal to the mean diameter of fibers, which is approximately 7 microns. The suitable filter is an APFB type from Millipore. The material of this membrane is a binder-free borosilicate glass fiber filter. The stable nature of borosilicate glass gives a really good resistance to strong acids. It can also go under high temperature without being affected. The porosity of about 2 microns is recommended to use for particles from 1 to 8 microns and higher which is perfect for this study.

Constituent Content Method

After the examination and justification of all the specific steps, the method can be summarized as follows:

1. Cut about 1,0 g of material and weigh accurately.
2. Dry the sample using a drying temperature of 35-40°C, and a drying time of 2 days.
3. Measure weight of sample in air, record as M_a.
4. Measure weight of sample immersed in water, record as M_w.
5. Dry a filtering membrane in a pre-identified aluminium weighing-pan with a drying temperature of 110 °C and drying time of 2 hours. Keep the weighing pan clean for further manipulations.
6. Weigh empty filter in weighing pan, record as M_f.
7. Add coupon to the digestion flask containing 200 ml of digestion medium.
8. Stir for two hours with a magnetic stirrer at boiling point of digestion medium.
9. Filter the digestion product using preheated analytical filtering apparatus (Figure 6.7) with an hot air blower directed on the filtering apparatus.
10. Dry the filter with the fibers inside the weighing pan, using a drying temperature of 110 °C and a drying time of 3 hours.
11. Weigh the weighing pan filled with the filter and the fibers, record as M_d.

6.4.2. Calculations

The calculated values are the weight fraction of fibers (W_f), the actual density (ϱ_a), the theoretical density (ϱ_t), and the void content (X_v). The basic equations for those values are:

$$W_f = \frac{M_{fibers}}{M_{composite}} \tag{6.4}$$

$$\rho_a = .9976 \frac{M_a}{M_a - M_w} \tag{6.5, ASTM D792}$$

$$\rho_t = \frac{\rho_f \rho_m}{\rho_f (1 - W_f) + \rho_m W_f} \tag{6.6}$$

$$X_v = \frac{\rho_t - \rho_a}{\rho_t} \tag{6.7}$$

In the previous equations, ϱ_f is the density of the fibers, ϱ_m is the density of the matrix, M_a is the weight of the laminate in air and M_w is the weight of the laminate in water. The measured values consist in the weight of the dry laminate in air (M_a), the weight of the dry laminate in water (M_w), the weight of the empty and dry filter in the weighing pan before filtration (M_f) and finally the weight of the filter plus the fibers in the weighing pan after filtration and proper drying (M_d). Rearranging equations 6.4 to 6.7 in terms of the measured values gives the following equations:

$$W_f = \frac{M_d - M_f}{M_a} \tag{6.8}$$

$$\rho_a = .9976 \frac{M_a}{M_a - M_w} \tag{6.9}$$

$$\rho_t = \frac{\rho_f \rho_m}{\rho_f + \frac{(M_d - M_f)(\rho_m - \rho_f)}{M_a}} \tag{6.10}$$

$$X_v = 1 - \frac{.9976\, M_a \left(\rho_f + \frac{(M_d - M_f)(\rho_m - \rho_f)}{M_a} \right)}{(M_a - M_w)\rho_f \rho_m} \tag{6.11}$$

The accuracy of all the above-calculated values can be determined by quadratic propagation of errors. The effect of the error of each measurement is determined by the partial derivative of the calculated value with respect to the measured value. The general equation is given below for the void content error:

$$\delta X_v = \sqrt{\left(\left(\frac{\partial}{\partial M_d} X_v\right)\delta M_d\right)^2 + \left(\left(\frac{\partial}{\partial M_f} X_v\right)\delta M_f\right)^2 + \left(\left(\frac{\partial}{\partial M_a} X_v\right)\delta M_a\right)^2 + \left(\left(\frac{\partial}{\partial M_w} X_v\right)\delta M_w\right)^2} \tag{6.12}$$

Complete equations are shown in Appendix D. Precision of each measured values are stated in Table 6.2 depending on the precision of the measuring instruments. ASTM standard D792 recommends a precision of ± 0.0001 gram, but no analytical balance that adapts a density measurement device with that precision is available in the lab.

Measured Value	Symbol	Measuring device	Unit	Range	Precision
Weight of coupon in air	M_a	Analytical Balance	g	1.0 ± .3	± 0.0001
Weight of coupon in water	M_w	Analytical balance, ASTM D792-98 compliant	g	0.25 ± .2	± 0.001 (ASTM recommendation: ± 0.0001)
Weight of the empty and dry filter	M_f	Analytical Balance	g	2.0 ± .2	± 0.0001
Weight of filter containing the fibers	M_c	Analytical Balance	g	2.7 ± .5	± 0.0001

Table 6.2: Precision on Measured Values.

Resulting precisions on the calculated values are stated in Table 6.3. Note that the fiber and matrix densities are considered as given values. This accuracy analysis shows that not having a ± 0.0001 gram precision on the weight of the coupon immersed in water doubles the error on the void content and changes by a factor of 10, the error on the actual density.

Calculated Value	Symbol	Unit	Range	Precision	Precision (with ± 0.0001 g precision on immersed weight)
Fiber Weight Fraction	W_f	-	0.0 – 1.0	± 0.0002	± 0.0002
Actual Density	ρ_c	g/cm³	1.0 - 1.78	± 0.0019	± 0.0002
Theoretical Density	ρ_t	g/cm³	1.0 - 1.78	± 0.0001	± 0.0001
Void Content	X_v	-	0.0 - 0.10 or 0% - 10%	± 0.0004 or ± 0.04%	± 0.0002 or ± 0.02%

Table 6.3: Precision on Calculated Values

Even though the precision is affected, the results are still reliable and accurate because the error on void content is only ±0.04%. Finally, the experiment is repeated 3 or more times to calculate the average, the standard deviation and the 95% confidence interval.

6.4.3. Results

The laminate density measurement and dissolution experiments, presented in Table 6.4, lead to 4 different results: the fiber weight ratio, fiber volume content, the laminate measured density, and the void content. Note that the fiber volume content includes the void in its calculation.

No	Braid Name	Local Angle	Fiber Weight Fraction (W_f)	Fiber Volume Content (V_f)	Measured Density (ρ_a)	Void Content (X_v)
	-	Deg	-	-	g/cm^3	-
1	30B72	±35.0	65.9% ± 0.5%	51.7% ± 0.6%	1.397 ± 0.008	1.1% ± 0.3%
2	45B72	±49.4	66.1% ± 1.1%	52.3% ± 1.2%	1.408 ± 0.008	0.5% ± 0.3%
3	60B72	±64.0	65.7% ± 0.3%	51.7% ± 0.3%	1.401 ± 0.002	0.7% ± 0.1%
4	78B72	±72.3	65.9% ± 0.2%	52.0% ± 0.2%	1.403 ± 0.003	0.7% ± 0.2%
5	30S72	±35.4	66.8% ± 0.2%	52.8% ± 0.1%	1.408 ± 0.003	0.9% ± 0.3%
6	45S68	±50.0	66.1% ± 0.5%	52.0% ± 0.7%	1.400 ± 0.006	1.1% ± 0.2%
7	60S60	±60.3	66.1% ± 0.7%	51.9% ± 0.8%	1.399 ± 0.008	1.1% ± 0.1%

Table 6.4, Consolidation Quality Examination Results

To ensure reliability of the dissolution technique, a sample of recovered fibers has been examined under SEM. As seen in Figure 6.9, no trace of un-dissolved nylon was identifiable on the fibers.

Figure 6.9, SEM Image of Clean Fibers After Coupon Dissolution

6.4.4. Discussion

From Table 6.4, it is observed that the fiber volume fraction of all the plates manufactured is around 52%. Compared to the fiber volume content in the raw commingled yarn, which is 51.6%, it can be stated that virtually no matrix flow out of the braided preforms is occurring even if the configuration of the mold allowed such flow out. This is explained by the high viscosity of the resin combined to the network of fibers constraining the resin flow.

The void contents for all the laminates are around the 1%. Indicating good quality consolidation.

6.5. Conclusion

The consolidation quality investigation showed braids manufactured with the Carbon/Pa12 commingled fibers consolidate well into plates. No flow out of the preform is occurring. Even if preforms have low cover factors, resin and reinforcement flow well to form laminates with good fiber/matrix distribution and with virtually no voids.

Chapter 7

MECHANICAL PROPERTIES

7.1. Background

Mechanical Properties of various forms of braids have been broadly tested for traditional braided composites using thermoset matrices. However, such experimental data is less accessible with thermoplastic hybrid yarns. For the Carbon/Pa12 Schappe Techniques yarn used in this study, recent publications are available presenting mechanical properties for various types of preforms [7, 23, 36, 38, 39]. Those data are shown in Table 7.1.

Laminate Type	Vf	Flexural Strength	Flexural Modulus	Tensile Strength	Tensile Modulus	Source	Ref
		MPa	GPa	MPa	GPa		
UD 0°	53%	1010	107	1400	98	Schappe Techniques	[23]
UD 90°	53%					Schappe Techniques	[23]
±20° Braid	53%	700	70	650	65	Schappe Techniques	[23]
UD 0°	53%	1035	96	1584	113	Di Florio et al.	[36]
UD 0°	52%	879	72	-	-	L-Lebel et al.	[39]
UD 90°	52%	65	4	-	-	L-Lebel et al.	[39]
2-2 Twill Weave	56%	-	-	832	64	MCDonnel et al.	[7]
5 HS Weave	56%	619	52	788	63	MCDonnel et al.	[7]
±31° Braid	56%	-	-	338	29	MCDonnel et al.	[7]
±42° Braid	56%	-	-	195	15	MCDonnel et al.	[7]
±58° Braid	56%	-	-	89	5	MCDonnel et al.	[7]

Table 7.1: Reported Mechanical Properties for Schappe Technique Carbon/Pa12 Commingled Yarn

Flexural strengths and moduli in Table 7.1 have all been determined by 3 point bending tests. It can be seen that the fiber content for the different studies is not constant. This is due to the fact that during the years, Schappe Techniques changed the fiber volume

fraction in their products. Nowadays, a commingled yarn has a fiber volume fraction of around 53%. It also depends on the constituent content test from each study.

This chapter will present a characterization of the flexural and tensile mechanical properties for a large range of braid angles, and apply the classical lamination theory to the consolidated braided laminates to predict the tensile modulus.

7.2. Flexural Testing

The 3-point bending tests are performed in accordance with standard test method ASTM D790, procedure A. Samples are extracted from the plates manufactured in this study, coming from the braidings.

7.2.1. Experimental

The coupons have a 3-inch (76 mm) length and a 1-inch width (25 mm). Twelve coupons are cut out from each plate with the diamond blade saw. Half of them (6) are cut along the braid axis direction and the other half are cut along the hoop direction. The fiber orientation in axial test coupons is $\pm\theta°$, where θ is the braid angle. For the hoop test coupons, the fiber orientation is the complementary angle, i.e. $\pm(90-\theta)°$ (see figure 7.1).

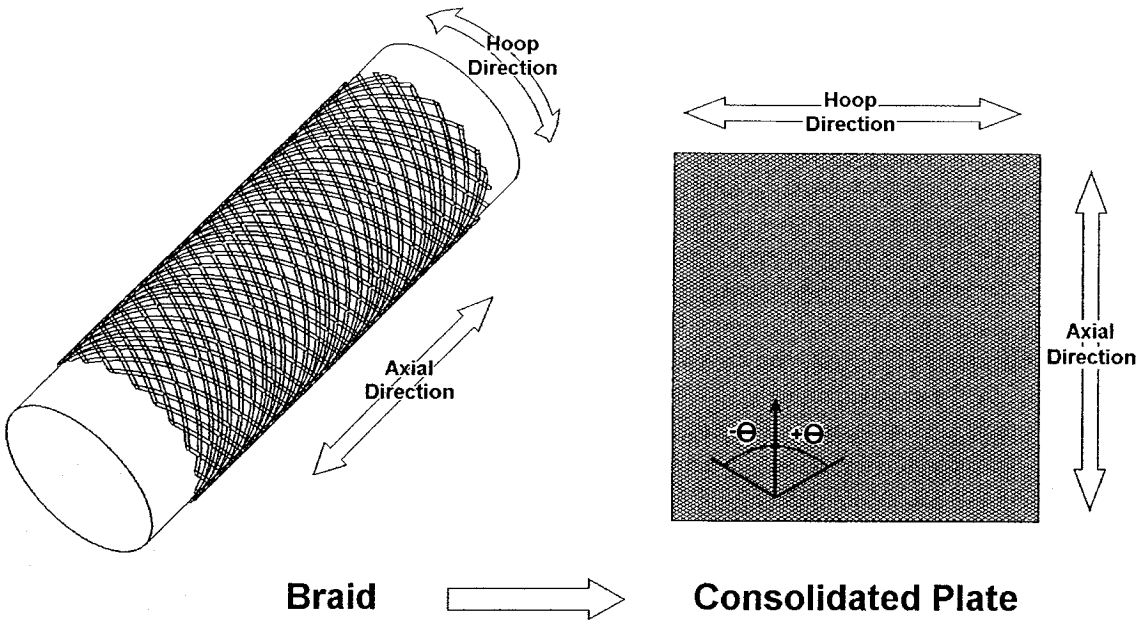

Figure 7.1: Samples Geometry.

The tests are performed on a MTS unidirectional testing machine and a 3-point flexural testing apparatus. The support span-to-depth and the ramp rate of testing vary according to the sample thickness but respect the strain rate of 0.01 mm/mm/min of the outer fiber of the specimen (Specified for ASTM D790 procedure A). The tested angles, the thickness, and specific ramp rate for each sample are shown in table 7.2.

Braid Name	Test Direction	Test Angle	Span	Plate Thickness	Ramp Rate
-	-	Deg	mm	mm	mm/min
30B72	Axial	35	63	0.63	10.0
	Hoop	55	51.4	0.63	7.0
45B72	Axial	49	63	0.81	8.0
	Hoop	n/a	n/a	n/a	n/a
60B72	Axial	64	63	1.20	5.5
	Hoop	26	63	1.20	5.5
78B72	Axial	72	63	1.80	3.7
	Hoop	18	63	1.80	3.7
30S72	Axial	35	51.4	1.11	4.0
	Hoop	55	51.4	1.11	4.0
45S68	Axial	50	51.4	1.32	3.3
	Hoop	40	51.4	1.32	3.3
60S60	Axial	60	51.4	1.54	2.9
	Hoop	30	51.4	1.54	3.9

Table 7.2: Testing Ramp Rates for Different Braided Laminates

7.2.2. Results

Flexural properties for tested laminates are presented in Table 7.3. Hoop flexural strength and modulus for the 45B72 braid are not available.

	Testing Direction ->		Axial			Hoop		
No	Braid Name	Braid Angle	Testing Angle	Bending Strength	Bending Modulus	Testing Angle	Bending Strength	Bending Modulus
	-	Deg	Deg	MPa	Gpa	Deg	MPa	Gpa
1	30B72	±35.0	±35.0	365.4 ± 23.0	26.6 ± 2.4	±55.0	323.8 ± 18.7	10.0 ± 0.7
2	45B72	±49.4	±49.4	333.8 ± 11.0	21.1 ± 1.5	±40.7	n/a	n/a
3	60B72	±64.0	±64.0	128.7 ± 5.1	6.0 ± 0.4	±26.0	577.3 ± 21.3	44.6 ± 0.7
4	78B72	±72.3	±72.3	122.6 ± 21.4	5.2 ± 0.6	±17.7	789.1 ± 40.1	72.8 ± 2.5
5	30S72	±35.4	±35.4	444.6 ± 20.0	26.2 ± 1.4	±54.6	252.0 ± 12.2	8.5 ± 0.8
6	45S68	±50.0	±50.0	284.1 ± 12.4	10.8 ± 0.8	±40.0	408.5 ± 10.4	20.6 ± 0.6
7	60S60	±60.3	±60.3	195.4 ± 1.9	6.7 ± 0.2	±29.7	538.6 ± 13.6	40.6 ± 0.6

Table 7.3, Flexural Mechanical Properties of Consolidated Braids in Axial and Hoop Directions

7.2.3. Discussion

The results for flexural strength and modulus are expressed as a function of fiber orientation in Figures 7.2 and 7.3 respectively.

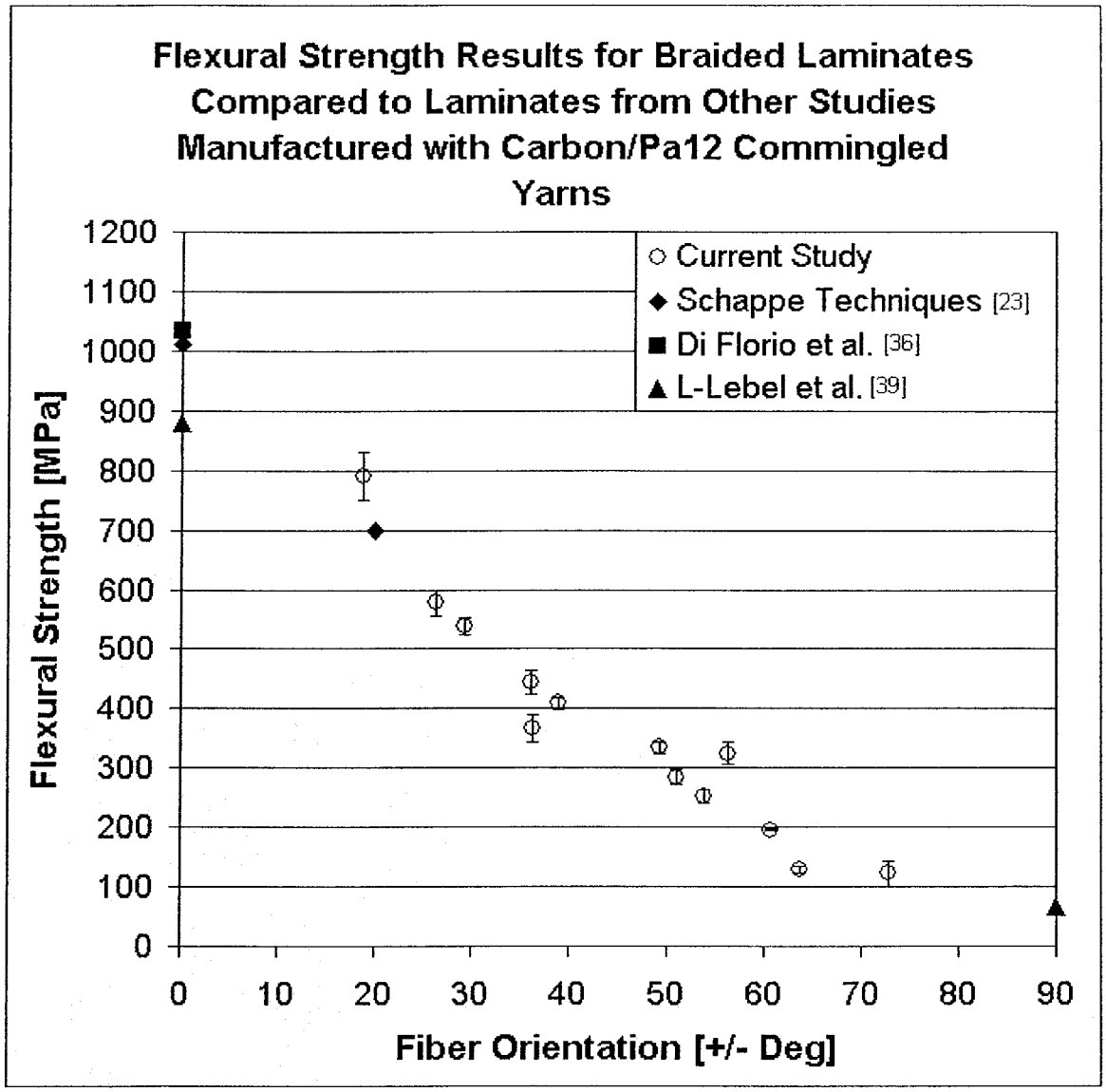

Figure 7.2: Flexural Strength as a Function of Fiber Orientation

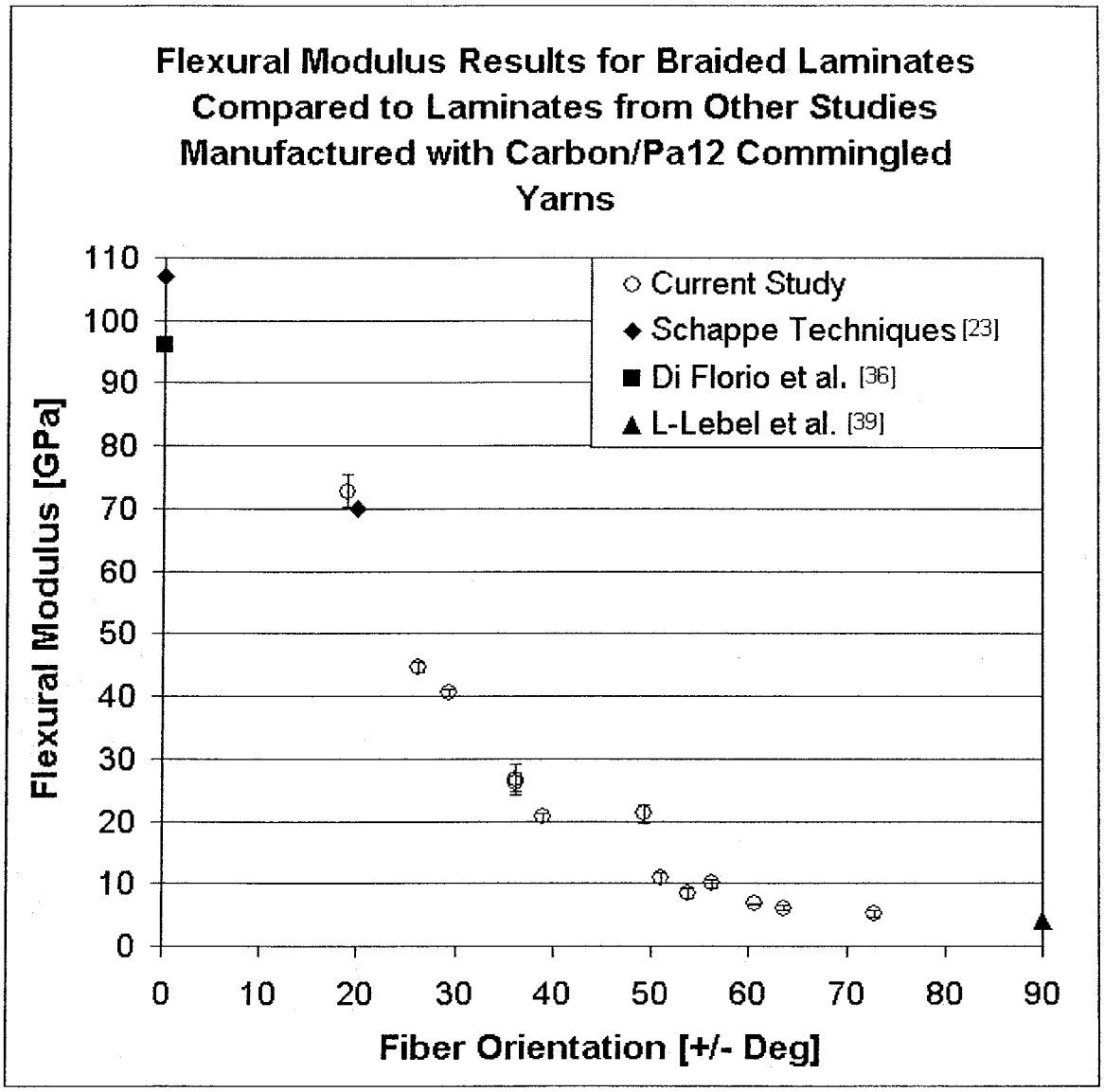

Figure 7.3: Flexural Modulus as a Function of Fiber Orientation

Both the flexural strength and modulus values have a bell shaped distribution where the maximum is approached when the angle approaches 0°. Also, the modulus approaches the transverse modulus obtained in L-Lebel et al. study [39] (see Table 7.1) when the angle approaches 90°. The values obtained in this study fits well to the values obtained in other studies.

7.3. Tensile Testing

Tensile testing has been realized in accordance with the standard test method ASTM D3039. Samples are extracted from the plates manufactured in this study. This completes the experimental cycle starting from the yarn examination until mechanical testing of the consolidated braids.

7.3.1. Experimental

From each plate, five coupons having the same orientation were cut out using a diamond blade saw. On three of them, unidirectional strain gages were placed to determine modulus. Every braid is tested in both their axial and hoop directions (See Figure 7.1).

The coupon dimension was 10 by 1 inch (254 x 25 mm) except for the coupons used to measure hoop strength and modulus of braids manufactured on the small mandrel (2-3/8", 60 mm). Those have dimensions of 7 inch (178 mm) by 5/8 inch (16 mm). Sample thickness changes according to fiber orientation, mandrel diameter and number of carriers used in the braiding operation. Because of the dimensions of the plates manufactured, two plates were needed from the same braid to obtain all the necessary coupons for axial and hoop directions

MTS testing machine with hydraulic gripping heads was used to apply the tension. The ramp rate for all the samples was 1 mm/min.

Materials for the gripping tabs used in this study are a 3000 series aluminium sheet and a 100-count stainless steel mesh. A specimen-wide mesh is fold over the tips of specimen on a 2-inch (51 mm) length. Then a piece of aluminium of same dimension as the mesh is bent-over the assembly. A picture of the assembly is shown in figure 7.4.

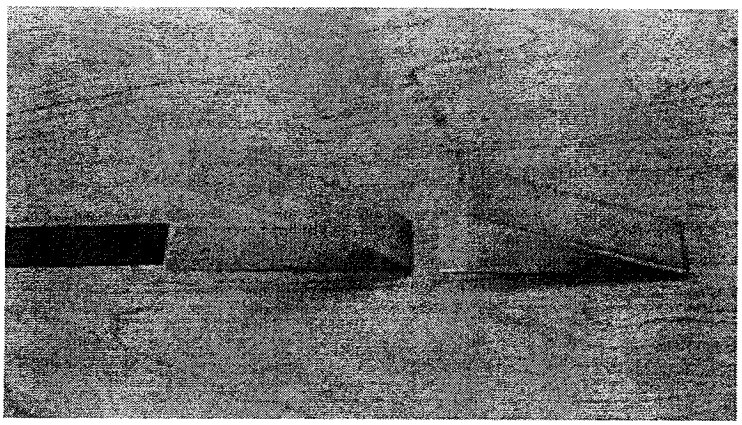

Figure 7.4, Gripping Assembly

This gripping method, widely used in Concordia by the thermoplastic composites research group [36], has proven its efficiency in allowing unidirectional and braided thermoplastic composites coupons to break in the examination zone at gripping pressure of 10 MPa.

7.3.2. Results

Tensile properties for braided laminates are presented in Table 7.5. Hoop strength and modulus for the 45B72 braid are not available. Modulus value for the 60S60 braid is uncertain, due to strain gage delamination. Except for the 78B72 tested in the hoop direction (± 17.7°), where the fracture occurred in fibers, all the coupons broke in resin rich regions at yarn interfaces.

Testing Direction ->			Axial			Hoop		
No	Braid Name	Braid Angle	Testing Angle	Tensile Strength	Tensile Modulus	Testing Angle	Tensile Strength	Tensile Modulus
	-	Deg	Deg	MPa	Gpa	Deg	MPa	Gpa
1	30B72	± 35.0	± 35.0	213.9 ± 12.6	16.8 ± 0.5	± 55.0	70.8 ± 1.5	7.4 ± 2.5
2	45B72	± 49.4	± 49.4	160.2 ± 4.7	14.4 ± 1.8	± 40.7	n/a	n/a
3	60B72	± 64.0	± 64.0	58.4 ± 2.1	5.2 ± 0.1	± 26.0	440.6 ± 19.0	34.9 ± 0.4
4	78B72	± 72.3	± 72.3	51.0 ± 1.1	6.0 ± 0.6	± 17.7	883.5 ± 42.8	73.0 ± 6.4
5	30S72	± 35.4	± 35.4	200.7 ± 12.8	16.6 ± 1.4	± 54.6	79.3 ± 1.7	7.7 ± 0.6
6	45S68	± 50.0	± 50.0	99.5 ± 5.1	8.2 ± 0.2	± 40.0	176.3 ± 8.0	15.7 ± 1.6
7	60S60	± 60.3	± 60.3	65.0 ± 2.7	6.0 ± 0.2	± 29.7	312.6 ± 9.4	56.4 ± 26.6

Table 7.4, Tensile Mechanical Properties of Consolidated Braids in Axial and Hoop Directions

7.3.3. Discussion

The tensile strength and modulus can be arranged in graphs as function of the tested angles. Figure 7.5 presents the tensile strength and Figure 7.6 the modulus. Both graphs include the reported values from the literature.

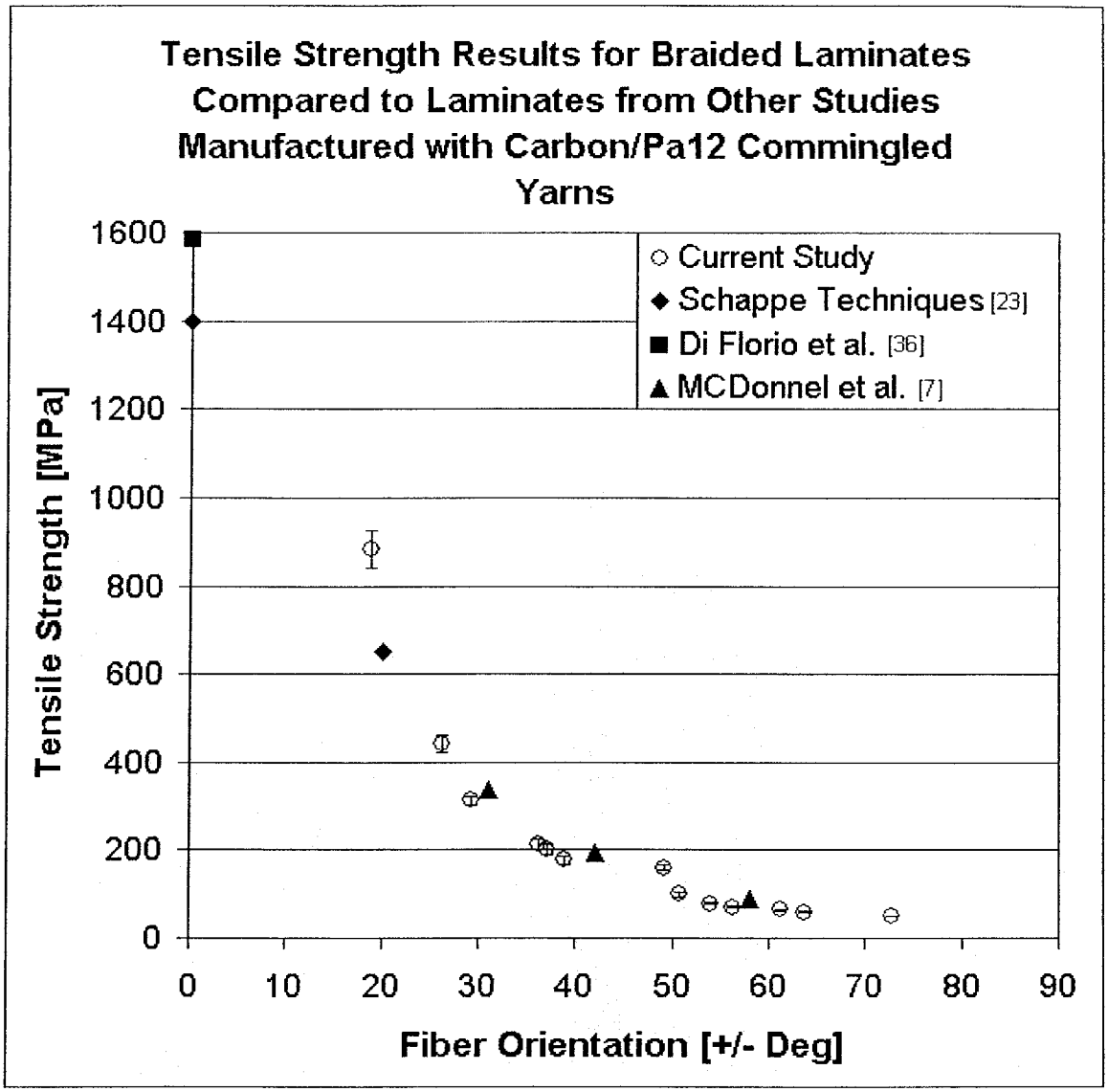

Figure 7.5: Tensile Strength as a Function of Fiber Orientation

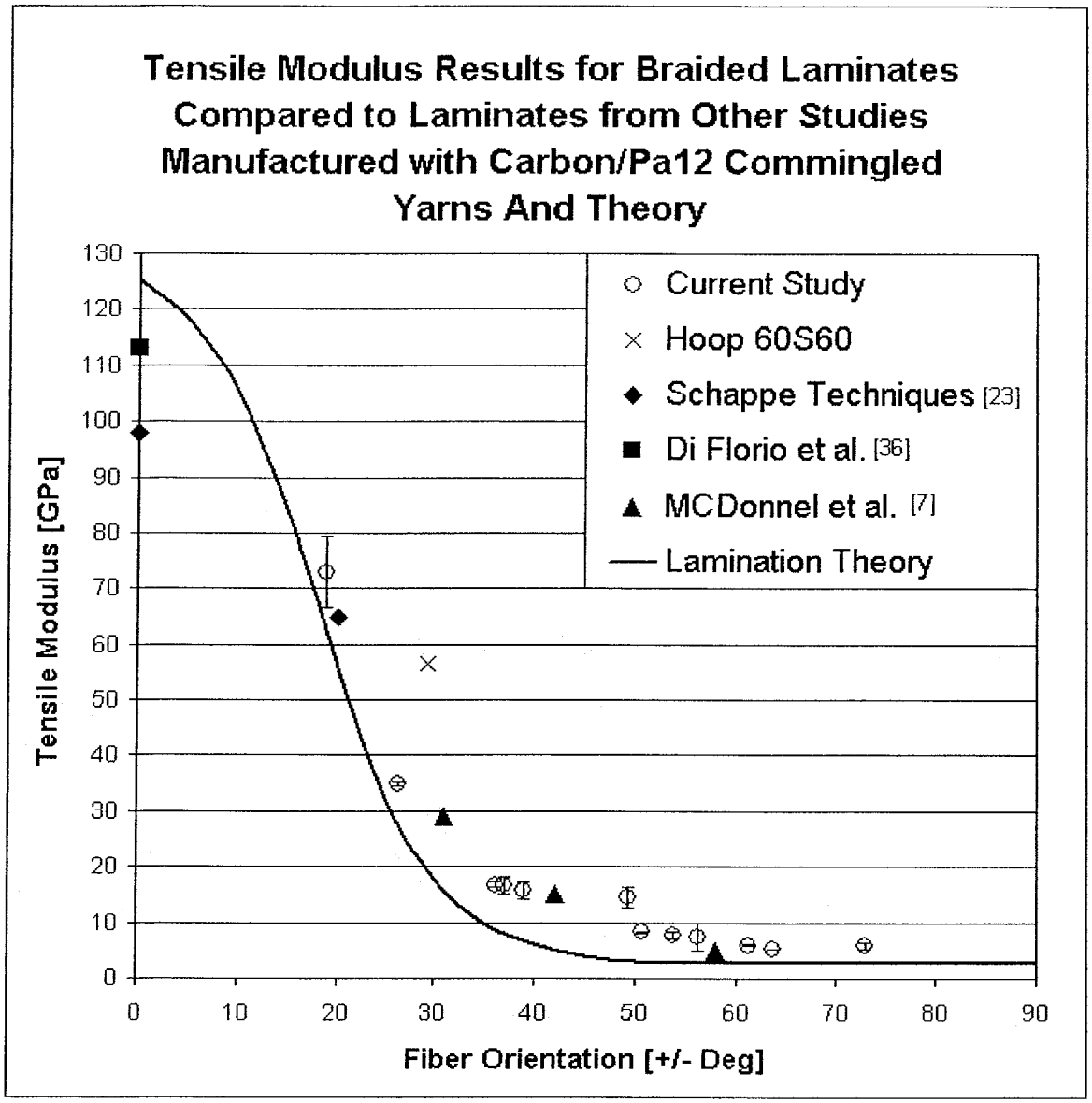

Figure 7.6: Tensile Modulus as a Function of Fiber Orientation

It can be seen from both graphs that the values from the current study are comparable to values obtained from other studies. Also, it is seen that the results have a bell shaped nature where the maximum is approached when the braid angle approach 0°.

7.3.4. Tensile Modulus Prediction

The tensile modulus can be predicted using the classical lamination theory [40]. Using this theory, the braided laminate of this study may be modeled as a stack of 6 unidirectional layers, having an angle of $\pm\theta°$ alternatively. The braid laminate model is shown in figure 7.7.

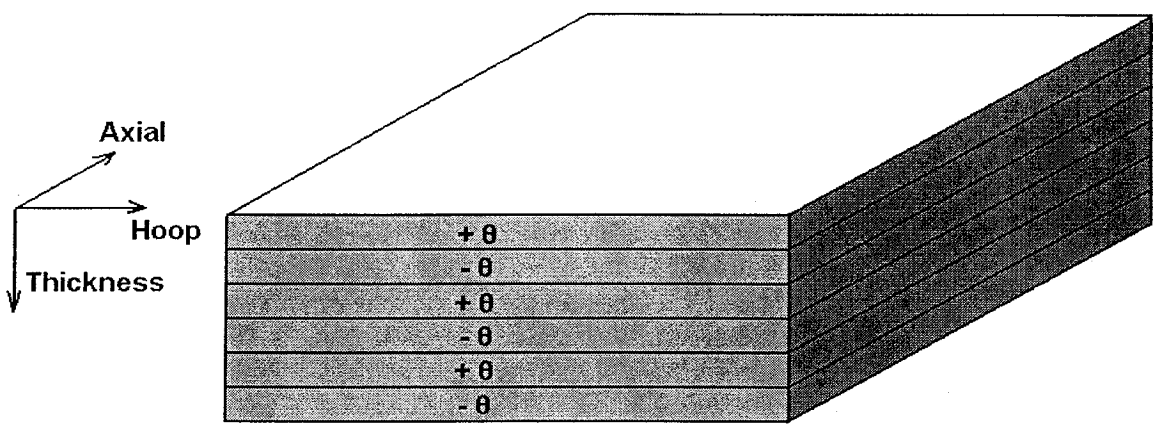

Figure 7.7: Braided Laminate Model

The modelled braided laminate stiffness in axial and hoop directions are calculated from a global laminate stiffness matrix. The process, extracted from reference [40] is summarized as follows:

1. Calculate the engineering properties of a unidirectional composite lamina in the 1-2-3 coordinates system, direction 1 being the fiber direction, 2 the lamina width direction and 3 being the thickness direction. (Figure 7.8)

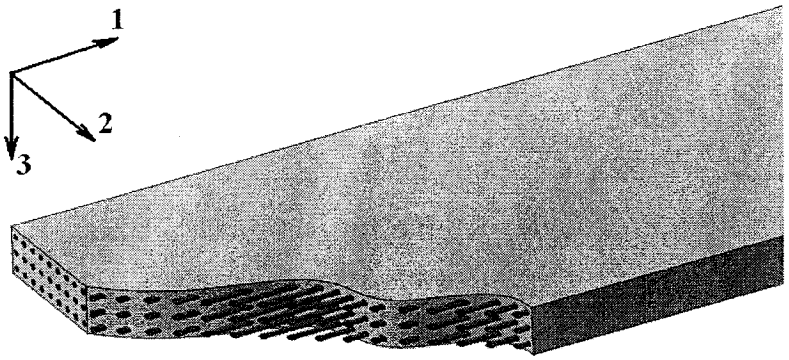

Figure 7.8: Unidirectional Lamina

2. Calculate a reduced stiffness matrix

3. Calculate two transformed reduced stiffness matrix to obtain the lamina properties at $\pm\theta°$. Rotating the reduced stiffness matrix around the axis 3 performs this calculation.

4. Assembly a global ABD matrix describing the braided laminate stiffness, using the transform reduced stiffness matrix and the position of each interfaces of the braided laminate. The position of the interfaces is deducted from the braided laminate thickness.

5. Inverse the ABD matrix to obtain an abd matrix describing the braided laminate compliance.

6. Calculate the axial and hoop modulus of the braided laminate using the following equations, specific values from the abd matrix, and the thickness of the braided laminate (t_C)

$$E_{AXIAL} = \frac{1}{abd_{11} \cdot t_C} \tag{7.1}$$

$$E_{HOOP} = \frac{1}{abd_{22} \cdot t_C} \tag{7.2}$$

Step one is performed using rules of mixtures, available theories [40], and properties of the matrix and the fiber (Table 7.5). The fiber volume content value used for this calculation was 52%, as measured in all laminates (Table 6.4) and in the unconsolidated yarn state (Section 3.3.2).

Property / Material	E_{11}	E_{22}	G_{12}	ν_{12}	ν_{23}
	GPa	GPa	GPa	-	-
Carbon Fiber	240	21.1	8.3	0.25	0.27
Pa12 Resin	1.1	1.1	0.4	0.33	0.33

Table 7.5: Fiber and Matrix Mechanical Properties [22]

Appendix E presents an example of the development of the method described (step 1 to 6) for an arbitrary laminate of $\pm 20°$ braid angle with a thickness of 2 mm. With the same spreadsheet, but changing the braid angle, the calculated values used to produce the curve in Figure 7.6 are also presented.

From this lamination theory, it is first seen that changing the angle of the braided laminate will produce a bell-shaped curve shown in Figure 7.6. Then, increasing the fiber volume content V_f used to model the laminate will increase the laminate theoretical moduli. Finally, the thickness of the modelled braided laminate does not have an effect on the final calculated axial and hoop tensile modulus if the braid angle and the fiber volume fraction are not changed. Because the thickness used to model the laminate stiffness matrix in step 4, is the

same as the thickness used to calculate the axial and hoop tensile modulus in step 6 (Equations 7.1 and 7.2). This particularity applies well to the case of braided thermoplastic laminates from commingled fibers, because the fiber volume fraction does not change from the unconsolidated yarn state until the fully consolidated braided laminate. As seen in chapter 5 and 6, the final plate thicknesses changed when the braiding conditions were different, but the fiber volume fraction was the same for all the manufactured plates.

When the mechanical results are compared to the theory (Figure 7.6), it is first seen that the results fits well the curve obtained with classical lamination theory. The results seem to follow the same curve even if the thicknesses of the individual laminates are all different. Also, the measured tensile modulus values are all higher than the predicted values even if the fiber waviness and the fiber interlocking effect of the braided structure are not modelled.

7.4. Conclusion

The mechanical properties characterization of braided laminates produced in this study has been performed. Tensile and flexural strength and modulus have been obtained for a wide range of braid angles. The distribution of the results when observed as a function of angle and compared to available values in literature confirms the validity of the results. Also, modelling of the tensile modulus has been performed using the classical lamination theory. It is noticed that the thickness of a laminate has no effect on final calculated tensile modulus because the fiber volume fraction does not change. Results fit well the calculated values from the classical lamination theory.

Chapter 8

CONCLUSIONS, CONTRIBUTIONS AND RECOMMENDATIONS

In this study, the evaluation of commingled fibers in braided laminates has been performed. After a brief overview of thermoplastic composites and their different manufacturing processes, chapter 3 presents the material used in this study: the carbon/nylon commingled fiber produced by Schappes Techniques in France. In chapter 4, a detailed analysis of braiding is performed. A general introduction on 2D biaxial braiding introduces the subject, then, a theoretical review of the mathematical relations linking the braid parameters together is done. The work on the machine calibration in the lab is presented followed by the braid manufacturing and analysis of results. In chapter 5 is shown the manufacturing of plates from the commingled fiber braids using commingled fiber. The evaluation of the consolidation quality is presented in chapter 6 where a constituent content method by matrix dissolution is used and an optical analysis by microscopy is realized. Finally the mechanical properties of the plates manufactured with the commingled yarn braids are shown in chapter 7 with flexural and tensile testing. Also, the modelling of the tensile modulus using laminate theory is presented.

Contributions

In this study, the contributions brought are as follows:

(1) The braid angle and the aerial weight of braided preforms from thermoplastic commingled yarns are well predicted by theory.

(2) The thickness of the final plate is dependent of the commingled yarn characteristics and the cover factor of the manufactured braid.

(3) The development of a good constituent content determination method leads to precise knowledge of the quality of the final composite, through quantification of reinforcement content and porosity.

(4) The existence of a flow of greater importance than an intra-bundle consolidation has been observed. Fibers and matrix tends to flow to cover the whole surface of the mold even at low cover factors.

(5) When using commingled yarns, the fiber and matrix content from the raw commingled yarn until the consolidated fabric, stays constant for every braid conditions.

(6) The consolidation quality of the plates manufactured with commingled fiber braids are independent of the braid characteristics such as braid angle, thickness and cover factor.

(7) The tested mechanical properties of the consolidated braids follow results from other works.

(8) The thickness of the consolidated braids does not have an effect on the modulus value because the fiber content does not change.

(9) The tensile modulus is well predicted with classical lamination theory.

Recommendations for Future work

To enrich the analysis of thermoplastic composites manufactured with braided commingled yarn fabrics, the following future work is suggested:

(1) Evaluation of the importance of the particular cross-section architecture of commingled yarns should be realized to see its effect on final braided fabric properties.

(2) A model should be developed to predict the preform thickness prior consolidation to help the design of complex molds.

(3) A detailed analysis of consolidated fabric should be performed to model the mechanical properties of the composite.

(4) A complete mechanical characterization of composites manufactured with braided commingled yarn fabrics should be performed to fully state the potential of thermoplastic composites for commercial, industrial and aerospace applications. For example, shear properties, creep behaviour, and resistance after impact should be investigated

References

1. Gutowsky, T.G., ed. *Advanced Composite Manufacturing*. 1997, John Wiley and Sons: New York. 581.

2. Chu, R.L., Bayha, T.D., Davis H., Ingram J.E., and J.G. Shukla, *Advanced Composites Structural Concepts and Material Technologies for Primary Aircraft Structures*. 1992, Lockheed Aeronautical System Company, for NASA: Marietta, Georgia.

3. Fedro, M.J. and K. Willden. *Characterisation and Manufacture of Braided Composites for Large Commercial Aircraft Structures*. in Ninth DoD/NASA/FAA Conference on Fibrous Composites in Structural Design. 1991. Lake Tahoe, Nevada: Nasa.

4. Renieri, M.P., S.J. Burpo, and L.M. Roundy, *Design and Manufacturing Concepts For Thermoplastic Structures*, McDonnel Aircraft Company: St-Louis, Missouri. p. 179206.

5. Ferdo, M.J., C. Gunther, and F.K. Ko, *Mechanical and Analytical Screening of Braided Composites for Transport Fuselage Applications*, Boing Defense and Space Group and Drexel University: Philadelphia, PA. p. 677-704.

6. Svensson, S. and R. Shishoo, *Manufacturing of Thermoplastic Composites from Commingled Yarns - A Review*. Journal of Thermoplastic Composite Materials, 1998. 11: p. 22-56.

7. McDonnell, P., McGarvey, K.P., Rochfort, L., and C.M. O Bradaigh., *Processing and Mechanical Properties evaluation of a Commingled Carbon-Fiber/PA 12 Composite*. Composites Part A: Applied Science and Manufacturing, 2001. 32: p. 925-932.

8. Leach, D., *PEKK Polymer and Composites*. 2004, Cytec Engineered Materials: Montreal.

9. Carlsson, L.A., ed. *Thermoplastic Composite Materials*. Composite Materials Series, ed. R.B. Pipes. Vol. 7. 1991, Elsevier Science: New York. 389.

10. Cirino, M. and T.P. Watson. *Composite Structure Fabrication with In-Situ Consolidation of APC-2/AS4*. in 36th Internationnal Sampe Symposium. 1991.

11. Bernet, N., Michaud, V., Bourban, P.E., and J.-A. E. Manson, *Commingled Yarn Composites for Rapid Processing of Complex Shapes*. Composites Part A: Applied Science and Manufacturing, 2001. 32: p. 1613-1626.

12. Bernet, N., Michaud, V., Bourban, P.E., and J.-A. E. Manson, *An Impregnation Model for the Consolidation of Thermoplastic Composites Made From Commingled Yarns*. Journal of Composites Materials, 1999. 33(8): p. 751-772.

13. Ye, L., Friedrich, K., Kastel, J., and Y.-W. Mai., *Consolidation of Unidirectionnal CF/PEEK Composites From Commingled Yarn Prepreg*. Composites Science and Technnology, 1995. 54: p. 349-358.

14. West, B.P.V., R.B. Pipes, and S.G. Advani, *The Consolidation of Commingled Thermoplastic Fabrics*. Polymer Composites, 1991. 12(6): p. 417-427.

15. Ramasamy, A., Y. Wang, and J. Muzzy, *Braided Thermoplastic Composites From Powder-Coated Towpregs. Part III: Consolidation and Mechanical Properties*. Polymer Composites, 1996. 17(3): p. 515-522.

16. Ramasamy, A., Y. Wang, and J. Muzzy, *Braided Thermoplastic Composites From Powder-Coated Towpregs. Part II: Braiding Characteristics of Towpregs*. Polymer Composites, 1996. 17(3): p. 505-514.

17. Ramasamy, A., Y. Wang, and J. Muzzy, *Braided Thermoplastic Composites From Powder-Coated Towpregs. Part I: Towpreg Characterization*. Polymer Composites, 1996. 17(3): p. 497-504.

18. Davis, S. and B. Blonski. *The Development of Vortex, The First Continuous Fiber Reinforced Thermoplastic Tennis Racquet*. in 39th Internationnal SAMPE Symposium. 1994. Anaheim, CA.

19. Nakai, A., et al. *Application of Micro-Braiding Technique to Long-Fiber Reinforced Thermoplastic Composite*. in ANTEC 2001. 2001. Dallas, TX.

20. Hamada, H., A. Fujita, and H. Tsunasawa. *Application of Micro Braided Fabric to Composite Materials*. in 27th International SAMPE Technical Conference. 1995. Albuquerque, NM.

21. Sakaguchi, M., et al., *The Mechanical Properties of Unidirectional Thermoplastic Composites Manufactured by a Micro-Braiding Technique*. Composites Science and Technnology, 2000. 60: p. 717-722.

22. Bernet, N., *Commingled Yarn Composites for Rapid Processing of Complex Shapes*, Ph D Thesis in Department of Materials. 2000, École Polytechnique Fédérale de Lausanne: Lausanne. p. 180.

23. Bontemps, G., *Propriétés des préimprégnés TPFL*,. 2005, Schappes Techniques: Charnoz.

24. Ko, F. and C. Pastore. *CIM of Braided Preforms for Composites*. in Computer Aided Design in Composite Material Technology, Proceedings of the International Conference. 1988. Southampton, England.

25. Yang, G.U.I., Pastore, C., Tsai, Y. Soebroto, H., and F. Ko, *CAD/CAM of Braided Preforms for Composites*. in Advanced composites III: Expanding the technology; Proceedings of the Third Annual Conference. 1987. Detroit, MI.

26. Hamada, H., Fujita, A., Maekawa, Z., and M. Nakao, *Enhancement of Tensile Modulus and Strength of Braided Composites*. in 40th Internationnal Sampe Symposium. 1995.

27. Braley, M. and M. Dingelin. *Advancements in Braided Materials Technology*. in 46th Internationnal SAMPE symposium. 2001.

28. Yan, Y., *A Study of Two Dimensional Braided Composites*, M Sc in Mechanical Engineering. 1998, Concordia University: Montreal. p. 137.

29. Du, G.W., P. Popper, and T.w. Chou. *Process Model of Circular Braiding for Complex-Shaped Preform Manufacturing.* in Processing of Polymers and Polymeric Composites, ASME Winter Annual Meeting. 1990. Dallas, TX.

30. Eustace, S.A., *Process Model for 2D Braiding of Elliptical Cross-Sections Preforms*, M. Sc in Department of Mechanical Engineering. 1998, University of Ottawa: Ottawa.

31. Mazzawi, A., *The Steady State and Transient Behaviour of 2D Braiding*, in Mechanical and Aerospace Engineering. 2001, University of Ottawa: Ottawa. p. 75.

32. Head, A. *New Braid Design Spreadsheet Calculates Fiber Architecture and Aerial Weight Simplifying the Design of Braid Reinforced Composites.* in 43rd International SAMPE Symposium. 1998. Anaheim, CA.

33. Bernhardsson, J. and R. Shishoo, *Effect of Processing Parameters on Consolidation Quality of GF/PP Commingled Yarn Based Composites.* Journal of Thermoplastic Composite Materials, 2000. 13: p. 292-313.

34. Ma, Y. and R. Shishoo, *The influence of Processing Parameters on the Fiber Distribution and Matrix Flow of Unidirectional Glass Fiber/Polyethylene Terephthalate (GF/PET) Commingled Yarns.* Journal of Thermoplastic Composite Materials, 1999.

35. Mayer, C., X. Wang, and M. Neitzel, *Macro- and Micro-Impregnation Phenomena in Continuous Manufacturing of Fabric Reinforced Thermoplastic Composites.* Composites Part A: Applied Science and Manufacturing, 1998. 29A: p. 783-793.

36. Di Florio, D. and Dr. S.V. Hoa, *Composite Manufacturing Technologies at CONCOM.* 2004, Concordia University: Montreal.

37. Bayldon, J.M., P.M. Schubel, and I.M. Daniel. *Measurement of Void Content in Composites through Image Analysis.* in 18th Technical conference of American Society for Composites. 2003. Gainesville, FL.

38. Connor, M.T., *Mechanical Properties of 56% CF-PA 12 Composites*. 1999, EMS-CHEMIE. p. 15.

39. Laberge-Lebel, L., Nakai, A., Salek, H., Guay, F., Hoa, S.V., and H. Hamada, *Processing and Properties of Carbon/Nylon Thermoplastic Composites Made by Commingled Tows and Micro-Braided Tows*. in Design, Manufacturing and Applications of Composites, Fifth Joint Canada-Japan Workshop on Composite. 204. Yonezawa, Yamagata, Japan.

40. Hyer, M.W., *Stress Analysis of Fiber-Reinforced Composite Materials*. 1997, Boston: WCB McGraw-Hill. 627.

APPENDIX A

4 inch (103 mm) O.D. Braiding Mandrel Drawings

NO.	DESCRIPTION	QTY.	MATERIAL
1	MANDREL (12 FOOT LONG) TUBING O.D.4"X1/8"X12'	1	ALU
2	DOWEL PIN 1/8"X 3/4"	8	STEEL
4	END CAP	2	ALU

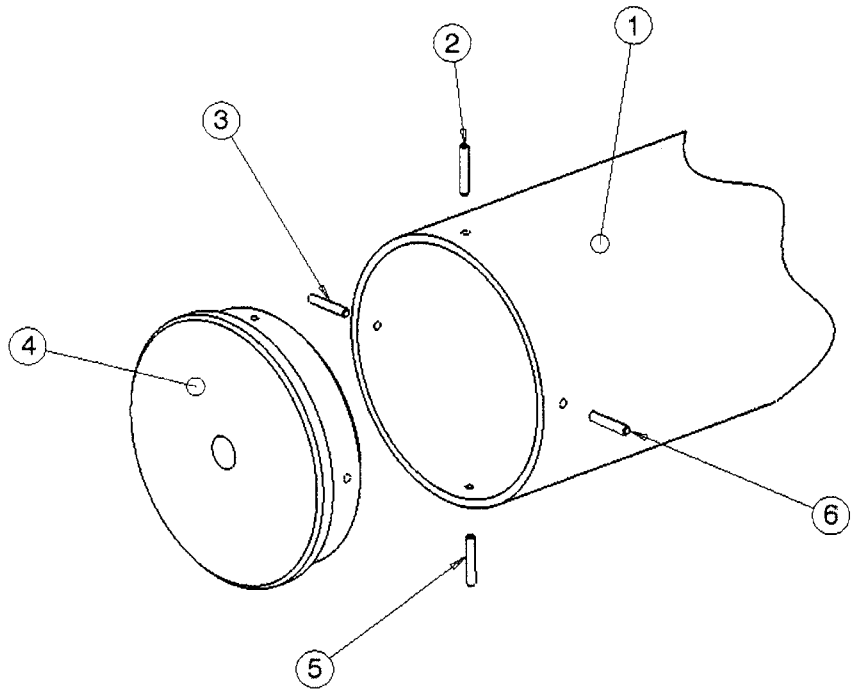

NOTES:
1- DRILL PIN HOLES AFTER END CAP ASSEMBLY WITH DRILL SIZE 31 (DIA. .120");
2- GLUE END CAP WITH MANDREL WITH PROPER ADHESIVE;
3- SAME ASSEMBLY FOR BOTH MANDREL ENDS;

CONCORDIA UNIVERSITY
MONTREAL

BRAIDING MANDREL ASSEMBLY

DRAFTED BY: LOUIS LABERGE-LEBEL	23/10/02
APROUVED BY:	
SCALE: 1/2 DWG NO: 1	PAGE: 1/2

4 END CAP

MATERIAL: ALUMINIUM
SCALE: 1/1

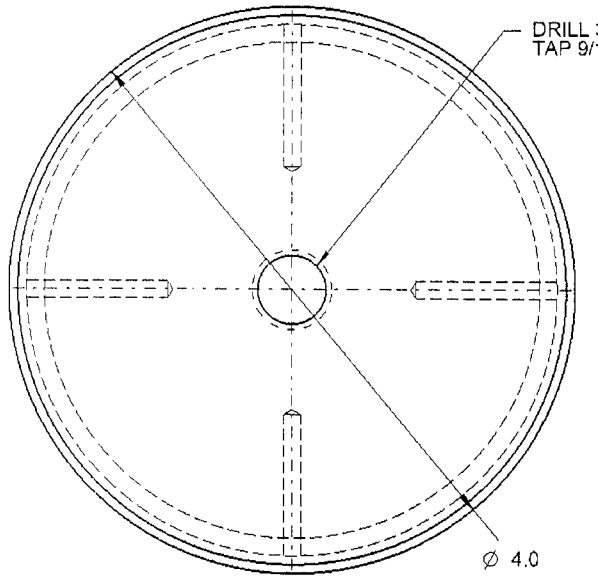

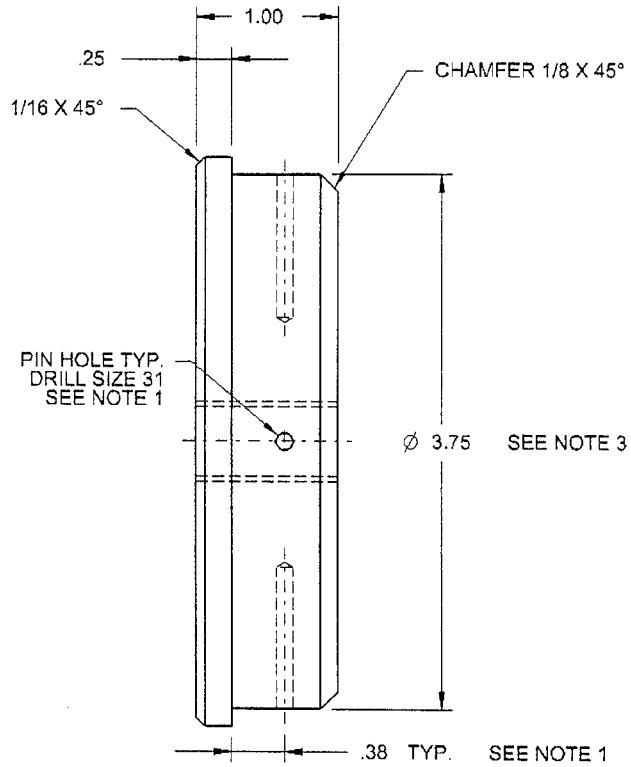

NOTES:
1- DRILL PIN HOLES AFTER END CAP ASSEMBLY WITH MANDREL. DRILL SIZE 31 (DIA. .120"), HOLE DEPTH HAVE TO FIT WITH DOWEL PIN ASSEMBLY;
2- DIMENSIONS IN INCHES;
3- MODIFY DIA. 3.75 TO OBTAIN A INTERFERENCE LOCATIONNAL FIT WITH THE MANDREL RAW MATERIAL INNER DIAMETER;

CONCORDIA UNIVERSITY MONTREAL	
BRAIDING MANDREL ASSEMBLY	
DRAFTED BY: LOUIS LABERGE-LEBEL	22/10/02
APROUVED BY:	
SCALE: 1/1 DWG NO: 1	PAGE: 2/2

APPENDIX B

Contact Informations

Name:		Mrs. Diane R. Pilley
	Resource:	Surface preparation disposables for microscopy
	Organisation:	Anamet
	Web	http://www.anamet.com
	Address	655, Jean-Paul Vincent, suite 9 Longueuil, Québec Canada, J4G 1R3
	Phone:	1-450-646-1290
	Fax:	1-450-646-4309
	Email:	anamet@anamet.com

Name:		Mr. Guy Bontemps
	Title:	Directeur Recherche, Développement Qualité
	Resource:	Material Informations
	Organisation:	Schappes Techniques
	Web	http://www.schappe.com
	Address	B.P. 89 01800 Charnoz France
	Phone:	(33) 04 74 46 31 00
	Fax:	(33) 04 74 34 79 35
	Email:	salesrd@schappe.com

Name:		Dr. Philippe Merle
	Resource:	Laboratory facilities and equipment
	Organisation:	Concordia University
	Department:	Chemistry Department
	Telephone:	(514) 848-2424 ext.5802
	Email:	pgmerle@alcor.concordia.ca

Name:		Raymond Mineau
	Resource:	Scanning Electron Microscopy
	Organisation:	Université du Québec à Montréal (UQAM)
	Department:	Département des Sciences de la terre et de l'atmosphère
	Telephone:	(514) 987-3000 ext. 6148#
	Email:	mineau.raymond@uqam.ca

APPENDIX C

Micrographs of Consolidated Braids

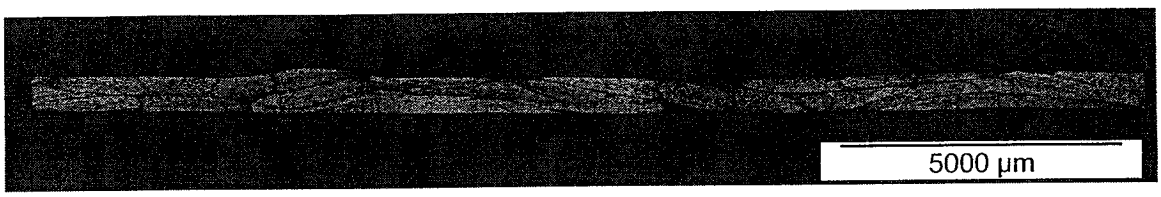

Figure 1: 50X Magnification of the Whole Coupon

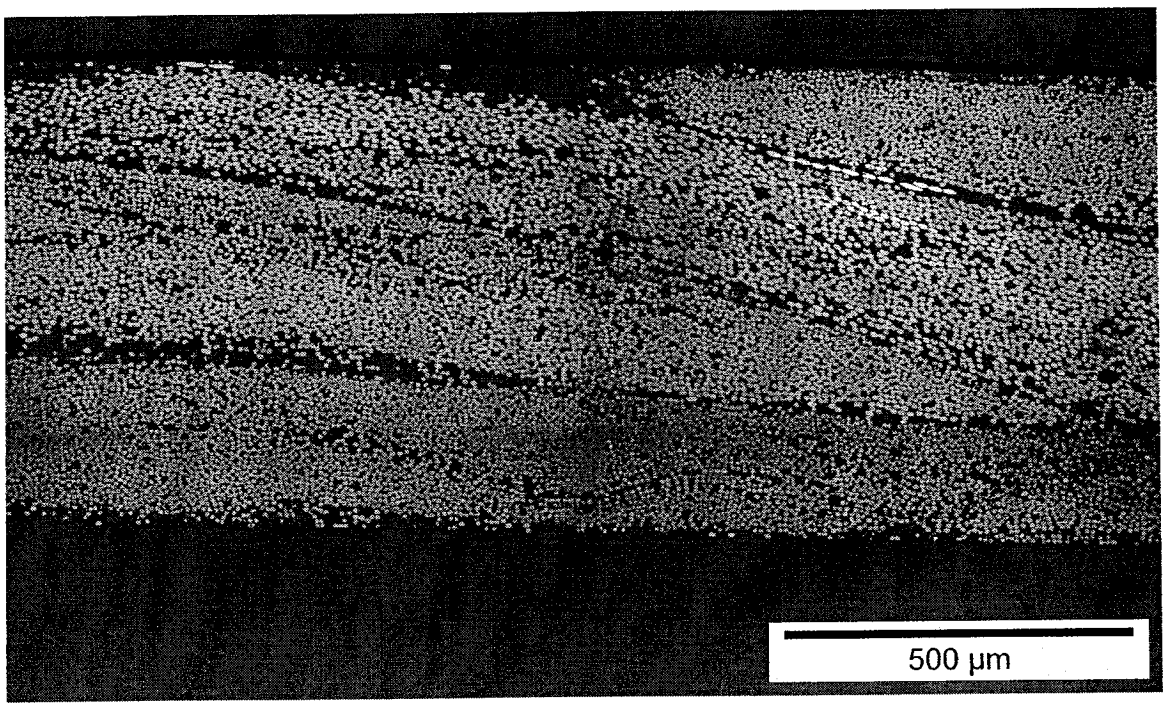

Figure 2: 200X Magnification of a selected Area

Sample: 45B72

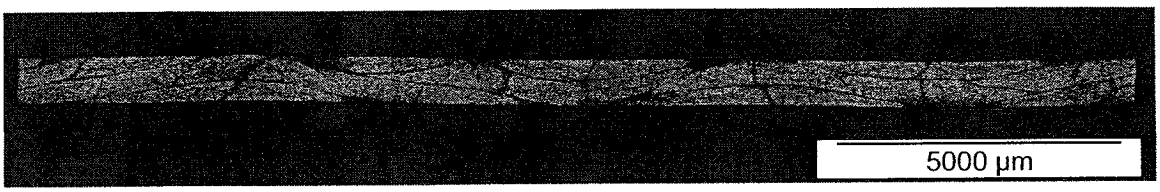

Figure 3: 50X Magnification of the Whole Coupon

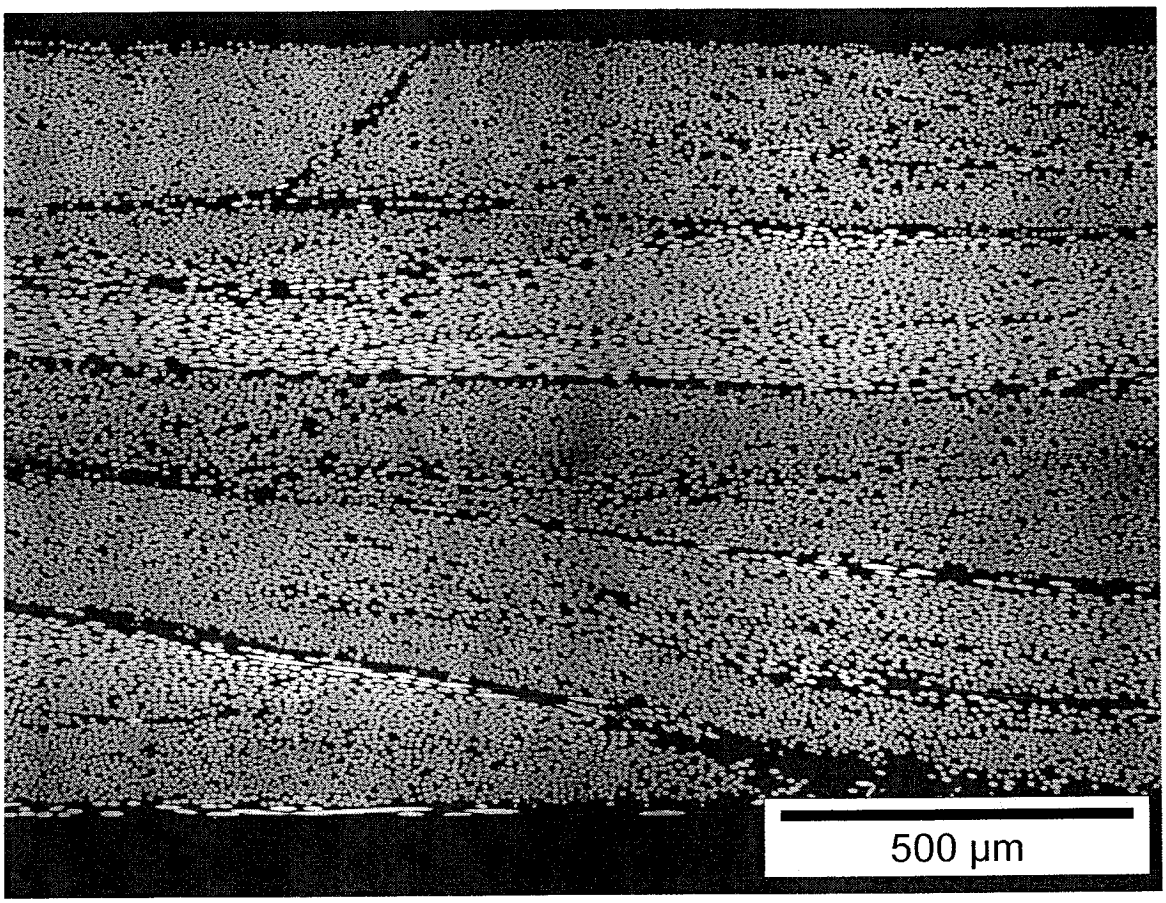

Figure 4: 200X Magnification of a selected Area

Sample: 60B72

Figure 5: 50X Magnification of the Whole Coupon

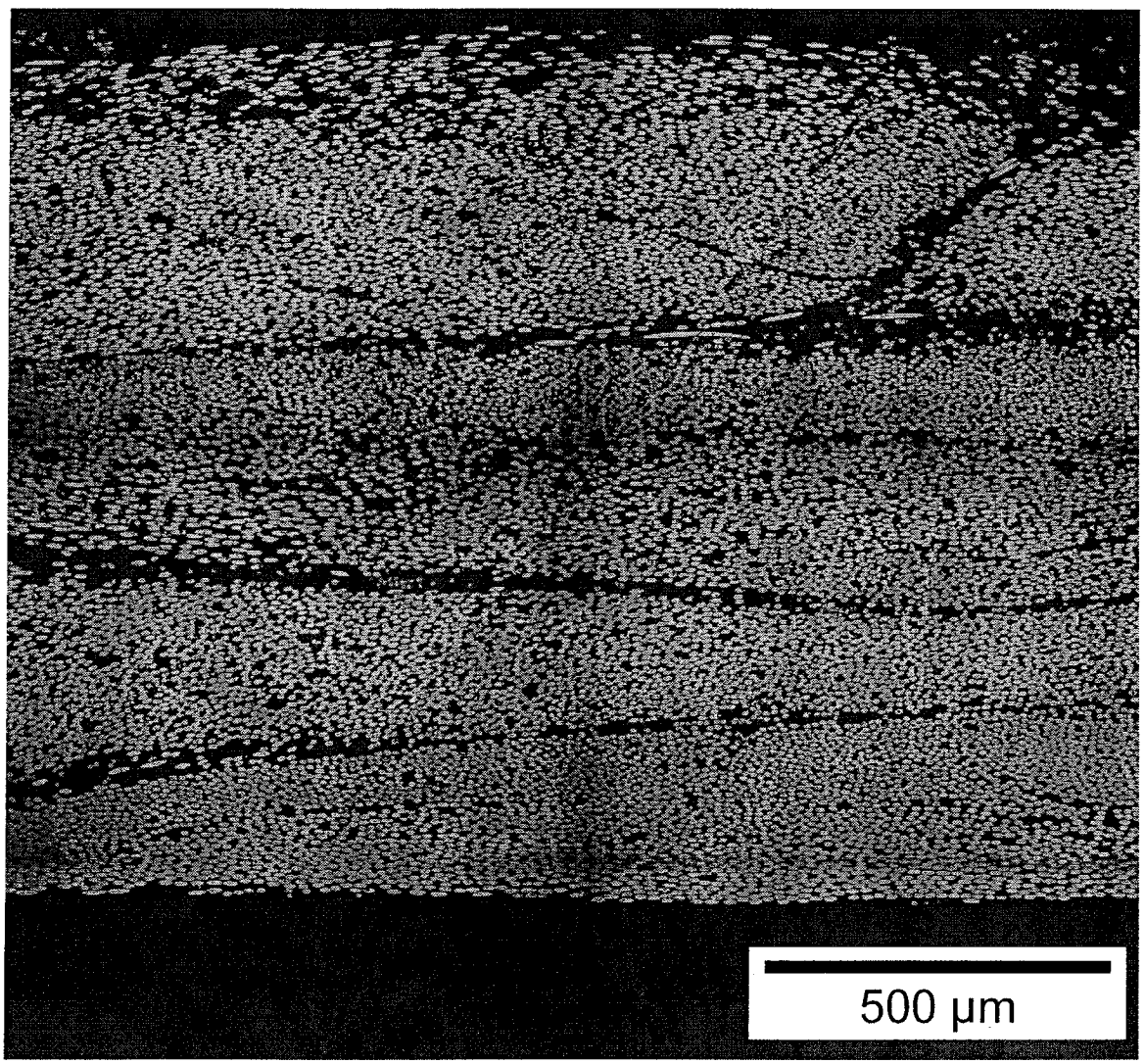

Figure 6: 200X Magnification of a selected Area

Sample: 78B72

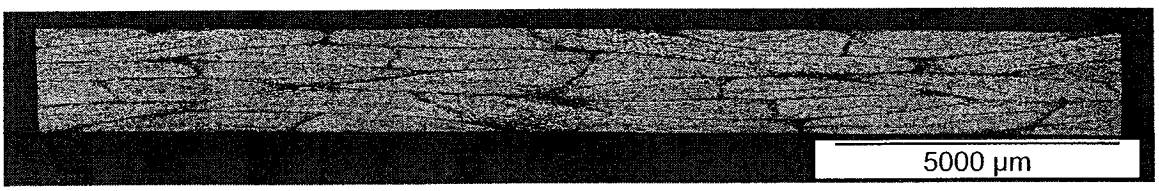

Figure 7: 50X Magnification of the Whole Coupon

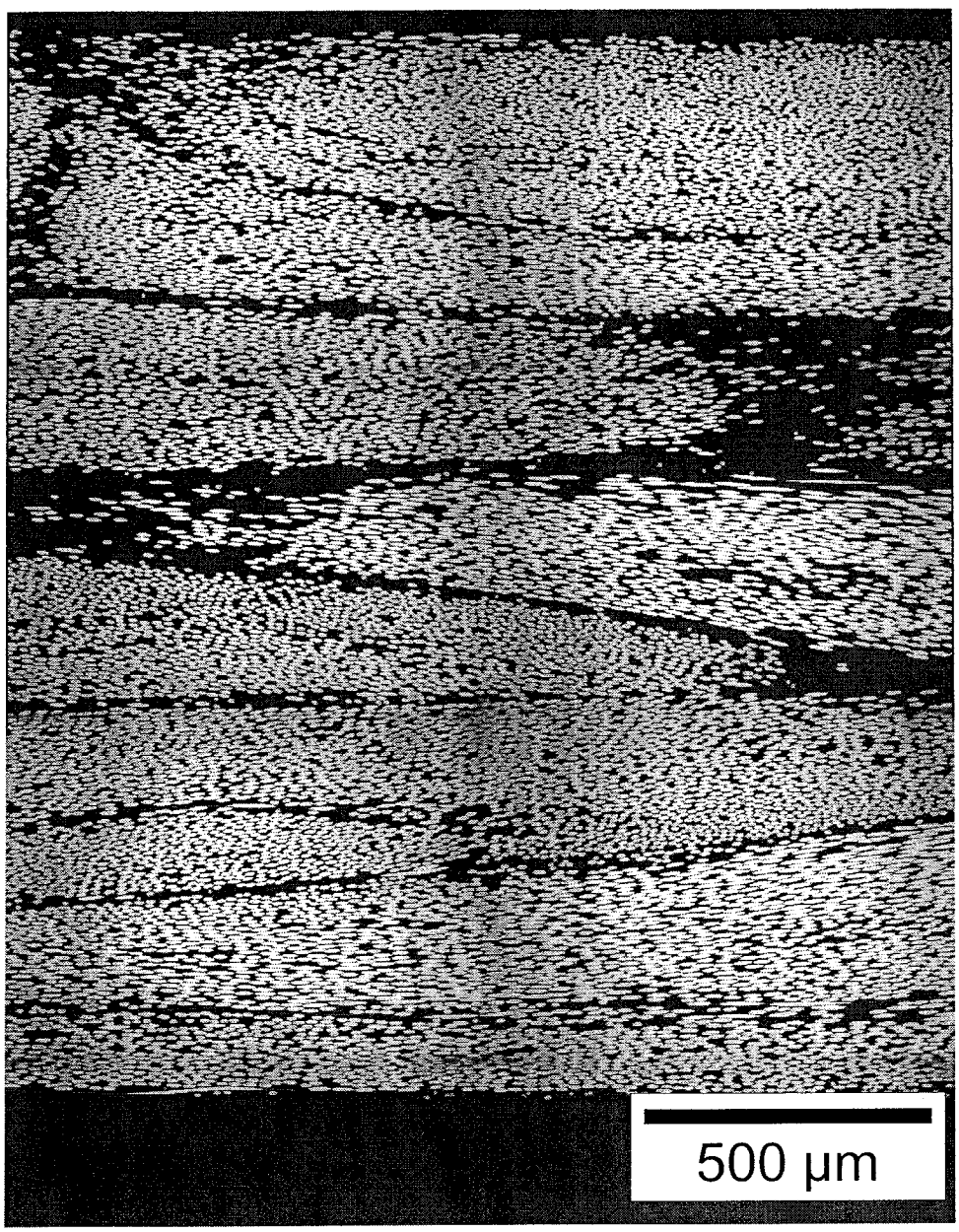

Figure 8: 200X Magnification of a selected Area

Sample: 30S72

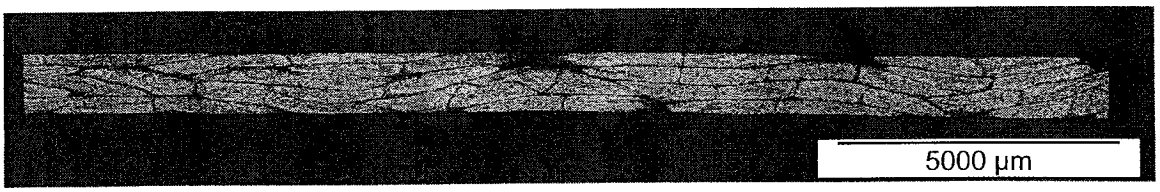

Figure 9: 50X Magnification of the Whole Coupon

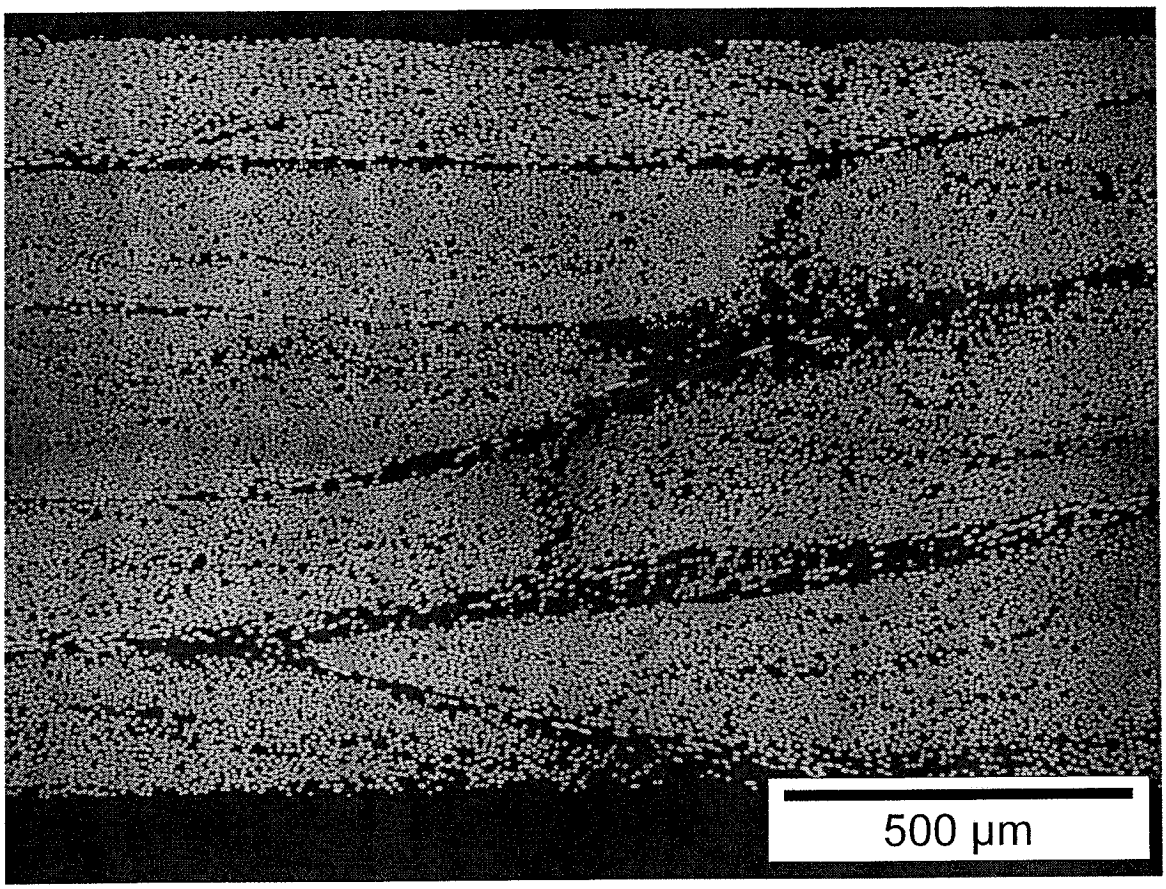

Figure 10: 200X Magnification of a selected Area

Sample: 45S68

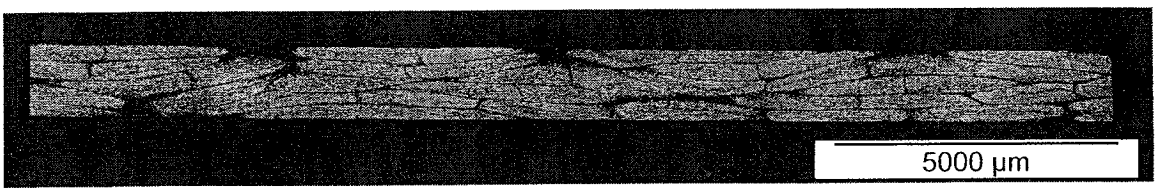

Figure 11: 50X Magnification of the Whole Coupon

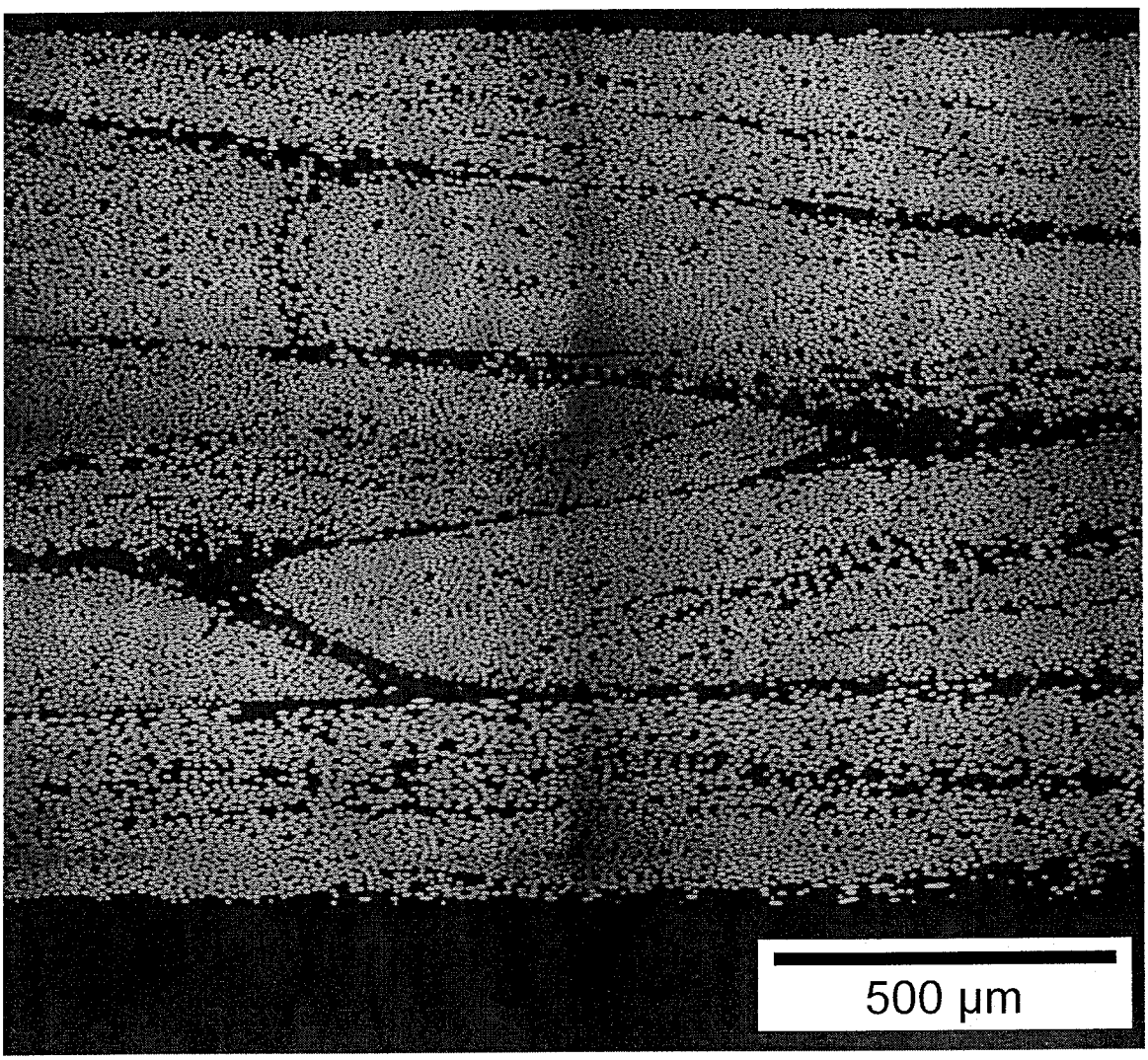

Figure 12: 200X Magnification of a selected Area

Sample: 60S60

Figure 13: 50X Magnification of the Whole Coupon

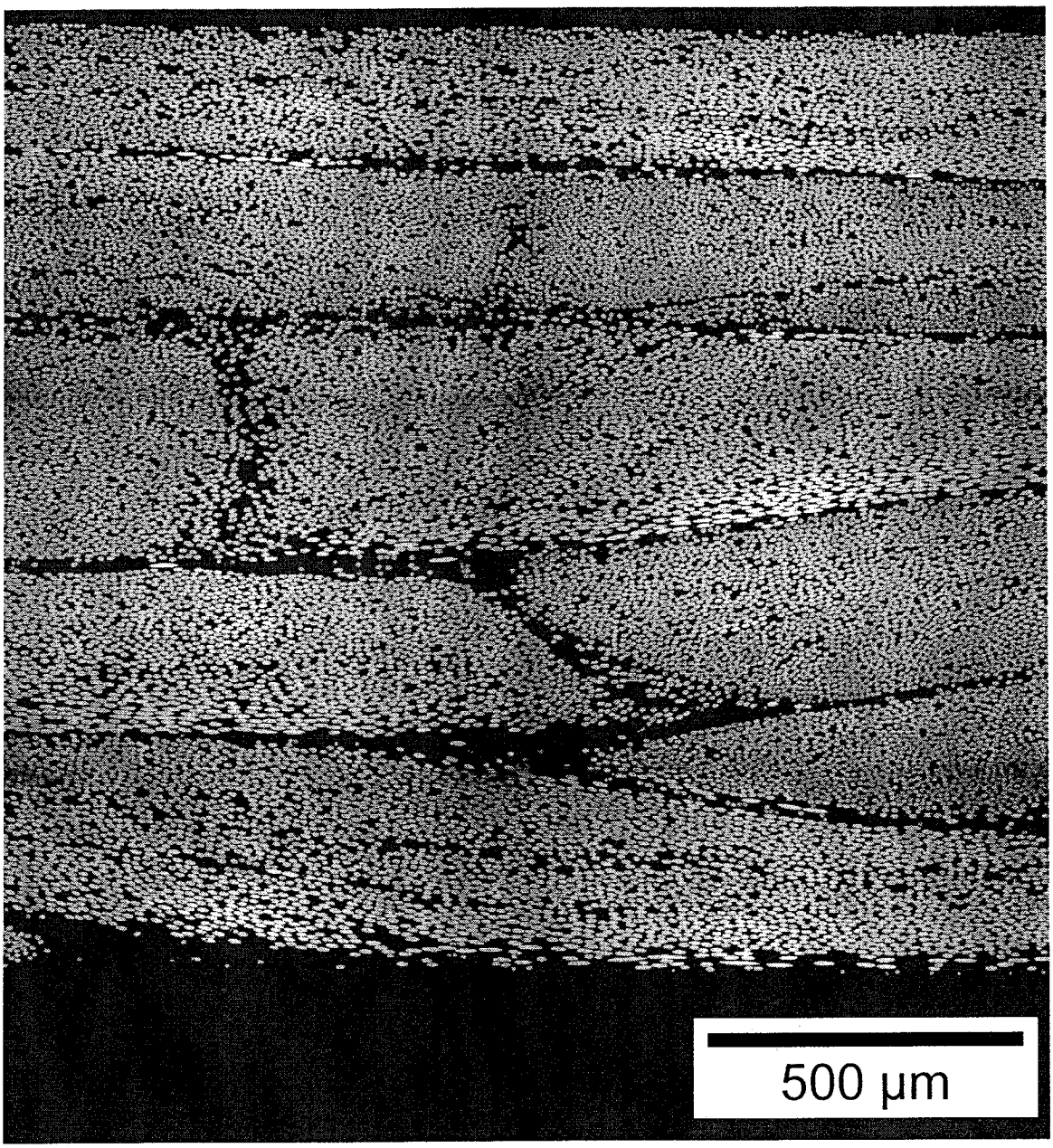

Figure 14: 200X Magnification of a selected Area

APPENDIX D

Precision Analysis on Constituent Content Method

Fiber Mass fraction formula and error propagation formulas

Fiber mass fraction in function of measured variables: mass of coupon in air (M_a), mass of empty and dry filter (M_f) and mass of dry filter filled with fibers (M_d):

$$W_f = \frac{M_d - M_f}{M_a} \tag{1}$$

Effect of the variation of the coupon mass in air (M_a) on the fiber mass fraction:

$$\frac{\partial}{\partial M_a} W_f = -\frac{M_d - M_f}{M_a{}^2} \tag{2}$$

Effect of the variation of the mass of empty and dry filter (M_f) on the fiber mass fraction:

$$\frac{\partial}{\partial M_f} W_f = -\frac{1}{M_a} \tag{3}$$

Effect of the variation of the mass of dry filter filled with fibers (M_d) on the fiber mass fraction:

$$\frac{\partial}{\partial M_d} W_f = \frac{1}{M_a} \tag{4}$$

Quadratic propagation of errors for the fiber mass fraction:

$$\delta W_f = \sqrt{\left(\left(\frac{\partial}{\partial M_d} W_f\right)\delta M_d\right)^2 + \left(\left(\frac{\partial}{\partial M_f} W_f\right)\delta M_f\right)^2 + \left(\left(\frac{\partial}{\partial M_a} W_f\right)\delta M_a\right)^2} \tag{5}$$

Actual density formula and error propagation formulas

Actual density in function of measured variables: mass of coupon in air (M_a), mass of coupon in water (M_w):

$$\rho_a = .9976 \frac{M_a}{M_a - M_w} \tag{6}$$

Effect of the variation of the coupon mass in air (M_a) on the actual density:

$$\frac{\partial}{\partial M_a} \rho_a = .9976 \frac{1}{M_a - M_w} - \frac{.9976\, M_a}{(M_a - M_w)2} \tag{7}$$

Effect of the variation of the coupon mass in water (M_w) on the actual density:

$$\frac{\partial}{\partial M_w} \rho_a = .9976 \frac{M_a}{(M_a - M_w)2} \tag{8}$$

Quadratic propagation of errors for the actual density:

$$\delta \rho_a = \sqrt{\left(\left(\frac{\partial}{\partial M_a}\rho_a\right)\delta M_a\right)^2 + \left(\left(\frac{\partial}{\partial M_w}\rho_a\right)\delta M_w\right)^2} \tag{9}$$

Theoretical density formula and error propagation formulas

Theoretical density in function of measured variables: mass of coupon in air (M_a), mass of empty and dry filter (M_f) and mass of dry filter filled with fibers (M_d):

$$\rho_t = \frac{\rho_f \rho_m}{\rho_f + \dfrac{(M_d - M_f)(\rho_m - \rho_f)}{M_a}} \tag{10}$$

Effect of the variation of the coupon mass in air (M_a) on the theoretical density:

$$\frac{\partial}{\partial M_a}\rho_t = \frac{\rho_f \rho_m (M_d - M_f)(\rho_m - \rho_f)}{\left(\rho_f + \dfrac{(M_d - M_f)(\rho_m - \rho_f)}{M_a}\right)^2 M_a^2} \tag{11}$$

Effect of the variation of the mass of empty and dry filter (M_f) on the theoretical density:

$$\frac{\partial}{\partial M_f}\rho_t = \frac{\rho_f \rho_m (\rho_m - \rho_f)}{\left(\rho_f + \dfrac{(M_d - M_f)(\rho_m - \rho_f)}{M_a}\right)^2 M_a} \tag{12}$$

Effect of the variation of the mass of dry filter filled with fibers (M_d) on the theoretical density:

$$\frac{\partial}{\partial M_d}\rho_t = -\frac{\rho_f \rho_m (\rho_m - \rho_f)}{\left(\rho_f + \dfrac{(M_d - M_f)(\rho_m - \rho_f)}{M_a}\right)^2 M_a} \tag{13}$$

Quadratic propagation of errors for the theoretical density:

$$\delta \rho_t = \sqrt{\left(\left(\frac{\partial}{\partial M_d}\rho_t\right)\delta M_d\right)^2 + \left(\left(\frac{\partial}{\partial M_f}\rho_t\right)\delta M_f\right)^2 + \left(\left(\frac{\partial}{\partial M_a}\rho_t\right)\delta M_a\right)^2} \tag{14}$$

Void content formula and error propagation formulas

Void content in function of measured variables: mass of coupon in air (M_a), mass of coupon in water (M_w), mass of empty and dry filter (M_f) and mass of dry filter filled with fibers (M_d):

$$X_v = 1 - \frac{.9976\, M_a \left(\rho_f + \dfrac{(M_d - M_f)(\rho_m - \rho_f)}{M_a} \right)}{(M_a - M_w)\, \rho_f \rho_m} \tag{15}$$

Effect of the variation of the coupon mass in air (M_a) on the void content:

$$\frac{\partial}{\partial M_a} X_v = -.9976 \frac{\rho_f + \dfrac{(M_d - M_f)(\rho_m - \rho_f)}{M_a}}{(M_a - M_w)\, \rho_f \rho_m} + \frac{.9976\, M_a \left(\rho_f + \dfrac{(M_d - M_f)(\rho_m - \rho_f)}{M_a} \right)}{(M_a - M_w)^2\, \rho_f \rho_m} + \frac{.9976\, (M_d - M_f)(\rho_m - \rho_f)}{M_a (M_a - M_w)\, \rho_f \rho_m} \tag{16}$$

Effect of the variation of the mass of coupon in water (M_w) on the void content:

$$\frac{\partial}{\partial M_w} X_v = -.9976 \frac{M_a \left(\rho_f + \dfrac{(M_d - M_f)(\rho_m - \rho_f)}{M_a} \right)}{(M_a - M_w)^2\, \rho_f \rho_m} \tag{17}$$

Effect of the variation of the mass of empty and dry filter (M_f) on the void content:

$$\frac{\partial}{\partial M_f} X_v = .9976 \frac{\rho_m - \rho_f}{(M_a - M_w)\, \rho_f \rho_m} \tag{18}$$

Effect of the variation of the mass of dry filter filled with fibers (M_d) on the void content:

$$\frac{\partial}{\partial M_d} X_v = -.9976 \frac{\rho_m - \rho_f}{(M_a - M_w)\, \rho_f \rho_m} \tag{19}$$

Quadratic propagation of errors for the void content:

$$\delta X_v = \sqrt{\left(\left(\frac{\partial}{\partial M_d} X_v \right) \delta M_d \right)^2 + \left(\left(\frac{\partial}{\partial M_f} X_v \right) \delta M_f \right)^2 + \left(\left(\frac{\partial}{\partial M_a} X_v \right) \delta M_a \right)^2 + \left(\left(\frac{\partial}{\partial M_w} X_v \right) \delta M_w \right)^2} \tag{20}$$

APPENDIX E

Tensile Modulus Prediction Using Classical Lamination Theory

The calculations are done in the software Matlab, An example is done for a 20 degree braid.

The proprties of the fiber and matrix are the following:

$$E1fibers := E_1^f = .240\ 10^{12}$$

$$E2fibers := E_2^f = .210\ 10^{11}$$

$$EMatrix := E^m = .11\ 10^{10}$$

$$NU12Fibers := \nu_{12}^f = .25$$

$$NUMatrix := \nu^m = .33$$

$$G12Fiber := G_{12}^f = .83\ 10^{10}$$

$$TheGMatrix := G^m = \frac{E^m}{2 + 2\,\nu^m}$$

$$GMatrix := G^m = .4135338346\ 10^9$$

$$VolumeFractionFibers := V^f = .52$$

The following etas are for the calculation of E2 and G.

$$ETHAE := \eta = .6$$

$$ETHAG := \eta = .6$$

Calculation of lamina properties in 1-2-3 coordinate system

$$Final\_E1 := E_1 = .125328\ 10^{12}$$

$$Final\_E2 := E_2 = .2819456193\ 10^{10}$$

$$Final\_NU12 := \nu_{12} = .2884$$

$$Final\_G12 := G_{12} = .1064436667\ 10^{10}$$

$$Final\_NU21 := \nu_{21} = .006488024752$$

$$Final\_NU23 := \nu_{23} = .33$$

2 - Reduced Stiffness Matrix

The next equations gives the parameters of the reduced stiffness matrix from the properties of the laminae, calculated in step 1. [Equation 4.17, ref. Hyer]

$$Q11 := Q_{11} = \frac{E_1}{1 - \nu_{12}\,\nu_{21}}$$

$$Q12 := Q_{12} = \frac{\nu_{12}\,E_2}{1 - \nu_{12}\,\nu_{21}}$$

$$Q22 := Q_{22} = \frac{E_2}{1 - \nu_{12}\,\nu_{21}}$$

$$Q66 := Q_{66} = G_{12}$$

The values of the reduced stiffness matrix in the 1-2-3 coordinate system are then:

$$Q11 := Q_{11} = .1255629466\ 10^{12}$$

$$Q12 := Q_{12} = .8146555057\ 10^{9}$$

$$Q22 := Q_{22} = .2824741698\ 10^{10}$$

$$Q66 := Q_{66} = .1064436667\ 10^{10}$$

3 - Rotation at +/- Braid Angle

The rotation equations to obtain the transform reduced stiffness matrix components, in global coordinate system:

$$first := Qbar_{11} = Q_{11}\,m^4 + 2\,(Q_{12} + 2\,Q_{66})\,m^2\,n^2 + Q_{22}\,n^4$$

$$second := Qbar_{22} = Q_{11}\,n^4 + 2\,(Q_{12} + 2\,Q_{66})\,m^2\,n^2 + Q_{22}\,m^4$$

$$third := Qbar_{12} = (Q_{11} + Q_{22} - 4\,Q_{66})\,m^2\,n^2 + Q_{12}\,(m^4 + n^4)$$

$$fourth := Qbar_{66} = (Q_{11} + Q_{22} - 2\,Q_{12} - 2\,Q_{66})\,m^2\,n^2 + Q_{66}\,(m^4 + n^4)$$

$$fifth := Qbar_{16} = (Q_{11} - Q_{12} - 2\,Q_{66})\,m^3\,n + (Q_{12} - Q_{22} + 2\,Q_{66})\,m\,n^3$$

$$sixth := Qbar_{26} = (Q_{11} - Q_{12} - 2\,Q_{66})\,m\,n^3 + (Q_{12} - Q_{22} + 2\,Q_{66})\,m^3\,n$$

PLUS THETA LAMINA

$$LeAngle := \theta = .3490684363$$

$$TheM := m = .9396917364$$

$$TheN := n = .3420225733$$

With values from the normal reduced stifness matrix calculated above we get, after the rotation:

$$QPTBar11 := QPTbar_{11} = .9855136666\ 10^{11}$$

$$QPTBar22 := QPTbar_{22} = .4528854852\ 10^{10}$$

$$QPTBar12 := QPTbar_{12} = .1346838891\ 10^{11}$$

$$QPTBar66 := QPTbar_{66} = .1371817007\ 10^{11}$$

$$QPTBar16 := QPTbar_{16} = .3480374477\ 10^{11}$$

$$QPTBar26 := QPTbar_{26} = .4643797053\ 10^{10}$$

MINUS THETA LAMINA

$$LeAngle := \theta = -.3490684363$$

$$TheM := m = .9396917364$$

$$TheN := n = -.3420225733$$

With values from the normal reduced stifness matrix calculated above we get, after the rotation:

$$QMTBar11 := QMTbar_{11} = .9855136666\ 10^{11}$$

$$QMTBar22 := QMTbar_{22} = .4528854852\ 10^{10}$$

$$QMTBar12 := QMTbar_{12} = .1346838891\ 10^{11}$$

$$QMTBar66 := QMTbar_{66} = .1371817007\ 10^{11}$$

$$QMTBar16 := QMTbar_{16} = -.3480374477\ 10^{11}$$

$$QMTBar26 := QMTbar_{26} = -.4643797053\ 10^{10}$$

4- Braided Laminate Construction

The ABD matrix is the following [Equation 7.85, ref. Hyer]:

$$ABD = \begin{bmatrix} A_{11} & A_{12} & A_{16} & B_{11} & B_{12} & B_{16} \\ A_{12} & A_{22} & A_{26} & B_{12} & B_{22} & B_{26} \\ A_{16} & A_{26} & A_{66} & B_{16} & B_{26} & B_{66} \\ B_{11} & B_{12} & B_{16} & D_{11} & D_{12} & D_{16} \\ B_{12} & B_{22} & B_{26} & D_{12} & D_{22} & D_{26} \\ B_{16} & B_{26} & B_{66} & D_{16} & D_{26} & D_{66} \end{bmatrix}$$

For the assembly of the laminate, i.e. the calculation of the ABD matrix terms, the positions in z of interfaces of the 6 layers are:

$$Z0 := z_0 = \frac{-1}{1000}$$

$$Z1 := z_1 = \frac{-1}{1500}$$

$$Z2 := z_2 = \frac{-1}{3000}$$

$$Z3 := z_3 = 0$$

$$Z4 := z_4 = \frac{1}{3000}$$

$$Z5 := z_5 = \frac{1}{1500}$$

$$Z6 := z_6 = \frac{1}{1000}$$

The terms of the matrix are calculated with Equation 7.86 of Hyer

First, For the As.

$$A11 := A_{11} = QPTbar_{11}(z_1 - z_0) + QMTbar_{11}(z_2 - z_1) + QPTbar_{11}(z_3 - z_2) + QMTbar_{11}(z_4 - z_3) + QPTbar_{11}(z_5 - z_4) + QMTbar_{11}(z_6 - z_5)$$

$$A12 := A_{12} = QPTbar_{12}(z_1 - z_0) + QMTbar_{12}(z_2 - z_1) + QPTbar_{12}(z_3 - z_2) + QMTbar_{12}(z_4 - z_3) + QPTbar_{12}(z_5 - z_4) + QMTbar_{12}(z_6 - z_5)$$

$$A16 := A_{16} = QPTbar_{16}(z_1 - z_0) + QMTbar_{16}(z_2 - z_1) + QPTbar_{16}(z_3 - z_2) + QMTbar_{16}(z_4 - z_3) + QPTbar_{16}(z_5 - z_4) + QMTbar_{16}(z_6 - z_5)$$

$$A22 := A_{22} = QPTbar_{22}(z_1 - z_0) + QMTbar_{22}(z_2 - z_1) + QPTbar_{22}(z_3 - z_2) + QMTbar_{22}(z_4 - z_3) + QPTbar_{22}(z_5 - z_4) + QMTbar_{22}(z_6 - z_5)$$

$$A26 := A_{26} = QPTbar_{26}(z_1 - z_0) + QMTbar_{26}(z_2 - z_1) + QPTbar_{26}(z_3 - z_2) + QMTbar_{26}(z_4 - z_3) + QPTbar_{26}(z_5 - z_4) + QMTbar_{26}(z_6 - z_5)$$

$$A66 := A_{66} = QPTbar_{66}(z_1 - z_0) + QMTbar_{66}(z_2 - z_1) + QPTbar_{66}(z_3 - z_2) + QMTbar_{66}(z_4 - z_3) + QPTbar_{66}(z_5 - z_4) + QMTbar_{66}(z_6 - z_5)$$

Calculations follow

[For the Bs

$$B11 := B_{11} = \frac{1}{2} QPTbar_{11} (z_1{}^2 - z_0{}^2) + \frac{1}{2} QMTbar_{11} (z_2{}^2 - z_1{}^2) + \frac{1}{2} QPTbar_{11} (z_3{}^2 - z_2{}^2)$$
$$+ \frac{1}{2} QMTbar_{11} (z_4{}^2 - z_3{}^2) + \frac{1}{2} QPTbar_{11} (z_5{}^2 - z_4{}^2) + \frac{1}{2} QMTbar_{11} (z_6{}^2 - z_5{}^2)$$

$$B12 := B_{12} = \frac{1}{2} QPTbar_{12} (z_1{}^2 - z_0{}^2) + \frac{1}{2} QMTbar_{12} (z_2{}^2 - z_1{}^2) + \frac{1}{2} QPTbar_{12} (z_3{}^2 - z_2{}^2)$$
$$+ \frac{1}{2} QMTbar_{12} (z_4{}^2 - z_3{}^2) + \frac{1}{2} QPTbar_{12} (z_5{}^2 - z_4{}^2) + \frac{1}{2} QMTbar_{12} (z_6{}^2 - z_5{}^2)$$

$$B16 := B_{16} = \frac{1}{2} QPTbar_{16} (z_1{}^2 - z_0{}^2) + \frac{1}{2} QMTbar_{16} (z_2{}^2 - z_1{}^2) + \frac{1}{2} QPTbar_{16} (z_3{}^2 - z_2{}^2)$$
$$+ \frac{1}{2} QMTbar_{16} (z_4{}^2 - z_3{}^2) + \frac{1}{2} QPTbar_{16} (z_5{}^2 - z_4{}^2) + \frac{1}{2} QMTbar_{16} (z_6{}^2 - z_5{}^2)$$

$$B22 := B_{22} = \frac{1}{2} QPTbar_{22} (z_1{}^2 - z_0{}^2) + \frac{1}{2} QMTbar_{22} (z_2{}^2 - z_1{}^2) + \frac{1}{2} QPTbar_{22} (z_3{}^2 - z_2{}^2)$$
$$+ \frac{1}{2} QMTbar_{22} (z_4{}^2 - z_3{}^2) + \frac{1}{2} QPTbar_{22} (z_5{}^2 - z_4{}^2) + \frac{1}{2} QMTbar_{22} (z_6{}^2 - z_5{}^2)$$

$$B26 := B_{26} = \frac{1}{2} QPTbar_{26} (z_1{}^2 - z_0{}^2) + \frac{1}{2} QMTbar_{26} (z_2{}^2 - z_1{}^2) + \frac{1}{2} QPTbar_{26} (z_3{}^2 - z_2{}^2)$$
$$+ \frac{1}{2} QMTbar_{26} (z_4{}^2 - z_3{}^2) + \frac{1}{2} QPTbar_{26} (z_5{}^2 - z_4{}^2) + \frac{1}{2} QMTbar_{26} (z_6{}^2 - z_5{}^2)$$

$$B66 := B_{66} = \frac{1}{2} QPTbar_{66} (z_1{}^2 - z_0{}^2) + \frac{1}{2} QMTbar_{66} (z_2{}^2 - z_1{}^2) + \frac{1}{2} QPTbar_{66} (z_3{}^2 - z_2{}^2)$$
$$+ \frac{1}{2} QMTbar_{66} (z_4{}^2 - z_3{}^2) + \frac{1}{2} QPTbar_{66} (z_5{}^2 - z_4{}^2) + \frac{1}{2} QMTbar_{66} (z_6{}^2 - z_5{}^2)$$

[Calculations follow

[For the Ds.

$$D11 := D_{11} = \frac{1}{3} QPTbar_{11} (z_1{}^3 - z_0{}^3) + \frac{1}{3} QMTbar_{11} (z_2{}^3 - z_1{}^3) + \frac{1}{3} QPTbar_{11} (z_3{}^3 - z_2{}^3) + \frac{1}{3} QMTbar_{11} (z_4{}^3 - z_3{}^3) + \frac{1}{3} QPTbar_{11} (z_5{}^3 - z_4{}^3) + \frac{1}{3} QMTbar_{11} (z_6{}^3 - z_5{}^3)$$

$$D12 := D_{12} = \frac{1}{3} QPTbar_{12} (z_1{}^3 - z_0{}^3) + \frac{1}{3} QMTbar_{12} (z_2{}^3 - z_1{}^3) + \frac{1}{3} QPTbar_{12} (z_3{}^3 - z_2{}^3) + \frac{1}{3} QMTbar_{12} (z_4{}^3 - z_3{}^3) + \frac{1}{3} QPTbar_{12} (z_5{}^3 - z_4{}^3) + \frac{1}{3} QMTbar_{12} (z_6{}^3 - z_5{}^3)$$

$$D16 := D_{16} = \frac{1}{3} QPTbar_{16} (z_1{}^3 - z_0{}^3) + \frac{1}{3} QMTbar_{16} (z_2{}^3 - z_1{}^3) + \frac{1}{3} QPTbar_{16} (z_3{}^3 - z_2{}^3) + \frac{1}{3} QMTbar_{16} (z_4{}^3 - z_3{}^3) + \frac{1}{3} QPTbar_{16} (z_5{}^3 - z_4{}^3) + \frac{1}{3} QMTbar_{16} (z_6{}^3 - z_5{}^3)$$

$$D22 := D_{22} = \frac{1}{3} QPTbar_{22} (z_1{}^3 - z_0{}^3) + \frac{1}{3} QMTbar_{22} (z_2{}^3 - z_1{}^3) + \frac{1}{3} QPTbar_{22} (z_3{}^3 - z_2{}^3) + \frac{1}{3} QMTbar_{22} (z_4{}^3 - z_3{}^3) + \frac{1}{3} QPTbar_{22} (z_5{}^3 - z_4{}^3) + \frac{1}{3} QMTbar_{22} (z_6{}^3 - z_5{}^3)$$

$$D26 := D_{26} = \frac{1}{3} QPTbar_{26} (z_1{}^3 - z_0{}^3) + \frac{1}{3} QMTbar_{26} (z_2{}^3 - z_1{}^3) + \frac{1}{3} QPTbar_{26} (z_3{}^3 - z_2{}^3) + \frac{1}{3} QMTbar_{26} (z_4{}^3 - z_3{}^3) + \frac{1}{3} QPTbar_{26} (z_5{}^3 - z_4{}^3) + \frac{1}{3} QMTbar_{26} (z_6{}^3 - z_5{}^3)$$

$$D66 := D_{66} = \frac{1}{3} QPTbar_{66} (z_1{}^3 - z_0{}^3) + \frac{1}{3} QMTbar_{66} (z_2{}^3 - z_1{}^3) + \frac{1}{3} QPTbar_{66} (z_3{}^3 - z_2{}^3) + \frac{1}{3} QMTbar_{66} (z_4{}^3 - z_3{}^3) + \frac{1}{3} QPTbar_{66} (z_5{}^3 - z_4{}^3) + \frac{1}{3} QMTbar_{66} (z_6{}^3 - z_5{}^3)$$

[Calculations follow

[ABD matrix assembly

$$FABD := \begin{bmatrix} .1971027334\,10^{9} & .2693677782\,10^{8} & 0. & 0 & 0 & -11601.24825 \\ .2693677782\,10^{8} & .9057709704\,10^{7} & 0. & 0 & 0 & -1547.932352 \\ 0. & 0. & .2743634015\,10^{8} & -11601.24825 & -1547.932352 & 0. \\ 0 & 0 & -11601.24825 & 65.70091110 & 8.978925940 & 0. \\ 0 & 0 & -1547.932352 & 8.978925940 & 3.019236568 & 0. \\ -11601.24825 & -1547.932352 & 0. & 0. & 0. & 9.145446712 \end{bmatrix}$$

5 - abd matrix.

Inversion of the ABD Matrix

$$abd :=$$

$$\begin{bmatrix} .897011957435218514\ 10^{-8} & -.254683720457118432\ 10^{-7} & 0. & 0. & 0. & .706813663755720110\ 10^{-5} \\ -.254683720457118432\ 10^{-7} & .186002736468104180\ 10^{-6} & 0. & 0. & 0. & -.825028401975643406\ 10^{-6} \\ 0. & 0. & .393901706180610474\ 10^{-7} & .706813663999959434\ 10^{-5} & -.825028419522066116\ 10^{-6} & 0. \\ 0. & 0. & .706813663999959520\ 10^{-5} & .0269103587464960478 & -.0764051162055901789 & 0. \\ 0. & 0. & -.825028419522065800\ 10^{-6} & -.0764051162055901789 & .558008209598894300 & 0. \\ .706813663755720110\ 10^{-5} & -.825028401975648384\ 10^{-6} & 0. & 0. & 0. & .118170511914353848 \end{bmatrix}$$

6 - Calculations of the axial and hoop modulus

The equation for the axial and hoop modulus are given by:

$$AxialModulus := E_{axial} = \frac{1}{abd_{11}\ Thickness}$$

$$HoopModulus := E_{hoop} = \frac{1}{abd_{22}\ Thickness}$$

The calculations of the moduli give:

$$AxialModulus := E_{axial} = .5574061705\ 10^{11}$$

$$HoopModulus := E_{hoop} = .2688132494\ 10^{10}$$

Using the same calculation spread sheet for different angles, the following tensile modulus values are calculated in function of the braid angle.

Angle	Tensile Modulus
Degrees	GPa
0	125.3
5	118.0
10	105.0
15	83.2
20	55.7
25	32.5
30	17.9
35	10.0
40	6.0
45	4.1
50	3.2
55	2.8
60	2.7
65	2.7
70	2.7
75	2.7
80	2.8
85	2.8
90	2.8